THE UNIVERSITY OF
WAIKATO
Te Whare Wānanga o Waikato

Mass Spectral Characterisation of Three New Groups of Algal Toxins

A thesis
submitted in partial fulfilment
of the requirements for the degree
of

Master of Science in Chemistry

at

The University of Waikato

by

BRENT KEVIN KNUDSEN

The University of Waikato
2009

Abstract

This thesis reports the mass spectral identification and characterisation of three new groups of algal compounds.

A series of novel pectenotoxins (PTXs) were identified in retained sub-samples of Irish mussel extracts that had previously been utilised to obtain bulk quantities of some other algal toxins. The first eluting of the novel pectenotoxins, when analysed on a C-18 column using an MeCN-H_2O gradient, afforded MNH_4^+ and MNa^+ ions at *m/z* 864 and 869 respectively. This compound was designated as PTX-i. Three minor isomers (possibly storage artefacts) of the dominant PTX-i compound were also detected in the retained extracts, together with several later eluting sulfonated and sulfonated fatty acid ester analogues of PTX-i. The dominant fatty acid analogues were found to be the 16:0 esters. Sulfonated PTX-i isomers and their 16:0 fatty acid ester analogues showed strong *m/z* 925 and 1163 ion responses respectively in negative ion mode. High resolution mass spectrometry (HRMS) data showed the atomic composition of the *m/z* 925 ion to be $C_{47}H_{69}O_{17}S$. Full scan, MS^2, MS^3 and MS^4 mass spectral data determined in both positive and negative ion modes for the three series of PTX-i compounds was consistent with the proposal that they possessed a $C_5H_{11}O_3$ side chain attached to C-35, rather than a 36-hemiacetal ring system as found in other known pectenotoxins, and that the sulfate and fatty acid residues were attached to two of the hydroxyl groups believed to present in the $C_5H_{11}O_3$ side chain.

An algal water sample collected from Vigo, Spain (*Dinophysis acuta*, 12/12/05), that had previously been extracted with CH_2Cl_2 and Et_2O, was found to contain low levels of two new pectenotoxin-2 seco acid (PTX-2SA) analogues that showed MNH_4^+ and MNa^+ ions at *m/z* 896 and 901 respectively. Full scan, MS^2, MS^3 and MS^4 mass spectral data determined in positive ion mode, in combination with $NaBH_4$ and $NaBD_4$ reduction reaction product data determined for PTX-2SA and the two new compounds, established that the new compounds were 14-hydroxy analogues of PTX-2SA.

The Spanish algal water sample also found to contain an appreciable level of two glycosides which were identified from a combination of full scan, MS^2, MS^3 and MS^4 mass spectral data determined in both positive and negative ion modes as either 7- or 24-*O*-glycosides of okadaic acid (OA) and dinophysistoxin-2 (DTX-2), as MS^n data excluded C-2 or C-27 *O*-glycosylation. 1D and 2D-^{1}H NMR, obtained by co-workers while the mass spectral investigations reported in this thesis were in progress, showed that the glycosides were the 24-β-*O*-glucopyranosyl analogues of OA and DTX-2.

A set of three New Zealand derived algal water extracts, two from West Coast, South Island (*Dinophysis acuta*) and one from Akaroa Harbour (*Dinophysis acuminata*), were prepared and analysed for the three groups of new algal compounds reported in this thesis. PTX-i and its analogues were not detected in any of the New Zealand samples, the two 14-hydroxy PTX-2SA compounds were detected in one of the West Coast samples and the Akaroa Harbour samples and 24-*O*-glucoside OA and DTX-2 analogues were only detected in the Akaroa Harbour sample.

Table of Contents

Acknowledgements

My biggest thanks go out to my main supervisor, Professor Alistair Wilkins. He put in a lot of time and effort (in New Zealand and in Oslo) into helping me make this possible and there is no way I could have done it without him. His encouragement and advice will not ever be forgotten.

I also wish to give my many thanks to my other supervisor, Dr Christopher Miles for all his advice and help when I could not fully understand certain elements of this project. His knowledge helped me a great deal with getting my head around certain parts of my research and I valued it greatly.

Other thanks go to Alan Hawkes from AgResearch, Ruakura for his assistance with the processing of my samples, Wendy Jackson for her help with the LCMS system at Waikato University, Pat Gread for her work obtaining the HRMS mass spectra and to the various people in at NVI, Oslo and Cawthron Institute, New Zealand who provided information and samples for my project.

The project was carried out at Waikato University, Hamilton so thanks goes out to them for providing the means for me to make this project possible. Also, thanks to my numerous lecturers over the years at university.

To my family - Mum, Dad, Nana and Poppa for their continuing support and encouragement throughout my 5 years at Waikato University and the years before attending university. Without your help, I would most likely never of attended university and had the opportunity to advance myself to the level I am at now. Also thanks to Mum and Dad for helping me proof read my thesis.

My final thanks go out to my many friends who have come through the various stages of my Chemistry degree with me, to those who I have met in other parts of university and Hamilton and to those who I have known before coming to university. You know who you are.

Abbreviations

NVI	National Veterinary Institute
PTX	Pectenotoxin
SA	Seco acid
LCMS	Liquid chromatography-mass spectrometry
NMR	Nuclear Magnetic Resonance
OA	Okadaic acid
DTX	Dinophysistoxin
ESI	Electrospray ionisation
HR	High Resolution
MS	Mass spectrometry
UV	Ultra-violet
CE	Collision energy
YTX	Yessotoxin
Da	Dalton
SRM	Selected ion reaction monitoring
NOE	Nuclear overhauser effect
NOESY	Nuclear overhauser effect spectroscopy
ROESY	Rotating frame overhauser effect spectroscopy
TOCSY	Total correlation spectroscopy
COSY	Correlation spectroscopy
RDA	Retro Diels-Alder
RT	Retention time
SRM	Selected reaction monitoring

List of Figures

List of Tables

Chapter 1

Introduction and Review

1.0 Introduction

Aquatic algal blooms are a common occurrence around the world. They are caused by a localised increase of phytoplankton algae in an aquatic environment. This can be caused by a surplus of nutrients (mainly phosphorus and nitrogen) but many other factors are also thought to contribute.

Dinoflagellates are an algal group associated with the production of many marine toxins. In an algal bloom, these toxins can accumulate to a dangerous level in filter feeders (mussels, scallops etc) that they come into contact with, causing widespread closure of all affected areas because of the danger to people who consume toxic shellfish. Filter feeders can process between 1-9 L of water per hour in a bloom and thus can accumulate a large amount of toxic compounds over time.

Algal blooms have a serious financial effect on commercial fishing and shellfish operations and businesses, along with recreational activities such as fishing and diving. In the case of commercial shellfish operations, if a mussel bed comes into contact with a bloom, harvesting is sometimes suspended since eating shellfish sufficiently contaminated by the bloom could result in human poisonings. Normal cooking techniques like steaming or boiling generally do not destroy the toxins although some toxin groups are affected by such treatment.

The food chain (Figure 1-1) shows routes for the transfer of toxins in shellfish, which eventually accumulates from the microalgae to the highest point of the food chain which is humans.

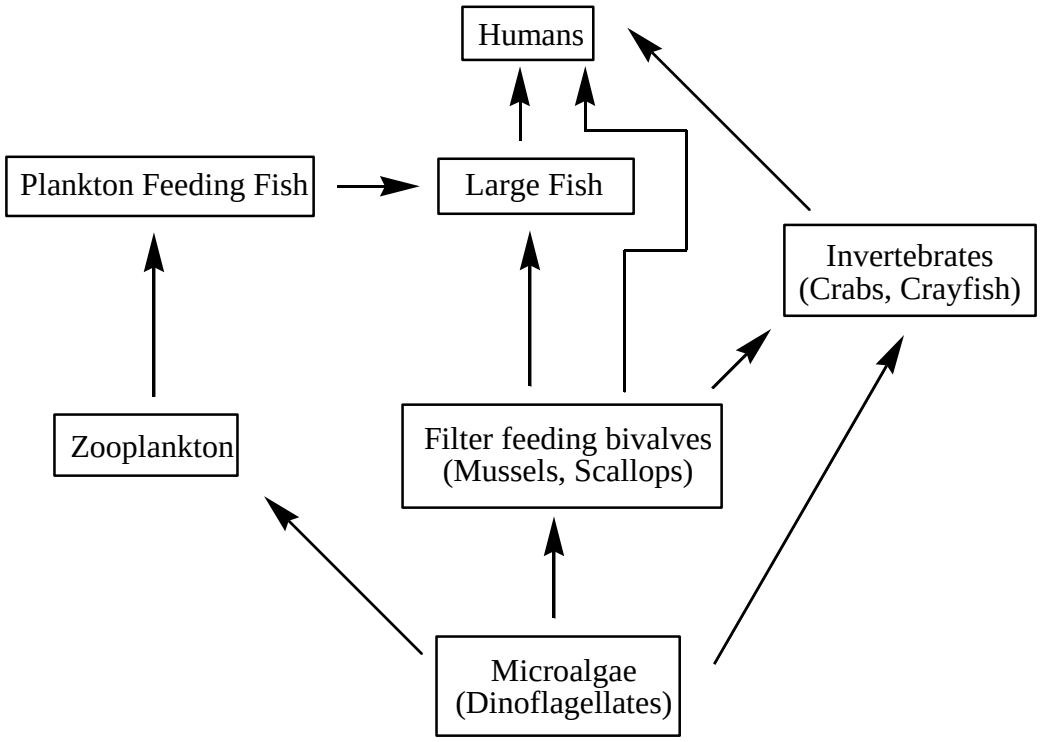

Figure 1-1: Food chain showing routes of toxin accumulation from microalgae to humans.

Algal bloom derived shellfish toxins used to be split into four groups depending on what the effect is of the toxin on the human body and/or the mouse bioassay, but are now classed by their structure into eight groups[1] because of confusion that resulted in classifying the compounds.

The four original groups were diarrhetic shellfish poisoning (DSP), paralytic shellfish poisoning (PSP), neurotoxic shellfish poisoning (NSP) and amnesic shellfish poisoning (ASP). DSP was one of the most common forms of shellfish poisoning. Symptoms of shellfish poisoning can occur as fast as 30 minutes from ingesting the poisoned shellfish and the main symptom is diarrhoea along with cramps, nausea and vomiting.

The eight modern groups that are used to classify the toxins according to their structures are:

1. azaspiracids
2. brevetoxins
3. cyclic imines
4. domoic acids
5. okadaic acids
6. pectenotoxins
7. saxitoxins
8. yessotoxins

Of particular interest in the investigations reported in subsequent chapters of this thesis are the pectenotoxins and okadaic acid analogues.

1.1 Pectenotoxins

Pectenotoxins (PTXs) are a group of polyether cyclic lactones produced by marine dinoflagellates of the genus *Dinophysis* and have been detected in shellfish worldwide. Isolation of pectenotoxins has been achieved from extraction of mussel tissue and from algal water extracts taken directly from algal bloom contaminated water.

The most commonly encountered PTX analogue in algal water samples is PTX-2 (**1**) which has been identified in *Dinophysis acuta* in New Zealand, Norway, Spain and Ireland[2-7], *Dinophysis acuminata* in Norway and New Zealand[5, 8], *Dinophysis caudata* from Spain[7] and *Dinophysis rotundata* from Norway[5] and *Dinophysis fortii* from Japan and Italy[9-11]. PTX-2 is hydrolysed enzymatically by many shellfish species into its seco acid form - PTX-2SA[12] (**6a**) which is the most commonly found pectenotoxin in mussel-derived extracts. A 7-*epi* form of PTX-2SA (7-*epi*-PTX-2SA) (**6b**) has also been reported although it has been shown to isomerise from PTX-2SA in storage and is probably not formed by the enzymatic processes in shellfish[13].

PTX-2 and its analogues were originally regarded as DSP toxins based on their activity in the mouse bioassay[14]. PTX-2SAs were also for a short time regarded as members of the DSP group of toxins based on Australian mice bioassay results that showed a mixture of PTX-2SA and 7-*epi*-PTX-2SA given orally caused gastrointestinal damage to the mice so these compounds were thought to be the cause of severe diarrheic illness[15]. It was later found that the PTX-2SA mixture used in the bioassay was contaminated with esters of OA and this was most likely the cause of the sickness. Subsequent toxicological evaluation with a pure sample showed no effect on mice, putting doubt into PTX-2SA as a toxin effecting the human body[16].

Other PTX analogues have been identified including PTX-3 (**2**)[17], PTX-6 (**3**)[17], PTX-11 (**4**)[18] and PTX-13 (**5**)[19], along with the 7-*epi* analogues (opposite stereochemistry at C-7) of some of these compounds.

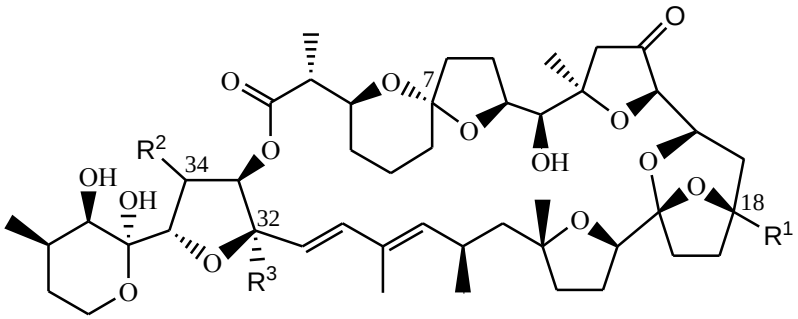

	R^1	R^2	R^3
PTX-2 (**1**)	CH_3	H	H
PTX-3 (**2**)	CHO	H	H
PTX-6 (**3**)	COOH	H	H
PTX-11 (**4**)	CH_3	OH	H
PTX-13 (**5**)	CH_3	H	OH

Figure 1-2: Structures of a selection of pectenotoxins.

Recently a series of fatty acids of PTX-2SA and 7-*epi*-PTX-2SA have been identified from extracts of Irish mussels[20]. The 37-*O*-acyl esters (**7**) were found to be the most common along with smaller amounts of 11-*O*-acyl (**9**) and the 33-*O*-acyl esters (**8**). The 18:4, 20:5, 22:6, 14:0, 16:1 and 16:0 fatty acid analogues were found to be

present in an approximate ratio of 1:1:1:1:1:1. Other *O*-acyl esters present in minor amounts included the 15:0, 15:1, 17:0, 17:1, 18:0, 18:1, 18:2, 18:3, 20:2 and 20:3 fatty acid esters[20].

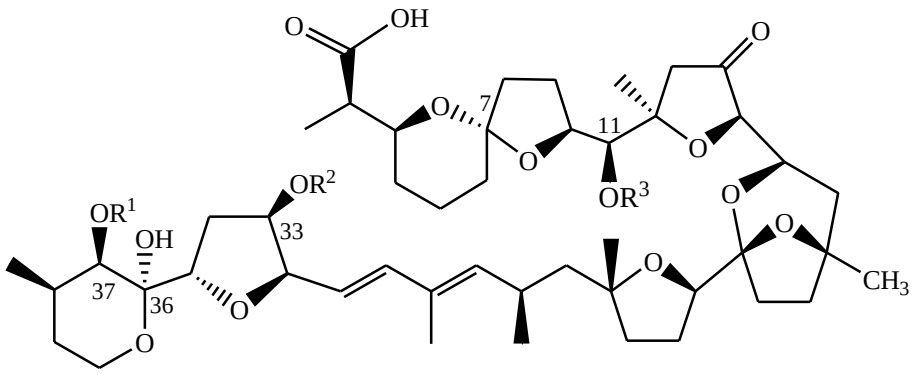

	R^1	R^2	R^3	C-7 Stereochemistry
PTX-2SA (**6a**)	H	H	H	*R*
7-*epi*-PTX-2SA (**6b**)	H	H	H	*S*
37-*O*-Acyl PTX-2SA (**7**)	Fatty acid ester	H	H	
33-*O*-Acyl PTX-2SA (**8**)	H	Fatty acid ester	H	
11-*O*-Acyl PTX-2SA (**9**)	H	H	Fatty acid ester	

Figure 1-3: Structures of PTX-2SA and its fatty acid ester analogues.

The point of predominant attachment of the dominant esters was tentatively found from a combination of LCMS and periodate reaction data. Mass spectral data showed that the ester group was not attached to C-11, since an *m/z* 551 ion was seen in the MS^2 MNH_4^+ mass spectra of the dominant 14:0, 16:0, 16:1, 18:4, 22:5 and 22:6 esters (as in the corresponding spectra of PTX-2 and PTX-2SA).

Treatment of PTX-2SA cleaves the carbon-carbon bond between the vicinal 36,37-diol portion of the PTX-2SA skeleton. This affords oxidised analogues

containing a 37-aldehyde group and a 36-keto group (**10, 11**). The structures of **10** and **11** were verified using NMR and MS^n LCMS data. NMR spectroscopy confirmed the formation of an aldehyde containing product. The NMR data was acquired by monitoring signals generated in a small scale reaction of PTX-2 with $NaIO_4$ in CD_3OD over several hours[20]. The MNa^+ MS^2 mass spectra of **10** and **11** included a daughter ion attributable to the loss of $HC(=O)CH(CH_3)\text{-}CH=CH_2$.

Since the dominant 14:0, 16:0, 16:1, 18:4, 22:5 and 22:6 esters did not react with sodium periodate (and MNH_4^+ MS^2 mass spectral data excluded C-11 substitution), it was concluded that the dominant esters were acylated at either C-36 (a tertiary carbon) or C-37 (a secondary carbon). Quantities of two of the dominant esters sufficient for NMR analyses were isolated and C-37 acylation (rather than C-36 acylation) was established[20].

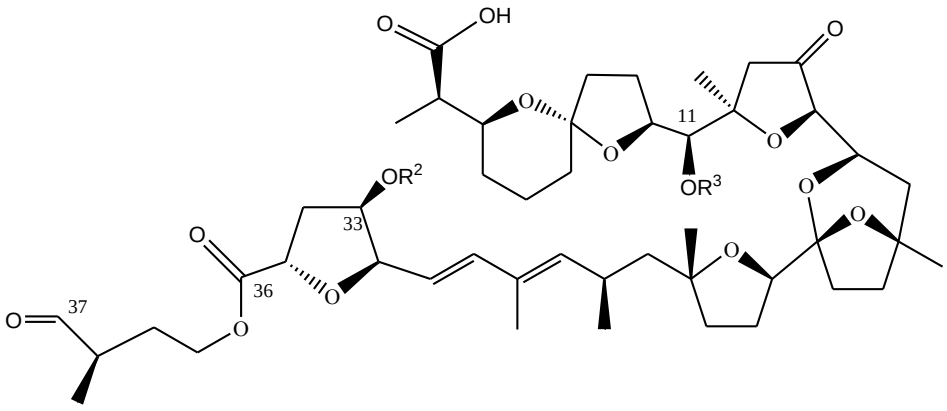

	R^2	R^3
IO_4^- oxidised 33-*O*-acyl PTX-2SA (**10**)	Fatty acid ester	H
IO_4^- oxidised 11-*O*-acyl PTX-2SA (**11**)	H	Fatty acid ester
IO_4^- oxidised PTX-2SA (**12**)	H	H

Figure 1-4: Structure of IO_4^- oxidised PTX-2SA and its fatty acid derivatives as confirmed by mass and NMR spectral analysis.

1.2 Okadaic acid analogues

Okadaic acid (OA) (**13**) is a toxin which has caused many shellfish poisonings around the world. It was first isolated and reported in 1981[21]. It was isolated from two marine sponges – one from Japan and one from the Caribbean near Florida and named after the Japanese sponge from which it was first isolated *Halichondria okadai.*

A variety of analogues of OA including, DTX-1 (**14**)[22], DTX-2 (**15**)[23], DTX-3 (**16**)[24] are now known. DTX-3 is not a single compound but rather a complex mixture of 7-*O*-acyl fatty acid ester analogues of OA, DTX-1 and DTX-2 which are produced by bivalves that metabolise OA, DTX-1 and DTX-2 into the various DTX-3 compounds[14, 24, 25].

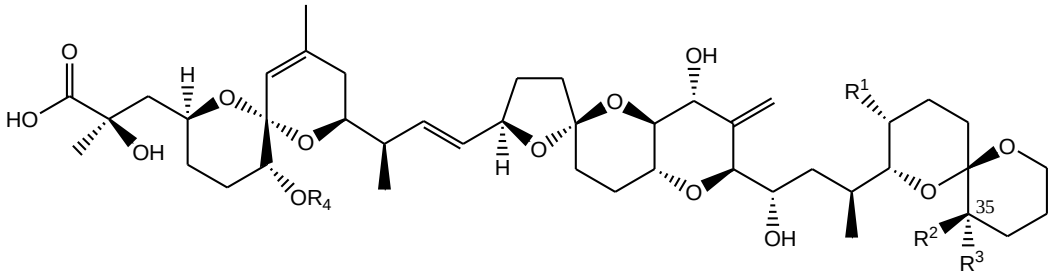

	R^1	R^2	R^3	R^4
OA (**13**)	CH_3	H	H	H
DTX-1 (35*R*) (**14**)	CH_3	CH_3	H	H
DTX-2 (35*S*) (**15**)	H	H	CH_3	H
DTX-3 (**16**)	CH_3	H	H	Fatty Acid Ester

Figure 1-5: Structures of okadaic acid and its dinophysistoxin derivatives.

Collectively, the group of toxins is known as the okadaic acid group of toxins. They are effective toxins because of their ability to inhibit protein phosphatases[26] which causes inflammation of intestinal tract and diarrhoea[27]. Tumour promoting activity has also been reported for OA and DTX-1[28].

Originally it was believed that DTX-1 and DTX-2 possessed the same C-35 stereochemistry, however it is now known that DTX-1 and DTX-2 possess opposite C-35 stereochemistries. The absolute configuration at C-35 is *R*- in DTX-1 and *S*- in DTX-2[29]. The difference in the C-35 configuration explains the differing protein phosphatase inhibitory activity between DTX-1 and DTX-2. Studies have also shown that if either the carboxyl group or all of the OH groups present are methylated, their ability to inhibit protein phosphatases is reduced[30]. Base hydrolysis at 78°C using a methanolic NaOH solution typically converts DTX analogues to OA[31].

A series of 'diol/triol-esters' of OA have also been reported in which conjugation of the carboxyl group of OA occurs with an unsaturated diol/triol[13, 32-35]. The structures of some of the diol/triol esters are represented in Figure 1-6. These compounds were mostly detected and isolated from cultures of *Prorocentrum* spp. such as *Prorocentrum lima*. One of the isolated C_8-diol esters was shown to be able to be hydrolysed to OA by enzymes in the hepatopancreas of *Perna canaliculus* (New Zealand green-lipped mussels)[36]. Recently some new 'diol-esters' have been reported along with a series of hybrid diol/triol fatty acid esters (mainly the 16:0 fatty acid ester analogues)[37].

Currently the regulatory method for OA/DTX group toxins is based on the levels of these compound present in extracts after base hydrolysis.

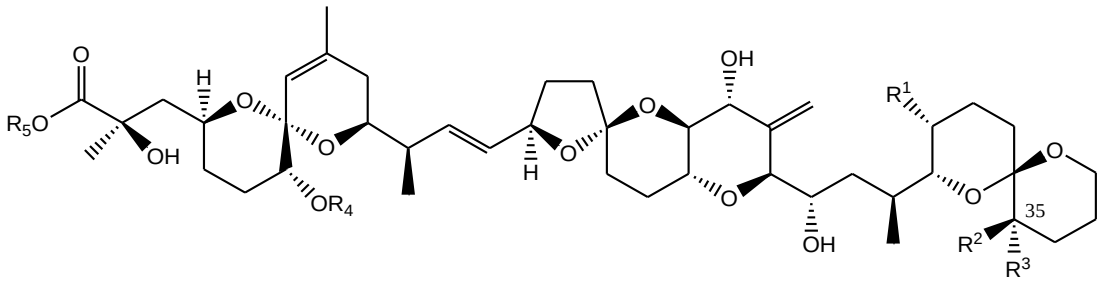

	R^1	R^2	R^3	R^4	R^5	Reference
C_4-diol OA	CH_3	H	H	H	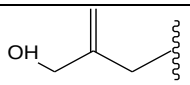	32
C_6-diol OA	CH_3	H	H	H	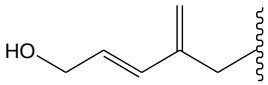	35
cis-C_7-diol OA	CH_3	H	H	H	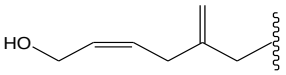	17
C_7-diol OA	CH_3	H	H	H	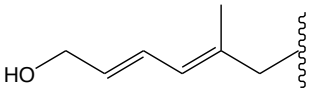	33
C_8-diol OA	CH_3	H	H	H	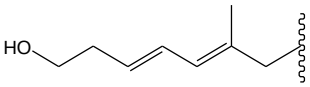	33
cis-C_8-diol OA	CH_3	H	H	H	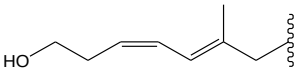	13
C_9-diol OA	CH_3	H	H	H	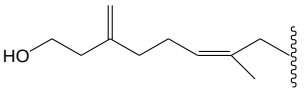	17
C_9-diol OA	CH_3	H	H	H	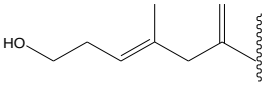	33
C_9-diol OA	CH_3	H	H	H	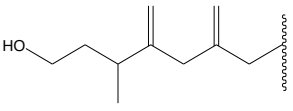	34
C_9-triol OA	CH_3	H	H	H	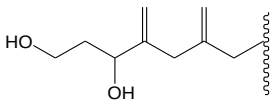	35
C_{10}-diol OA	CH_3	H	H	H	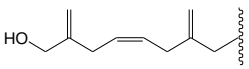	35

Figure 1-6: Structures of some esters of okadaic acid.

Chapter 2

Experimental Conditions and Methods

2.0 Experimental conditions

General experimental directions and factors which influenced the choice of specific instrumental settings are reported and where appropriate is discussed (e.g. the influence of the LCMS capillary temperature) in this Chapter.

2.1 General directions

Chemicals

HPLC grade solvents (MeOH, MeCN), Milli-Q H_2O and analytical grade reagents (NH_4COOH, HCOOH) were used for all LCMS analysis.

New Zealand Samples

Three crude algal water extracts supplied by Dr C. O. Miles, AgResearch Ruakura were used for the New Zealand investigation. The three samples were sourced from the South Island of New Zealand by Lincoln MacKenzie and Veronica Beuzenberg (Cawthron Institute) from three separate locations in 2001[8]. Sample 1A/1B was obtained from Buller Bay, West Coast on the 2/2/2001 and contained *Dinophysis acuta*. Sample 2A/2B was obtained from Akaroa Harbour on the 27/11/2001 and contained *Dinophysis acuminata*. Sample 3A/3B was obtained from Carters Beach, West Coast on the 21/1/2001 and contained *Dinophysis acuta*. Samples 1A/1B and 2A/2B were taken from various depths within the water column and Sample 3A/3B was taken by a surface tow method[8].

W8 Vigo (Spain) Algal Water Sample

The W8 Vigo (Spain) water sample, collected on the 12/12/05 from a *Dinophysis* acuta bloom, was supplied by the National Veterinary Institute, Oslo. The algal water

sample had previously been extracted with Et_2O and CH_2Cl_2 and stored in a refrigerator. LCMS data for the sample was determined by Professor Wilkins (in Oslo) and forwarded to New Zealand for detailed analysis.

2.2 Sample preparation (New Zealand samples)

Crude algal water extracts (as above) were prepared for analysis by passing each extract (50 mL) through solid phase extraction Strata X 33 μL polymetric sorbent (8B-S100-HCH, 500 mg/6 mL) columns on an Alltech vacuum SPE manifold. The columns were prewashed with MeOH (10 mL) followed by Milli-Q H_2O (10 mL). Glass wool was added to the top of the column to assist with filtration. The sample (50 mL) was loaded and eluted with H_2O (10 mL) followed by MeOH (10 mL) and the filtrate was made up in a volumetric flask with MeOH (25 mL). Extracts were stored at -20^oC until required for analysis. A sub-sample of each of the extracts was used for LCMS analysis.

Full scan MS and UV plots determined for each of the New Zealand extracts, acquired as described below using the LCQ-Duo instrument shown and a detailed discussion of the data determined for these samples appears in Chapters 3, 4 and 5.

2.3 LCMS analyses

Combined LC-UV-MS was performed at Waikato University using a Thermo-Finnigan LCQ-Duo instrument running under Xcalibur 1.2 software or the National Veterinary Institute, Oslo using an LTQ instrument running under Xcalibur 1.4 software. Some analysis (e.g. okadaic acid analyses: see below) were also performed using an LCQ classic instrument available at the National Veterinary Institute, Oslo. Detailed analyses of Oslo LCMS data (acquired in Oslo by Professor Wilkins during a 3 month secondment to the National Veterinary Institute), was carried out in New Zealand. Greater MS sensitivity was obtained using the LTQ instrument. MS^n

analyses were typically performed using collision energy (CE) settings of 30% for MNH_4^+ and 55% for MNa^+ ions, and fragment ions derived from these ions.

2.3.1 LCQ-Duo analyses

Separations were achieved using a 5 µm Phenomenex Prodigy ODS column (2.0 x 150 mm) which was typically eluted with a linear gradient from 30% MeCN/H_2O to 100% MeCN over 20 min, with a 10 min hold and a flow rate of 300 µL/min. Both mobile phases contained NH_4COOH (2 mM) and 0.05% HCOOH (v/v).

Typical instrument settings were:

Capillary interface temperature	250˚C
UV	220-600 nm
MS modes	Positive and negative
Mass range	*m/z* 400-1500
Spray Voltage	5.5 kV
Capillary Voltage	23 V Positive ion mode
	-25 V Negative ion mode
Lens Tube	50 V Positive ion mode
	-40 V Negative ion mode

2.3.2 LTQ analyses

Separations were achieved using a 3.5 µm Waters Symmetry C18 column (2.1 × 50 mm) which was typically eluted with a linear gradient from 30% MeCN/H_2O to 100% MeCN over 20 min, with a 10 min hold and a flow rate of 250 µL/min. Both mobile phases contained NH_4COOH (2 mM) and 0.1% HCOOH (v/v).

Typical instrument settings were:

Capillary interface temperature	250˚C

UV	220-600 nm
MS modes	Positive and negative
Mass range	*m/z* 400-1500
Spray Voltage	4.5 kV
Capillary Voltage	35 V Positive
	-20 V Negative
Lens Tube	50 V Positive
	-40 V Negative

2.3.3 LCQ-Classic analyses

Separations were achieved using 3.5 µm Waters Symmetry C18 column (2.1 × 50 mm) which was typically eluted with a with linear gradient from 30% MeCN/H_2O to 100% MeCN over 20 min, with a 10 min hold and a flow rate of 250 µL/min. Both mobile phases contained NH_4COOH (2 mM) and 0.05% HCOOH (v/v).

Typical instrument settings were:

Capillary interface temperature	150-250˚C
MS modes	Positive
Mass range	*m/z* 750 - 1200

2.4 High resolution mass spectral analyses

A recent Irish mussel extract, supplied by Dr C. O. Miles, was analysed using a high resolution Bruker Daltronics MicrOTOF spectrophotometer. The sample was infused via a Cole-Parmer syringe pump at 3 µL/min. The default instrument settings were used along with a nitrogen gas flow of 5 L/min, detector voltage 1000 V and a dry temperature of 200˚C.

2.5 Evaluation of the significance of the capillary interface temperature

During the course of the LCMS investigations reported in this thesis, it emerged that the detection (or not) of the MNH_4^+ ion of okadaic acid when using the LCQ-Duo instrument, but not the LTQ instrument, was strongly dependent on the choice of the capillary interface temperature. This observation prompted an evaluation of the significance of capillary temperature over the range of 150-250^{o}C using the LCQ-Duo instrument at Waikato University and the LCQ Classic instrument at the National Veterinary Institute, Oslo. This thermal degradation on the two LCQ instruments was found to only occur for the MNH_4^+ ions of OA and its derivatives. This thermal degradation did not occur for the MNH_4^+ ions of PTX-2 or PTX-2SA or for the MNa^+ ions of any of the PTXs or OA and its derivatives on the two LCQ instruments. The LTQ instrument, when operated with a capillary temperature of 250°C was not prone to thermal degradation problems.

A graphical representation of the effect of the capillary temperature on the ratio of the MNH_4^+ ions to the MNa^+ ions on the Waikato University LCQ-Duo MS system is presented in Figure 2-7. Too low a capillary temperature appears to limit the passage of ions through the inlet capillary tube while too high a temperature results in thermal degradation of MNH_4^+, but not MNa^+ ions, during their passage through the capillary tube.

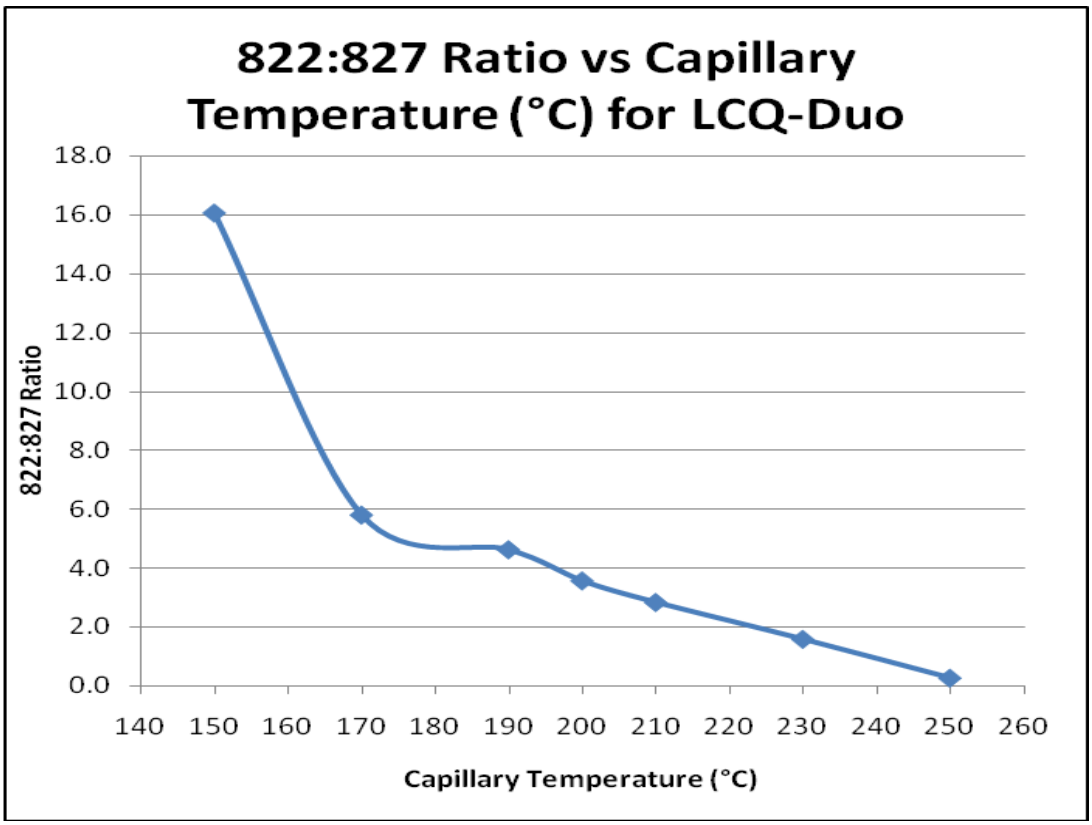

Figure 2-7: Capillary temperature vs. *m/z* 822:*m/z* 827 MNH_4^+:MNa^+ ratio determined for okadaic acid using the Waikato University LCQ-Duo LCMS system.

Chapter 3

MS^n Characterisation of a New Series of Modified Pectenotoxin Analogues

3.0 Introduction

Pectenotoxin-2 (PTX-2) (**1**) and pectenotoxin-2 seco acid (PTX-2SA) (**6a**), along with okadaic acid (OA) (**13**), dinophysistoxin-1 (DTX-1) (**14**) and dinophysistoxin-2 (DTX-2) (**15**) can be present in mussel and algal samples worldwide. PTX-2 (**1**) is the most common pectenotoxin found in *Dinophysis* algal extracts while its hydrolysed analogue, PTX-2SA (**6a**), is the most common pectenotoxin in mussel derived samples. PTX-2 has, for example, been identified in *Dinophysis acuta* in New Zealand, Norway, Spain and Ireland[2-7], *Dinophysis acuminata* in Norway and New Zealand[5, 8], *Dinophysis caudata* from Spain[7], *Dinophysis rotundata* from Norway[5] and *Dinophysis fortii* from Japan and Italy[9-11].

In our laboratories (AgResearch, Ruakura, The University of Waikato and the National Veterinary Institute, Oslo) extracts containing PTX-2, PTX-2SA, OA, DTX-1 and/or DTX-2 are routinely examined for presence of new, unreported analogues of these and other known algal toxins. This approach has lead to the identification of several new analogues of these compounds, including PTX-6[17] (**3**), PTX-11[18] (**4**) and PTX-13[19] (**5**) and fatty acid esters of PTX-2SA (**7- 9**)[20].

LCMS analyses of bulk Irish mussel extracts that were originally utilised to isolate azaspiracid analogues, showed that they also contained elevated levels of PTX-2, PTX-2SA, OA and DTX-2. Hitherto a series of PTX-2SA and 7-*epi*-PTX-2SA esters have been isolated from these extracts[20]. These extracts were utilised to secure a quantity of DTX-2 that enabled a detailed one and two dimensional NMR analyses to be performed on this compound. This study[29] clarified the difference in the C-35

stereochemistry between DTX-2 and DTX-1 and showed that they do not have the same C-35 stereochemistry as originally reported in the literature[24].

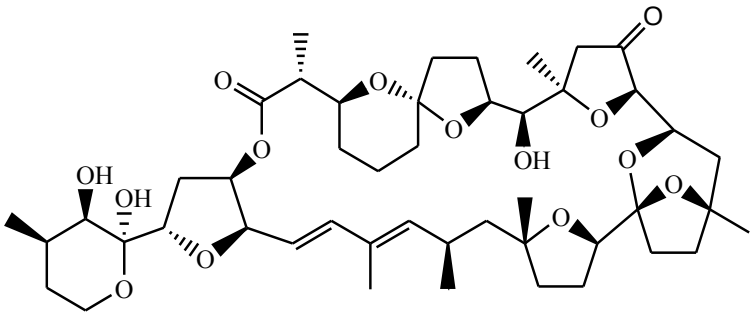

PTX-2 (**1**)

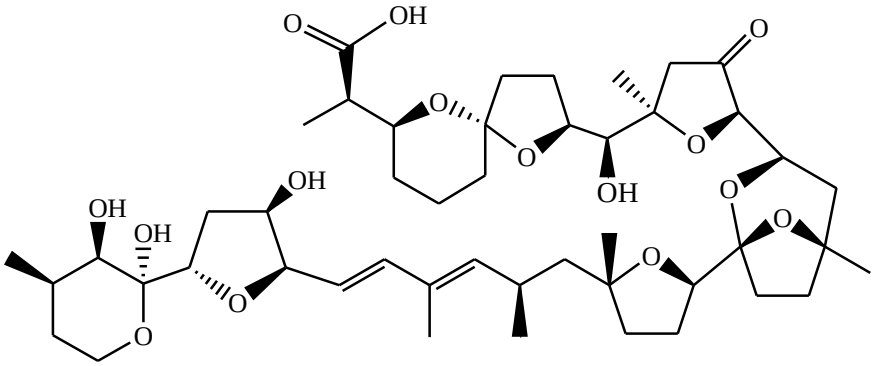

PTX-2SA (**6a**)

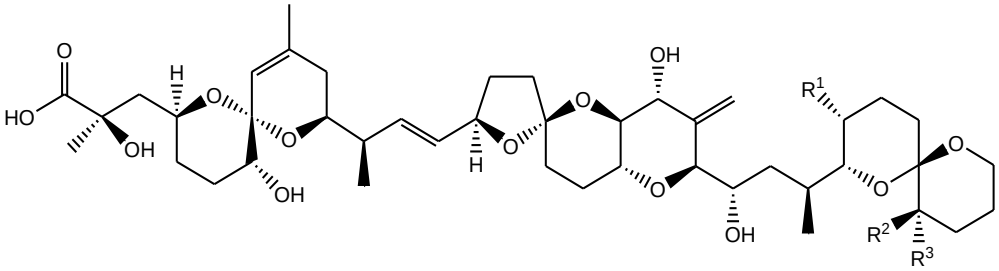

	R^1	R^2	R^3
OA (**13**)	CH_3	H	H
DTX-1 (35*R*) (**14**)	CH_3	CH_3	H
DTX-2 (35*S*) (**15**)	H	H	CH_3

Figure 3-1: Chemical structures of some pectenotoxins and okadaic acid analogues.

Subsequent to the DTX-2 investigation, an LCMS analyses of some retained (stored) sub-samples of the bulk Irish extracts showed that they also possessed moderate levels of some other compounds that (at least in part) exhibited PTX-2 like MS^n mass spectra.

This chapter reports the first detection and MS^n characterisation of a PTX-like compound which was designated as PTX-i (i.e. an isomeric form of a PTX-type compound) and a series of analogues of this compound, in sub-samples of processed bulk extracts of the Irish mussel extracts.

The intention of these investigations was to derive as much structural information as possible from mass spectral methods alone in the expectation that this information would contribute to defining the essential structural features of the new PTX-i compound prior to a sufficient quantity of it being isolated and its structure being unequivocally defined using more advanced methods such as one and two-dimensional NMR and high resolution MS.

It was also anticipated that the initial ion trap LCMS investigation would provide information that could be used to develop higher sensitivity analytical methods such as triple quad SRM methods to detect the PTX-i compound and related analogues in extracts of other mussel and algal water extracts from around the world.

3.1 MS^2 and MS^3 analyses of PTX-2 and PTX-2SA

In our laboratories, LCMS analyses of mussel and algal water extracts are typically performed using a C-18 reverse phase column and NH_4COOH/HCOOH/MeCN-H_2O mixtures. Under these conditions, pectenotoxins characteristically afford MNH_4^+ and MNa^+ ions of parent compounds in positive ion mode, and either $[M-H]^-$ or $[M+X]^-$ (X = COOH) in negative ion mode.

Under ESI-ion trap LCMS conditions, elution of PTX containing mixtures from a reverse phase column using a H_2O-MeCN gradient with 0.02 mM NH_4COOH and HCOOH (0.1% (v/v) (LTQ analysis) or 0.05% (v/v) on (LCQ-Duo analysis) added to each of the eluent phases typically affords a 1:1 ratio of MNH_4^+ and MNa^+ ions due to the presence of a significant background level of Na ions in solvents used to elute components and/or desorbed from surfaces in the MS environment. The bulk of the literature concerning the MS fragmentation of PTX-2 and its analogues describes the fragmentation of MNH_4^+ ions determined using either ion trap or triple-quad mass spectrometers, presumably because they can be fragmented under relatively mild conditions (e.g. 25-30% collision energy using a Thermo-Finnagin LCQ or LTQ series MS instruments). Higher collision energies (of the order 50-60%) are required to fragment MNa^+ ions.

3.1.1 MS^2 analyses of the *m/z* 876 $[PTX\text{-}2+NH_4]^+$ ion

Figure 3-2 shows the MS^2 mass spectrum of the *m/z* 876 ion which corresponds to the MNH_4^+ ion of PTX-2. When a collision energy (CE) in the range 25-30% is used, the dominant ions observed are those attributable to the loss of NH_4OH (or NH_3 and H_2O) and a subsequent series of H_2O losses[38]. These losses afford ions which occur at *m/z* 841 $[MNH_4^+\text{-}NH_4OH]^+$, *m/z* 823 $[MNH_4^+\text{-}NH_4OH\text{-}H_2O]^+$, *m/z* 805 $[MNH_4^+\text{-}NH_4OH\text{-}2H_2O]^+$, *m/z* 787 $[MNH_4^+\text{-}NH_4OH\text{-}3H_2O]^+$ and *m/z* 769 $[MNH_4^+\text{-}NH_4OH\text{-}4H_2O]^+$ respectively.

Figure 3-3 shows an expanded view of the lower mass region of the *m/z* 876 MNH_4^+ MS^2 mass spectrum. Low intensity *m/z* 551, 457 and 439 ions are apparent in the expanded MS^2 mass spectrum. The *m/z* 551, 457 and 439 daughter ions have been reported[6, 38] to arise from cleavages across the lower left hand portion of the PTX-2 skeleton as depicted in Figure 3-4.

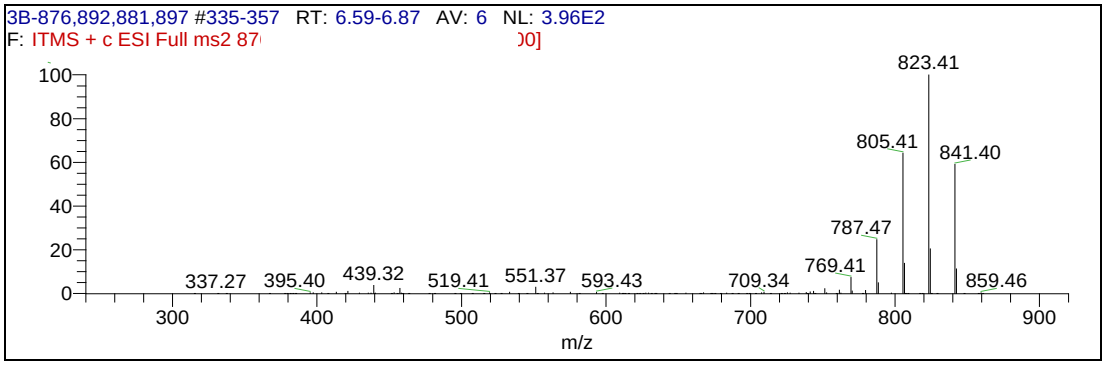

Figure 3-2: MS^2 mass spectrum of the *m/z* 876 ion MNH_4^+ ion of PTX-2.

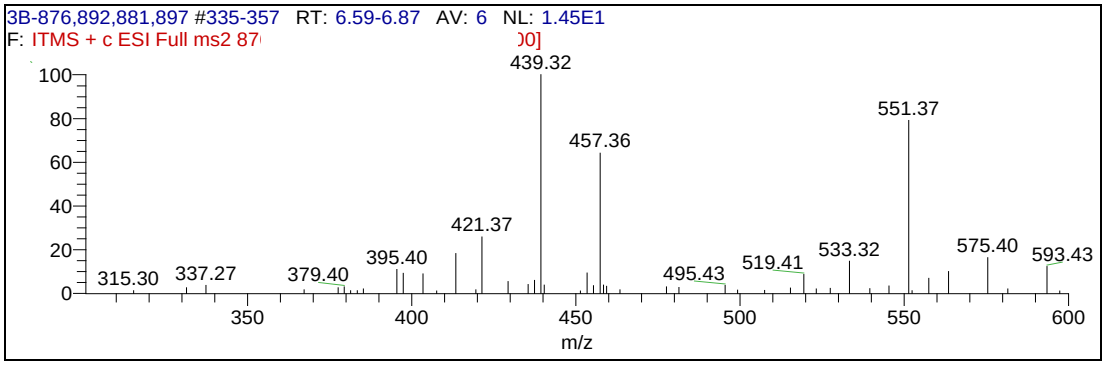

Figure 3-3: Expanded low mass range of the *m/z* 876 MNH_4^+ MS^2 mass spectrum of PTX-2.

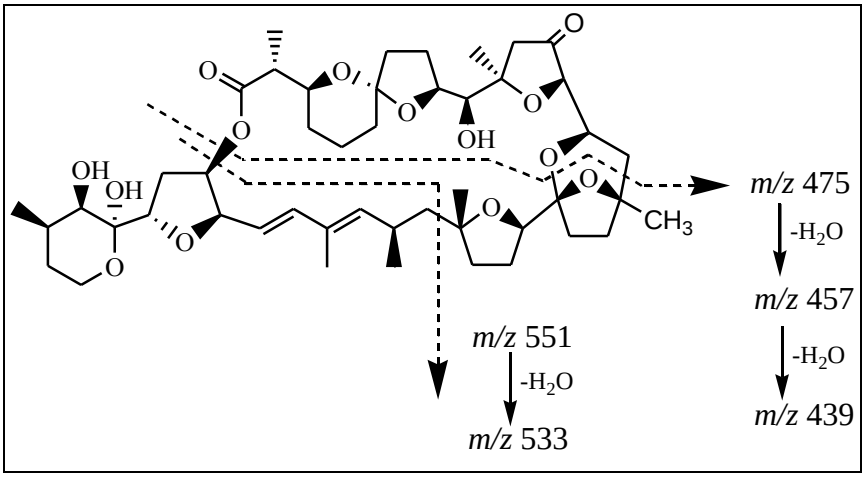

Figure 3-4: Scheme showing the proposed origin of some ions seen in the MNH_4^+ MS^2 mass spectrum of PTX-2.

3.1.2 MS^2 and MS^3 analyses of the *m/z* 881 $[PTX\text{-}2+Na]^+$ ion

Figure 3-5 shows the MS^2 and MS^3 mass spectra of the *m/z* 881 MNa^+ ion of PTX-2 determined with a CE of 55%. The MS^2 mass spectrum showed a daughter ion at *m/z* 837 attributable to the loss of CO_2 (Figure 3-5). The MS^3 mass spectrum of the *m/z* 837 daughter ion afforded an *m/z* 819 ion attributable to the loss of H_2O from the 837 ion and an *m/z* 539 ion attributable to the loss of 298 Da from the *m/z* 837 ion. This loss can be attributed to the loss of the upper portion of the PTX-2 skeleton as depicted in Figure 3-6

It is of note that for pectenotoxins such as PTX-2, a greater CE (50-60%) is required to fragment the MNa^+ ion compared to that (25-30%) required to fragment the MNH_4^+ ion. Two major advantages of MS^2, MS^3 or MS^4 MNa^+ ion data, compared to MNH_4^+ MS^2 data are:

i) the absence (in general) of a series of H_2O loss fragment ions.

ii) fragmentation to afford a limited number of high intensity structurally significant ions.

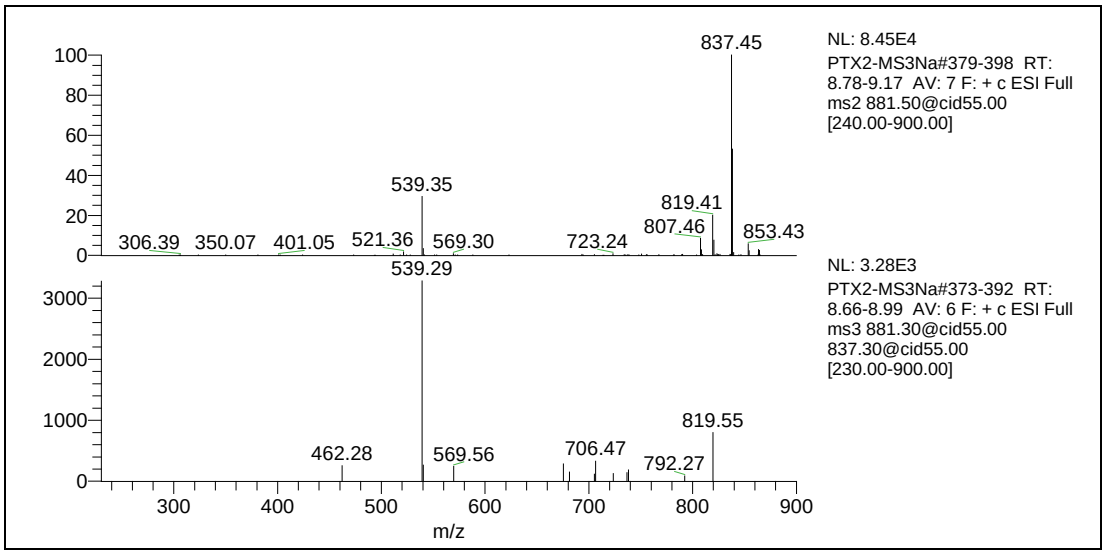

Figure 3-5: MNa^+ MS^2 (*m/z* 881) (upper) and MS^3 (*m/z* 881 → *m/z* 837) (lower) mass spectra determined for PTX-2.

The finding that MNa^+ and MNH_4^+ ions behave differently under ESI MS^n conditions can be attributed to the differing stabilities of the MNH_4^+ and MNa^+ ions.

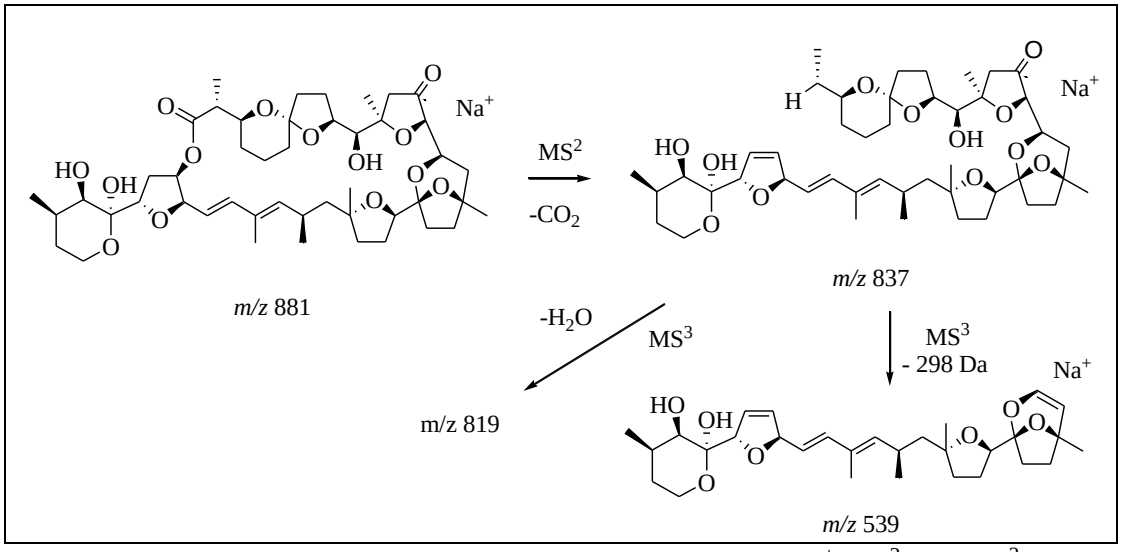

Figure 3-6: Proposed structures for some ions seen in the MNa^+ MS^2 and MS^3 mass spectra of PTX-2.

3.2 MS^2 and MS^3 analyses of PTX-2SA

The following section provides information on the fragmentation of PTX-2SA MNH_4^+ and MNa^+ ions.

3.2.1 MS^2 analyses of the *m/z* 894 $[PTX\text{-}2SA+NH_4]^+$ ion

The MS^2 mass spectrum of the *m/z* 894 $[PTX\text{-}2SA+NH_4]^+$ ion is shown in Figure 3-7. An expansion of the lower mass region is shown in Figure 3-8. The fragmentation pattern seen is reminiscent of that observed for PTX-2. In particular, the dominant ions in the MS^2 mass spectrum of PTX-2SA are those attributable to the loss of NH_4OH (or NH_3 and H_2O) and a subsequent series of H_2O losses. These losses afford ions which occur at *m/z* 859 $[MNH_4^+\text{-}NH_4OH]^+$, *m/z* 841 $[MNH_4^+\text{-}NH_4OH\text{-}H_2O]^+$, *m/z* 823 $[MNH_4^+\text{-}NH_4OH\text{-}2H_2O]^+$ and *m/z* 805 $[MNH_4^+\text{-}NH_4OH\text{-}3H_2O]^+$. The *m/z* 551, 457 and 439 daughter ions, as seen in the expanded MS^2 mass spectrum

of PTX-2SA (Figure 3-8), were previously also seen in the MS^2 mass spectrum of PTX-2 (Figure 3-2).

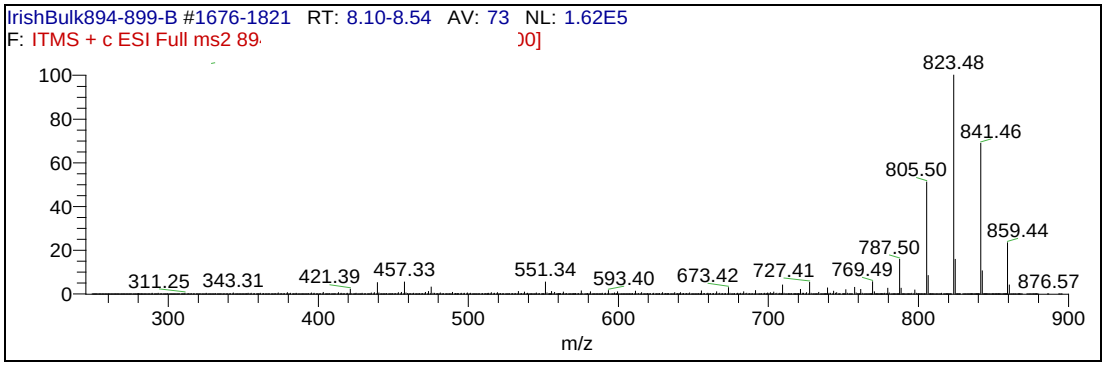

Figure 3-7: MS^2 mass spectrum of the *m/z* 894 $[PTX\text{-}2SA+NH_4]^+$ ion.

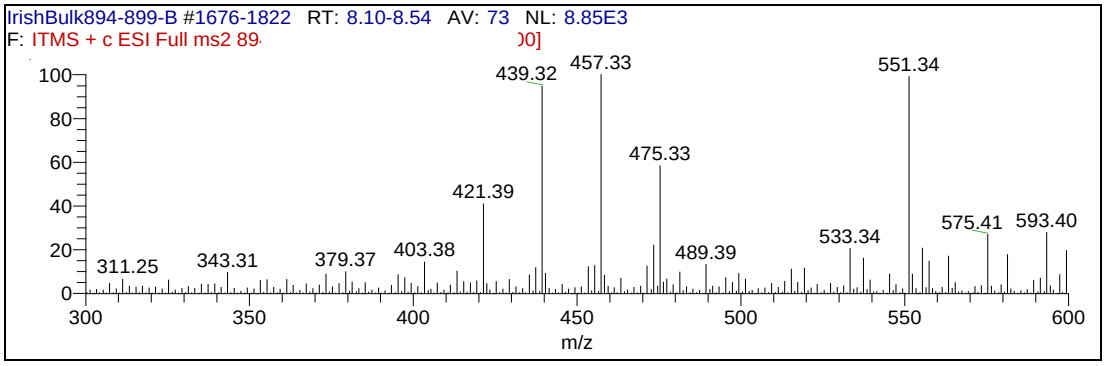

Figure 3-8: Expanded low mass region of the MS^2 mass spectrum of the *m/z* 894 $[PTX\text{-}2SA+NH_4]^+$ ion.

3.2.2 MS^2 analyses of the *m/z* 899 $[PTX\text{-}2SA+Na]^+$ ion

The MS^2 mass spectrum of the *m/z* 899 MNa^+ ion of PTX-2SA is shown in Figure 3-9. The strong *m/z* 855 ion can be attributed to the loss of CO_2 while the lower intensity daughter ion at *m/z* 557 can be attributed to the loss of the upper portion of the PTX-2SA molecule (a 342 Da loss) from the parent MNa^+ ion as depicted in Figure 3-10, or the loss of a 298 Da from the *m/z* 855 ion in a manner analogous to that seen in the MS^2 and MS^3 mass spectra of PTX-2.

Under MS^3 conditions, fragmentation of the *m/z* 855 daughter ion of PTX-2SA afforded an *m/z* 557 ion. Extracts containing PTX-2SA invariably also contain significant levels of 7-*epi*-PTX-2SA. The MNa^+ MS^2 and MS^3 mass spectra of this pair of compounds were essentially identical[2].

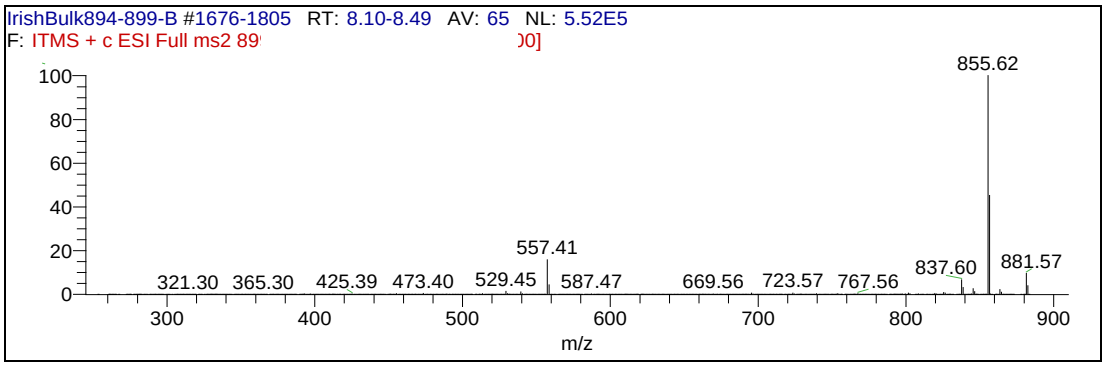

Figure 3-9: MS^2 mass spectrum of the MNa^+ ion (*m/z* 899) of PTX-2SA.

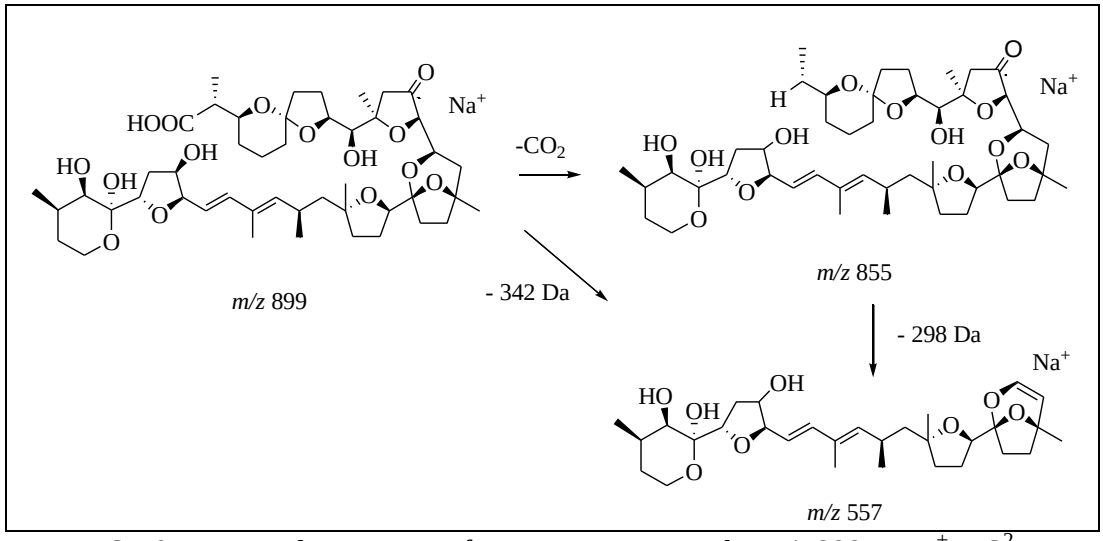

Figure 3-10: Proposed structures of some ions seen in the *m/z* 899 MNa^+ MS^2 mass spectrum of PTX-2SA.

3.3 The '864/869' compounds

The following section describes the detection and mass spectral analysis of the '864/869' group of compounds.

3.3.1 Introduction

Systematic analyses of full scan positive ion LCMS data determined for sub-samples of the bulk Irish extract that had previously been found to contain a series of PTX-2SA esters, revealed the presence of several early eluting peaks that exhibited a pair of ions at *m/z* 864 and 869 attributable to MNH_4^+ and MNa^+ ions respectively. These ions correspond to a compound of a molecular weight of 840 Da.

Since the Irish extracts were known to contain appreciable levels of compounds with molecular weights in the region 800-900 Da, including OA, DTX-2, PTX-2 and PTX-2SA, the possibility that the early eluting substances might be analogues of one of the foregoing algal toxins was investigated.

A comparison of the chromatograms showing the peaks and their RT relative to each other is shown by Figure 3-11. The major PTX-i peak elutes earlier than the peaks arising from the other known compounds.

A preliminary examination of the MS^2 mass spectra determined for the presumed *m/z* 864 MNH_4^+ and *m/z* 869 MNa^+ ions of the new compounds indicated them to be PTX-2 like compounds. The compounds are henceforth referred to as PTX-i analogues. The MNH_4^+ and MNa^+ MS^n data determined for the dominant '864/869' is presented in Sections 3.3.2 and 3.3.3 below.

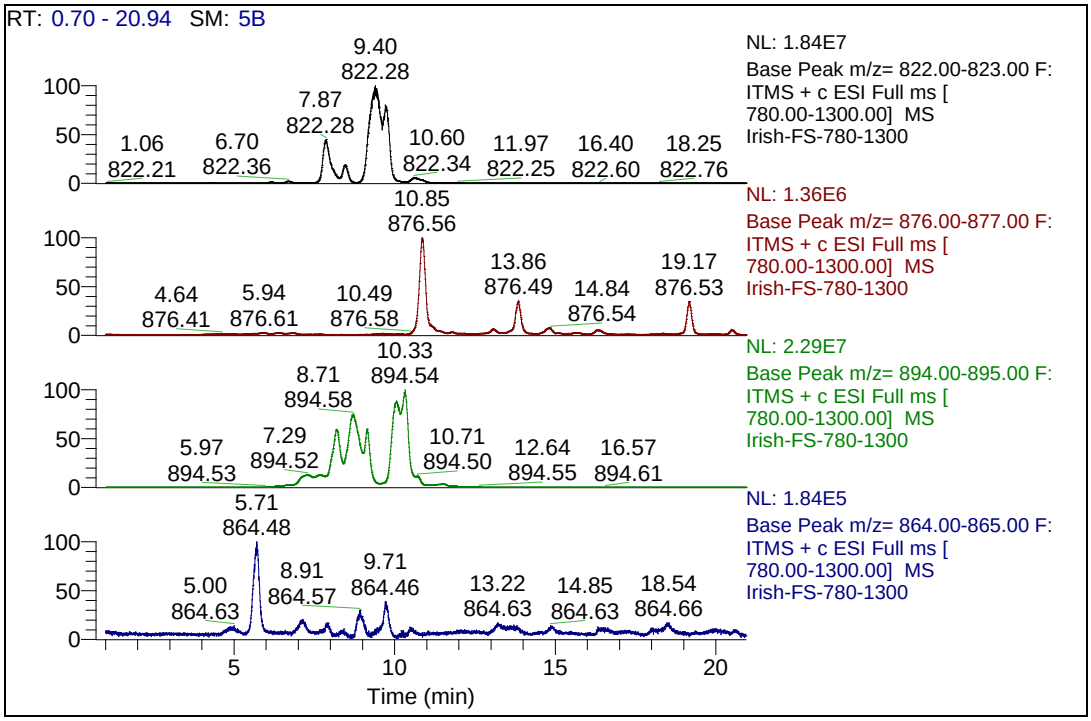

Figure 3-11: Extracted ion chromatograms comparing peak retention times of *m/z* 822 (OA MNH_4^+) (top), *m/z* 876 (PTX-2 MNH_4^+) (upper middle), *m/z* 894 (PTX-2SA MNH_4^+) (lower middle) and the *m/z* 864 compound (bottom).

3.3.2 MS^2 analyses of *m/z* 864 MNH_4^+ ion of PTX-i compounds

The MS^2 mass spectrum determined for the dominant earliest eluting peak which showed an *m/z* 864 MNH_4^+ ion is shown in Figure 3-12. This mass spectrum was reminiscent of MS^2 mass spectra determined for PTX-2 and PTX-2SA (Figure 3-2 and Figure 3-7 respectively).

The highest observed ion at *m/z* 847 can be attributed to the loss of NH_3 from a parent MNH_4^+ ion (*m/z* 864). A high intensity $[M\text{-}NH_4OH]^+$ ion was also observed at *m/z* 829, together with a series of subsequent H_2O loss ions (*m/z* 811, 793 and 775). These ions can be considered to arise from a substance that has a molar mass that is either 12 Da less than that of PTX-2 or 30 Da less than that of PTX-2SA.

Lower intensity *m/z* 681, 587, 551, 463, 445, 437 and 409 daughter ions were also observed in the MS^2 mass spectrum of the dominant early eluting PTX-i compound (Figure 3-13).

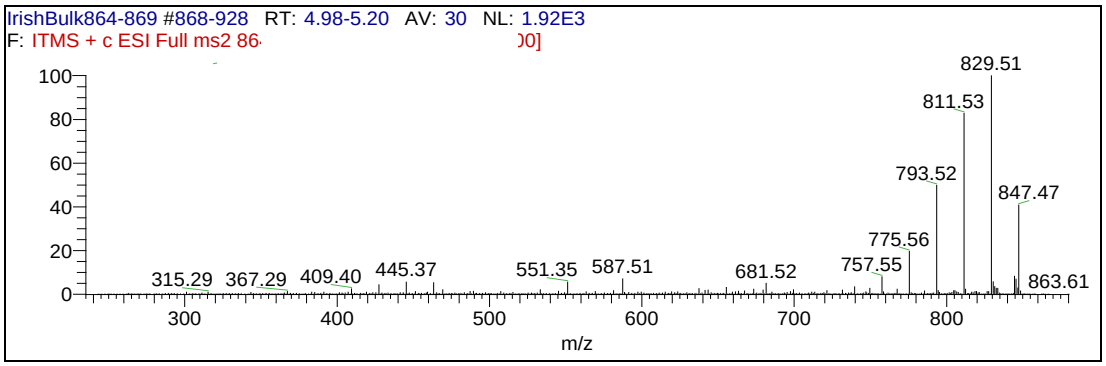

Figure 3-12: MNH_4^+ MS^2 mass spectrum of the dominant early eluting PTX-i peak.

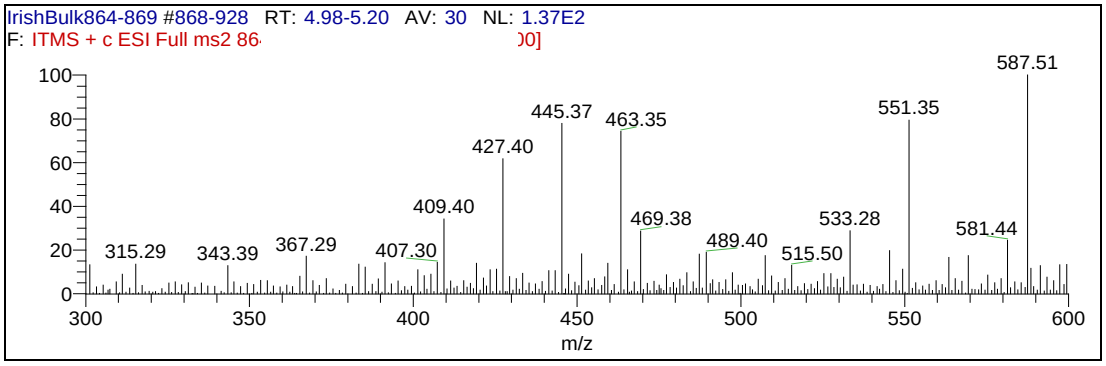

Figure 3-13: Expanded low mass region of the MNH_4^+ MS^2 mass spectrum of the dominant early eluting PTX-i peak.

The presence of a low intensity but readily detectable daughter ion at *m/z* 551 was consistent with the conclusion that the new compound possessed a modified PTX-2 or PTX-2SA like skeleton which retained the upper portion of the PTX-2 or PTX-2SA skeletons (Figure 3-14).

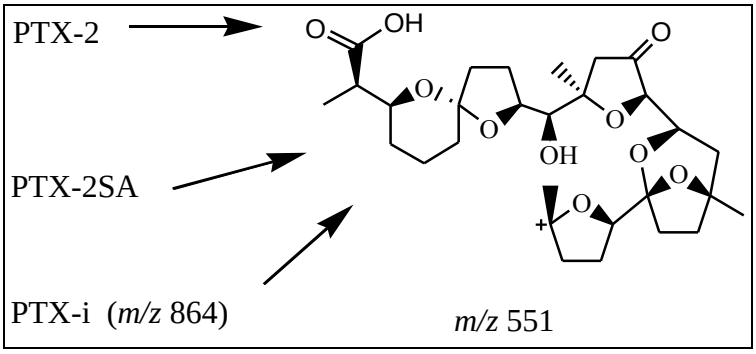

Figure 3-14: Scheme showing the proposed origin of the *m/z* 551 ion observed in the MNH_4^+ MS^2 mass spectra of PTX-2, PTX-2SA and the early eluting PTX-i compound.

On the other hand, the series of X-n(H_2O) ions which occurred at *m/z* 463, 445 and 437 can be viewed as arising from ions which are either 12 Da lower, or 6 Da higher than is case for the *m/z* 457, 439 and 421 ions seen in the MNH_4^+ MS^2 mass spectra of PTX-2 and PTX-2SA respectively. Low mass ions appearing in the *m/z* 280-740 region of the MNH_4^+ MS^2 mass spectra of the dominant early eluting PTX-i compound (top) and PTX-2 (middle) and PTX-2SA (bottom) are compared in Figure 3-15.

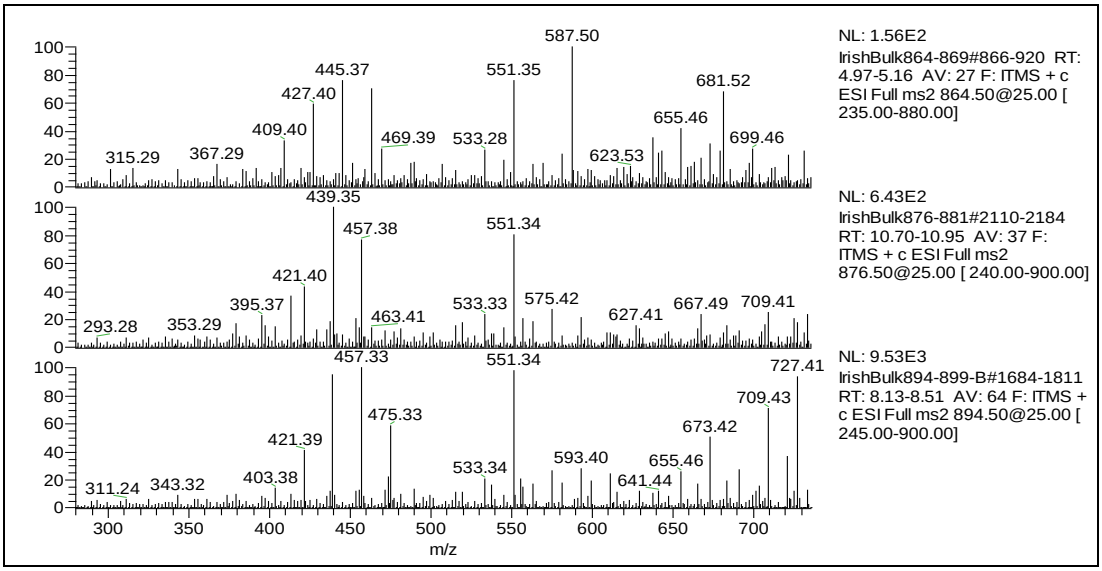

Figure 3-15: Comparison of daughter ions observed in the *m/z* 280-740 region of the MNH_4^+ MS^2 mass spectra of the dominant early eluting PTX-i compound (top), PTX-2 (middle) and PTX-2SA (bottom).

3.3.3 MS^2 analyses of the *m/z* 869 MNa^+ ion from the PTX-i compounds

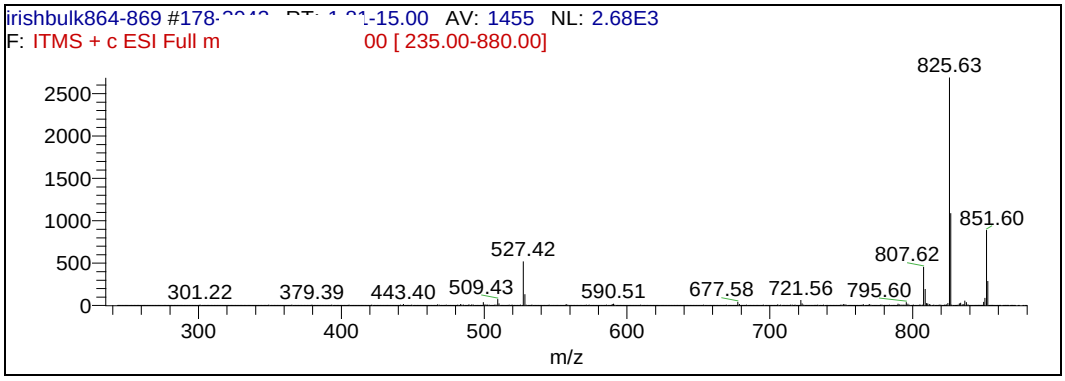

Figure 3-16: MNa^+ MS^2 mass spectrum of the dominant early eluting PTX-i peak.

The MS^2 mass spectrum of the presumed MNa^+ ion (*m/z* 869) of the dominant early eluting PTX-i compound is shown in Figure 3-16. The high intensity daughter ion which appeared at *m/z* 825 can be attributed to the loss of CO_2 as observed in the MS^2 MNa^+ mass spectra of PTX-2 and PTX-2SA. Less intense MS^2 fragment ions appeared at *m/z* 851 (H_2O loss from the MNa^+ ion), 807 (H_2O loss from the *m/z* 825 ion) and *m/z* 527. The latter ion can be attributed to the loss of the upper portion of a

PTX-2 or PTX-2SA like structure as a 342 Da residue or as a 298 Da residue after the prior loss of CO_2 (Figure 3-17). Equivalent 342 Da and/or 44+298 Da loss ions are seen in the MS^2 and MS^3 mass spectra of PTX-2 and PTX-2SA (refer to Sections 3.1 and 3.2 respectively).

Assuming the PTX-i compound was a PTX-2 like analogue rather than a PTX-2SA analogue (evidence confirming this was obtained at a later stage in the investigation: refer to Section 3.4), the MNH_4^+ and MNa^+ MS^n data thus far described is consistent with the presence in the dominant PTX-i compound of an intact PTX-2 like C-1 to C-36 structure and the attachment of a $C_5H_{11}O_3$ or a $C_4H_7O_4$ side chain to C-36, rather than the presence of a six membered hemiacetal ring as found for PTX-2 and PTX-2SA, as depicted in Figure 3-17.

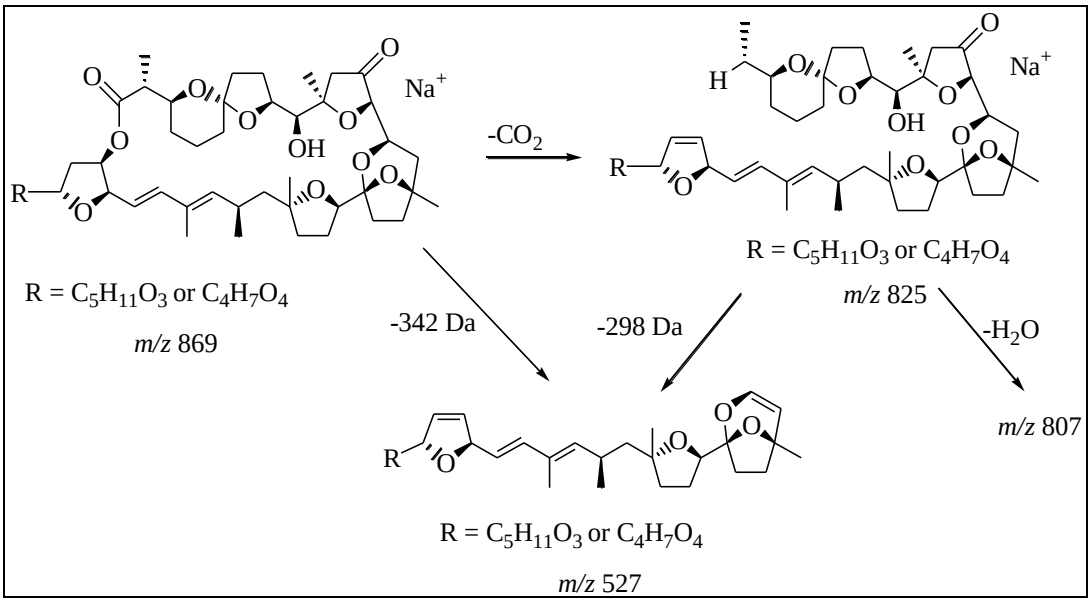

Figure 3-17: Scheme showing proposed origin of daughter ions in the *m/z* 869 MNa+ MS^2 mass spectrum of the dominant PTX-i compound.

A 12 Da difference between the molar mass of the new PTX-i compound (M = 846 Da, MNH_4^+ = *m/z* 864, MNa^+ = *m/z* 869) and that of PTX-2 (M = 858 Da, MNH_4^+ = 876, MNa^+ = *m/z* 881) can, for example, be accounted for by the absence of a CH_2 group (14 Da) and the inclusion of two additional hydrogen atoms by opening the

terminal hemiacetal system to afford a nor-seco-dihydro-PTX-2 analogue. Two such structures are depicted in Figure 3-18.

Another option would be the absence of three CH_2 groups combined with the presence of a carbonyl group and the inclusion of two additional hydrogen atoms by saturation of the terminal hemiacetal ring system to afford a dinor-seco-dihydro-PTX-2 analogue. The combination of a C=O group with that of an OH group (two OH groups are typically present in PTX-2, PTX-2SA and analogues of these compounds) could afford an analogue possessing a carboxyl group. An unsaturated ether structure is also possible (Figure 3-18).

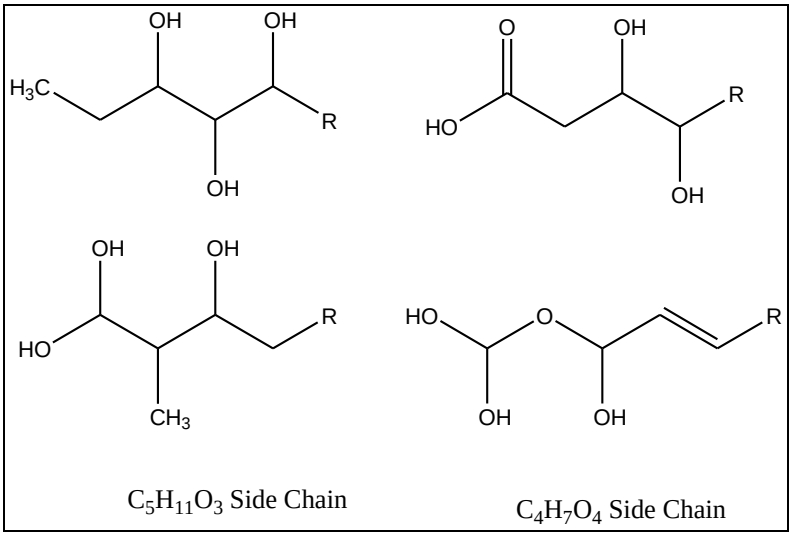

Figure 3-18: Possible side chain structures for PTX-i isomers: R = the C-1 to C-35 portion of the PTX-2 skeleton.

3.3.4 Evidence for PTX-i isomers

Selected ion profiling and targeted MS^2 ion acquisitions determined for sub-samples of the stored (aged) bulk Irish extracts examined in this investigation showed that in addition to the dominant early eluting PTX-i peak, there are also some minor peaks that showed essentially identical MS^2 mass spectral features suggesting that these peaks were structural isomers of the dominant compound.

Figure 3-19 shows the MS^2 MNH_4^+ (*m/z* 864) and MNa^+ (*m/z* 864) ion profiles determined for a representative sub-sample of the bulk Irish extract.

Three *m/z* 869 ion responses, arising from peaks eluting at 5.08, 7.25 and 9.28 min were readily apparent in the full scan MNa^+ MS^2 profile (Figure 3-19) of sub-samples of the stored (aged) bulk Irish extract. The three peaks showed essentially identical *m/z* 869 MS^2 mass spectra, each of which was dominated by an intense *m/z* 825 ion response (Figure 3-19). Only the dominant PTX-i compound (eluting at 5.06 min) afforded an adequate signal to noise ratio *m/z* 864 MS^2 MNH_4^+ mass spectrum when plotted in full scan mode (Figure 3-19).

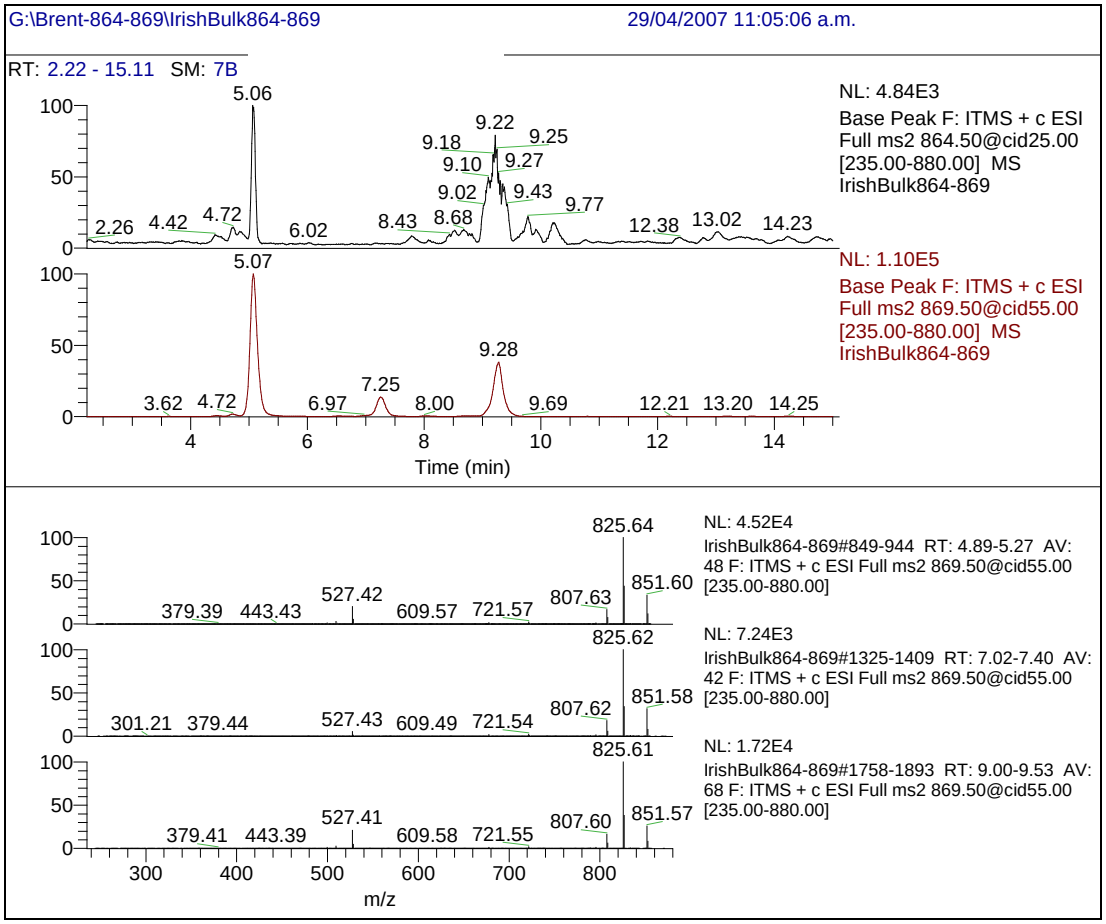

Figure 3-19: Extracted ion profiles (upper profiles) showing full scan MS^2 MNH_4^+ (*m/z* 864) and MNa^+ (*m/z* 869) MS^2 mass spectra (lower) determined for PTX-i peaks eluting at 5.07, 7.25 and 9.28 min respectively.

Since only sub-samples of processed (aged) bulk Irish mussel extracts were examined in the present investigation, it cannot be ascertained if the minor, later eluting peaks arose for naturally occurring PTX-i compounds or from isolation/storage artefacts of them such as 7-*epi* or other isomers. It is, for example, well documented that the level of the 7-*epi* isomer of PTX-2SA increases when extracts containing PTX-2SA are stored for extended times, especially so for samples stored in solution. In our laboratories, some other minor PTX-2SA isomers of unknown structure, have also been detected in aged PTX-2SA containing extracts.

3.4 Sulfonated PTX-i analogues

The following sections describe the detection and mass spectral analyses of the sulfonated PTX-i analogues.

3.4.1 Initial detection of sulfonated PTX-i analogues

In addition to appreciable levels of OA, DTX-2, PTX-2SA, 7-*epi*-PTX-2SA and some isomers of these compounds (possibly including some extraction and processing induced artefacts) together with significant levels of the PTX-i isomers (Figure 3-19), sub-samples of the stored bulk Irish extract afforded an LCMS profile which included a series of early eluting peaks that (some what confusingly, at least initially) afforded four MX^+ ions per compound with masses of *m/z* 944, 961, 966 and 971 (Figure 3-20). These peaks eluted at 4.73, 7.04 and 8.90 min (Figure 3-20). The apparent MX^+ ion clusters observed for the dominant 5.44 and 4.73 min peaks are shown in the lower section of Figure 3-20.

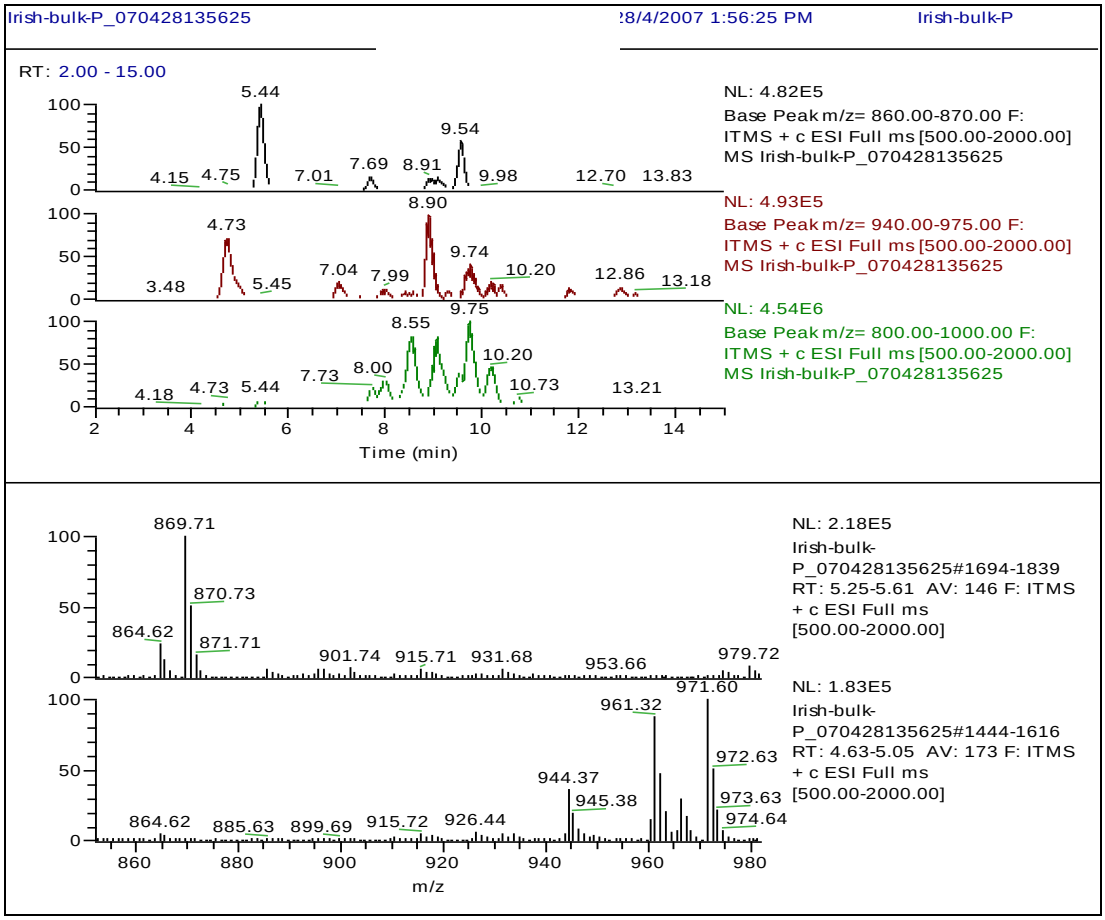

Figure 3-20: Chromatograms showing the *m/z* 860-870, 940-975 and 800-1000 ion profiles (upper profiles) and full scan mass spectra determined for the 5.44 min and 4.73 min peaks (lower spectra).

Initially, it appeared that only two out of three of the suspected MX^+ ions (namely *m/z* 944, 961 and 966 ions) were genuine MX^+ ions, since 17 and five Da are characteristic of the differences between MH^+, MNH_4^+ and MNa^+ ions respectively. Selected ion profiling (Figure 3-21) showed that an *m/z* 971 ion response was also associated with these peaks.

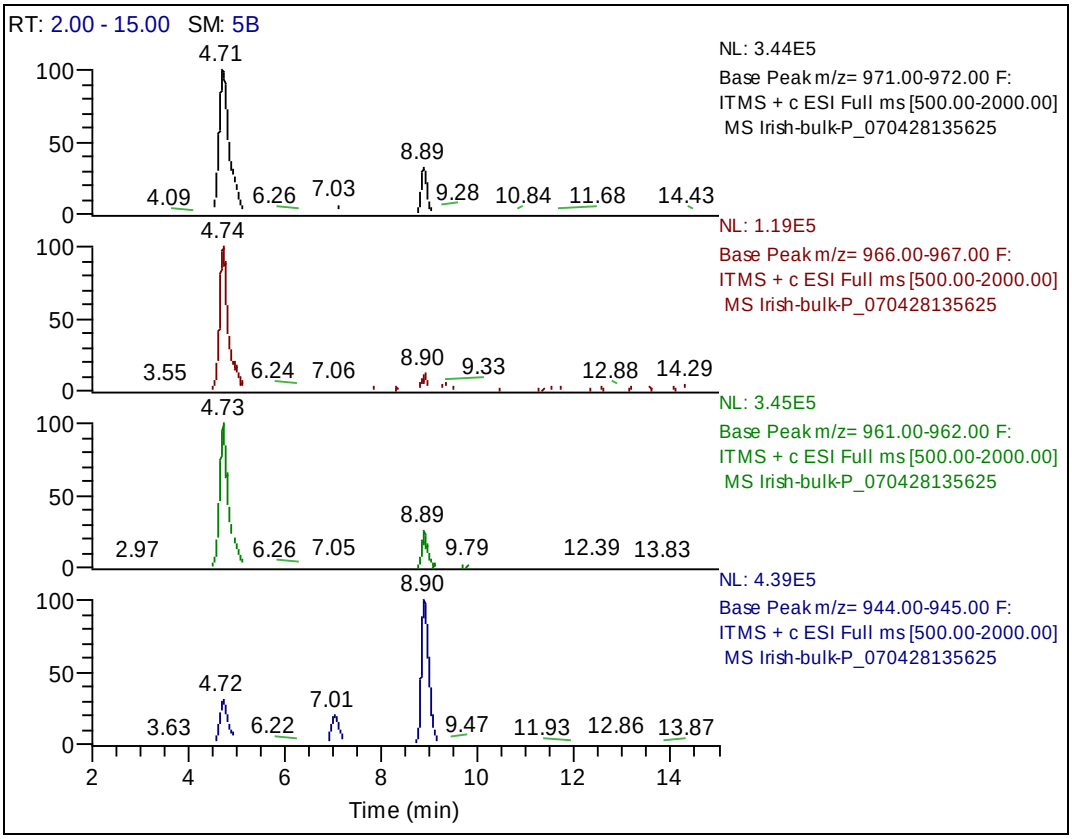

Figure 3-21: Extracted ion traces showing the relationship between the *m/z* 944 (lower), *m/z* 961 (lower centre), *m/z* 966 (upper centre) and *m/z* 971 (upper) ions.

Initially, this observation defied a logical interpretation since, if the *m/z* 944, 961 and 966 ions arose from MH^+, MNH_4^+ and MNa^+ ions respectively of a species of molecular weight 943 Da, the *m/z* 971 ion would be attributable to a $[M+28\ Da]^+$ species.

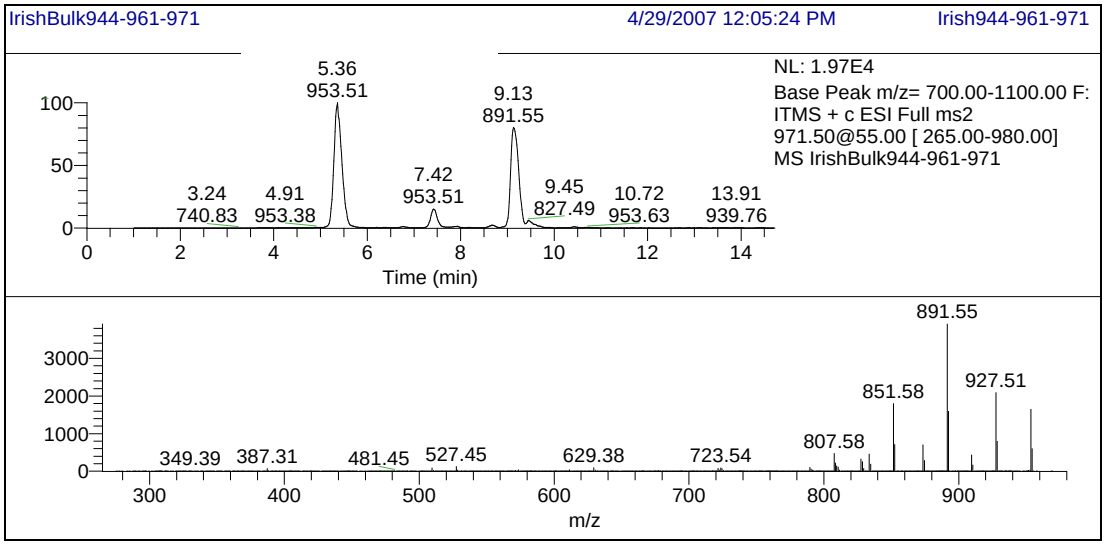

Figure 3-22: MS^2 mass spectrum of *m/z* 971 ion.

The MS^2 mass spectrum of the more dominant of the 'mystery' *m/z* 971 ions is shown in Figure 3-22. This spectrum showed ions at *m/z* 953 and 927 which can be attributed to losses of H_2O and CO_2 respectively. These losses are reminiscent of those seen in the MNa^+ MS^2 mass spectra of PTX-2 analogues, including the PTX-i isomers (refer to Section 3.2).

The daughter ions that appeared at *m/z* 891 and 851 correspond to losses of 80 and 120 Da respectively. These losses, which are reminiscent of those exhibited by sulfonated algal toxins (e.g. YTX and its analogues), can be attributed to the loss of SO_3 and $NaHSO_4$ respectively. The peak at *m/z* 873 (not labelled) corresponds to loss of 98 Da from the parent ion. This could be due to the loss of H_2O (18 Da) and an SO_3 group (80 Da) or vice versa to give an overall loss of 98 Da from the parent ion.

The foregoing observations are indicative of the four compounds which exhibited *m/z* 944, 961, 965 and 971 MX^+ ions possessing one or more ionisable groups such as sulfonate or acid groups (see below).

The recognition of the probable presence of a sulfate group, as revealed by 80 Da loss fragments, offered a rational explanation of the observation of a cluster of MX^+ ions

at *m/z* 944, 961, 966 and 971 since these could be attributed to ion arising from the following species:

(i) *m/z* 944: $[R\text{-}OSO_3H]NH_4^+$ or $[R\text{-}OSO_3NH_4]H^+$

(ii) *m/z* 961: $[R\text{-}OSO_3NH_4]NH_4^+$

(iii) *m/z* 966: $[R\text{-}OSO_3Na]NH_4^+$ or $[R\text{-}OSO_3NH_4]Na^+$

(iv) *m/z* 971: $[R\text{-}OSO_3Na]Na^+$

These observations lead to the hypothesis that the molecular weight of the parent compounds, namely the $R\text{-}OSO_3H$ variants which eluted at 4.73, 7.04 and 8.90 min respectively was 926 Da, and that the molecular weight of the non-sulfonated R-OH analogues was therefore 846 Da. Thus the MNH_4^+ and MNa^+ ions of the non-sulfonated compounds would therefore be expected to occur at *m/z* 864 and 869, as observed for the three PTX-i peaks which eluted at 5.44, 7.69 and 9.54 min respectively.

That the three early peaks were indeed sulfonated analogues of the slightly later eluting non-sulfonated PTX-i analogues (refer to Section 3.2) was supported by the similar relative contributions of the three pairs of sulfonated and non sulfonated peaks (peak 1 > peak 3 > peak 2) (Figure 3-21) and the detailed MS^2 analyses of the sulfonated analogues presented below.

3.4.2 MS^2 analyses of the *m/z* 961 and 944 ions from the sulfonated PTX-i analogues

Only the dominant early eluting sulfonated PTX-i peak afforded a detectable *m/z* 961 MNH_4^+ MS^2 mass spectrum. This MS^2 mass spectrum (Figure 3-23), which can be considered to arise for a double NH_4^+ ion of the type $[R\text{-}OSO_3NH_4]NH_4^+$, was characterised by a structurally uninformative H_2O loss ion which appeared at *m/z* 943.

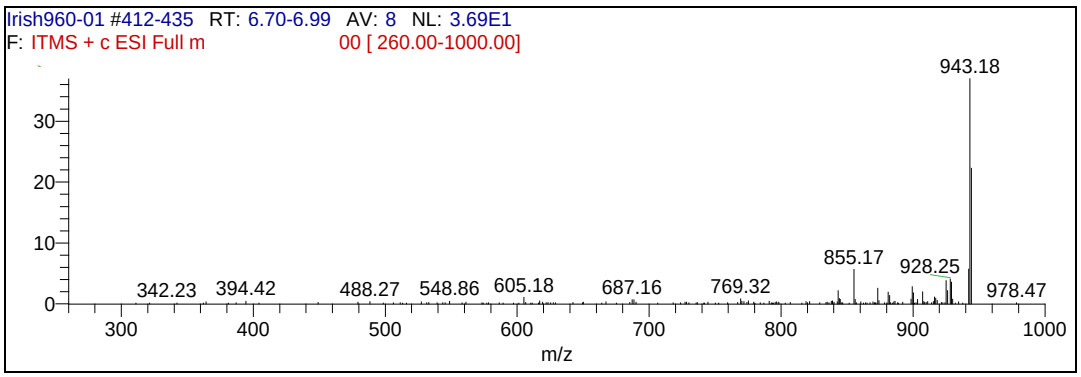

Figure 3-23: MS^2 mass spectrum of the *m/z* 961 ion.

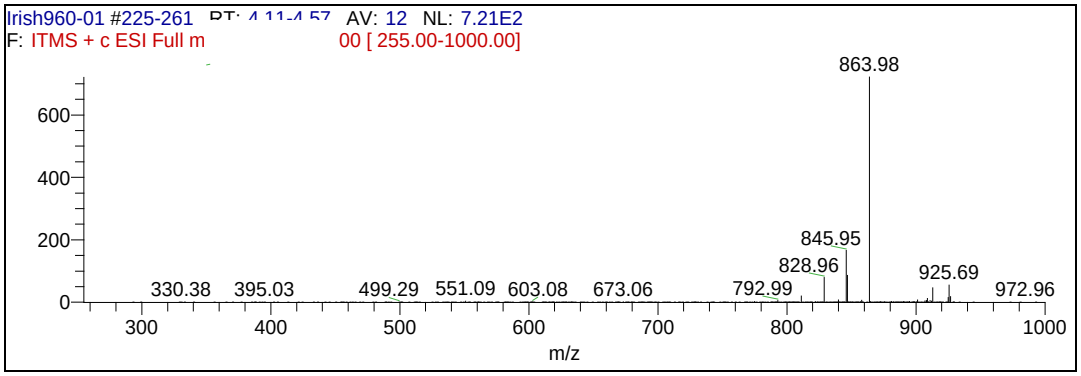

Figure 3-24: MS^2 mass spectrum of the *m/z* 944 ion.

The *m/z* 944 MS^2 mass spectrum (Figure 3-24) determined for the dominant sulfonated PTX-i peak showed an 80 Da loss to afford an *m/z* 864 ion. This loss of 80 Da can be attributed to the loss of a SO_3 group. A weak, but detectable *m/z* 551 ion was seen in the *m/z* 944 mass spectrum. The origin of this ion is believed to be identical to that of the *m/z* 551 ion observed in the MNH_4^+ MS^2 mass spectra of PTX-2 and PTX-2SA (refer to Sections 3.1.2 and 3.2.2).

3.4.3 MS^3 analyses of the *m/z* 971 ion from the sulfonated PTX-i analogues

MS^3 analyses were performed on five daughter ions observed in the MS^2 mass spectrum of *m/z* 971 $[R\text{-}OSO_3Na]Na^+$ ions (refer to Section 3.4.1) which occurred at *m/z* 953, 927, 891, 873 and 851 respectively. These mass spectra were variously characterised by losses of 18, 44, 80, 120, 298, 342 or 364 Da which can be attributed

to the loss of H_2O, CO_2, SO_3, and $NaHSO_4$ respectively or, in the case of the 298, 342 and 364 Da losses, the upper ring portion of the PTX-2 skeleton as formulated in Figure 3-25.

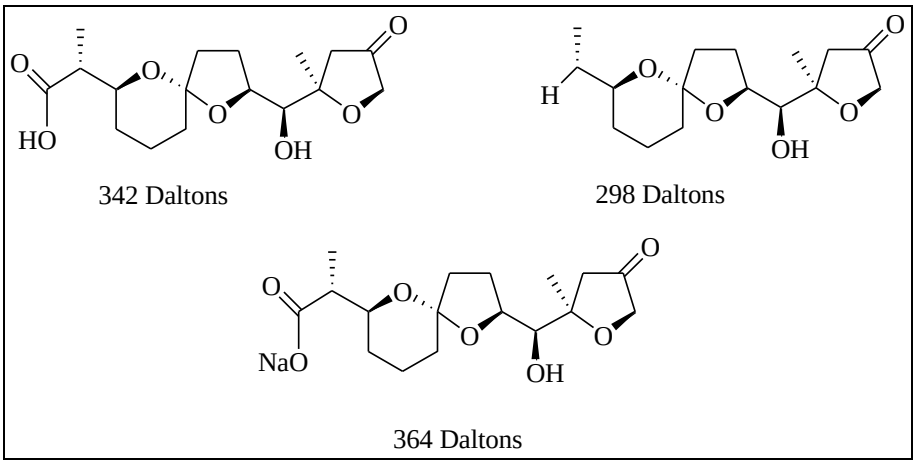

Figure 3-25: Proposed structures for three neutral losses seen in *m/z* 971 MS^3 mass spectra of sulfonated PTX-i analogues.

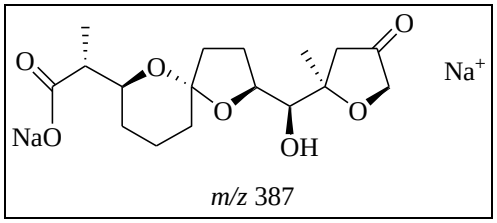

Figure 3-26: The proposed structure for the *m/z* 387 ion.

Some of the MS^3 mass spectra included an *m/z* 387 ion which can be formulated as the double Na (positively charged) analogue of the neutral 342 Da variant of the upper portion of the PTX-2 molecules (Figure 3-26). No literature information is presently available in respect of the MS^2 characteristics of positively charged double sodium ions of species such as the sodium adduct ion in Figure 3-26.

3.4.3.1 MS^3 analyses of the *m/z* 971 → *m/z* 953 ion sequence from sulfonated PTX-i analogues

The *m/z* 971 → *m/z* 953 (H_2O loss) MS^3 mass spectrum (Figure 3-27) included daughter ions at *m/z* 909, 873 and 833 arising for the loss 44 (CO_2), 80 (SO_3) or 120 ($NaHSO_4$) Da respectively.

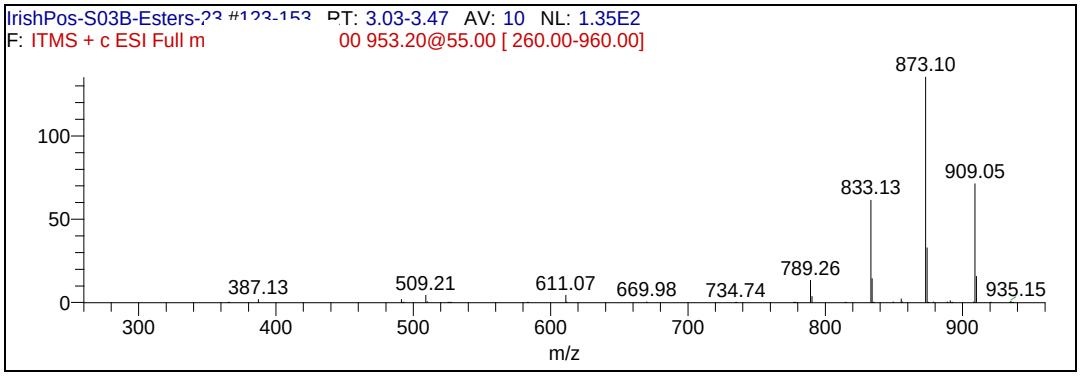

Figure 3-27: MS^3 mass spectrum of the *m/z* 971 → *m/z* 953 ion sequence from the PTX-i $[R\text{-}OSO_3Na]Na^+$ '971' compound.

3.4.3.2 MS^3 analyses of the *m/z* 971 → *m/z* 927 ion sequence from the sulfonated PTX-i analogues

The *m/z* 971 → *m/z* 927 (CO_2 loss) MS^3 mass spectrum (Figure 3-28) was dominated by the loss of $NaHSO_4$ (120 Da) to afford an *m/z* 807 ion. A weak but detectable *m/z* 509 ion, believed to arise by the loss of a 298 Da residue (corresponding to upper ring system of a PTX-2 like skeleton) molecule from the *m/z* 807 ion was also seen (Figure 3-25).

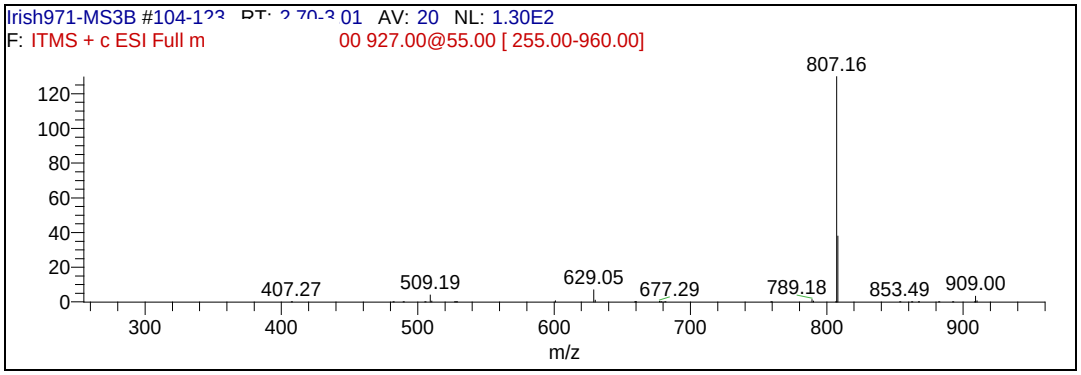

Figure 3-28: MS^3 mass spectrum of the *m/z* 971 → *m/z* 927 ion sequence from the PTX-i $[R\text{-}OSO_3Na]Na^+$ '971' compound.

3.4.3.3 MS^3 analyses of the *m/z* 971 → *m/z* 891 ion sequence from the *m/z* 971 sulfonated PTX-i analogues

The *m/z* 971 → *m/z* 891 (SO_3 loss) MS^3 mass spectrum (Figure 3-29) was characterised by an *m/z* 873 (H_2O loss), *m/z* 795 (96 Da loss), *m/z* 527 (364 Da loss) ions and by an *m/z* 387 ion. In the absence of high resolution data, the origin of the *m/z* 795 ion is uncertain while the 364 Da loss that affords appears the *m/z* 527 ion (as also seen in the MS^2 mass spectrum of PTX-i (refer to Section 3.3.3), is believed to be a sodium containing variant of the 342 Da loss commonly observed for PTX-2 like compound (Figure 3-25). The origin of the *m/z* 387 ion is believed to be as formulated in Figure 3-26.

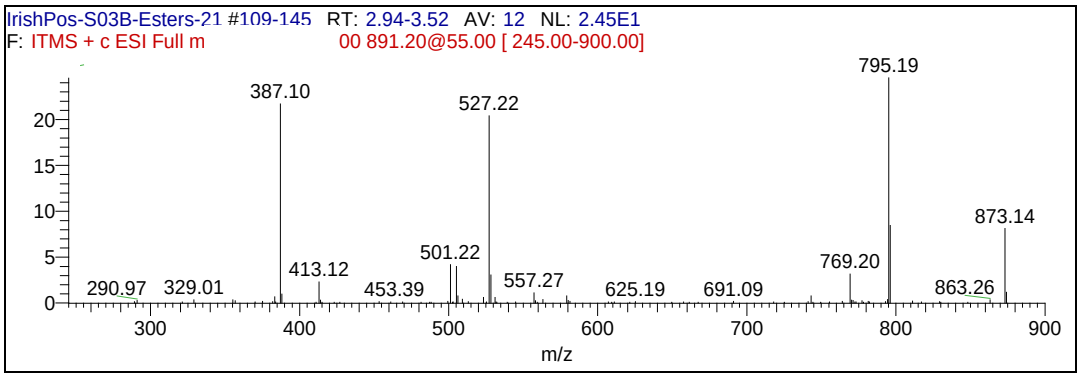

Figure 3-29: MS^3 mass spectrum of the *m/z* 971 → *m/z* 891 ion sequence from the PTX-i $[R\text{-}OSO_3Na]Na^+$ '971' compound.

3.4.3.4 MS^3 analyses of the *m/z* 971 → *m/z* 873 ion sequence from the sulfonated PTX-i analogues

The *m/z* 971 → *m/z* 873 (H_2O + SO_3 loss) MS^3 mass spectrum (Figure 3-30) was characterised by *m/z* 777 (96 Da loss), *m/z* 509 (364 Da loss) ions and by an *m/z* 387 ion. As noted above for *m/z* 971 → *m/z* 891 (SO_3 loss) MS^3 mass spectrum, the origin of the *m/z* 777 ion is uncertain while the 364 Da loss that affords the *m/z* 509 ion, is the H_2O loss analogue of the *m/z* 527 ion observed in the *m/z* 971 → *m/z* 891 (SO_3 loss) MS^3 mass spectrum. As noted above, the origin of the *m/z* 387 ion is believed to be as formulated in Figure 3-26.

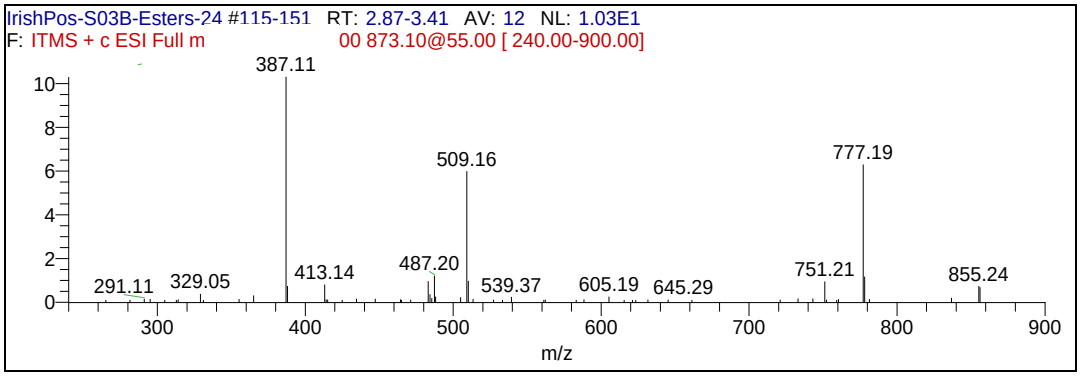

Figure 3-30: MS^3 mass spectrum of the *m/z* 971 → *m/z* 873 ion sequence from the PTX-i $[R\text{-}OSO_3Na]Na^+$ '971' compound.

3.4.3.5 MS^3 analyses of the *m/z* 971 → *m/z* 851 ion sequence from the sulfonated PTX-i analogues

The *m/z* 971 → *m/z* 883 ($NaHSO_4$ loss) MS^3 mass spectrum (Figure 3-31) was characterised by *m/z* 833 (H_2O loss), *m/z* 807 (CO_2 loss) ions and *m/z* 509 (342 or 44+298 Da) loss ions. The *m/z* 509 ion is the H_2O loss analogue of the *m/z* 527 ion observed in the *m/z* 971 → *m/z* 891 (SO_3 loss) MS^3 mass spectrum.

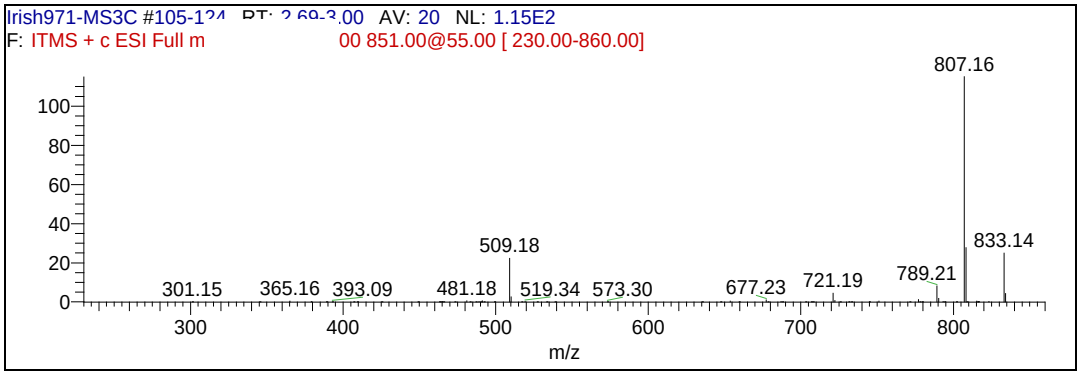

Figure 3-31: MS^3 mass spectrum of the *m/z* 971 → *m/z* 851 ion sequence from the PTX-i $[R\text{-}OSO_3Na]Na^+$ '971' compound.

The foregoing MS^2 and MS^3 mass spectral data is consistent with the view that the sulfonated compound possesses a PTX-i like structure in which one of the hydroxyl groups associated with $C_4H_7O_4$- or $C_5H_{11}O_3$- side chain attached to the right hand portion of the molecule is sulfonated.

3.5 MS^n analyses of the *m/z* 925 and 943 $[M\text{-}H]^-$ ions

Realisation that the compounds that exhibited the *m/z* 944-971 ions were sulfonated species prompted the hypothesis that when subjected to LCMS analyses, they should afford diagnostic negative ions. Unlike positive ion spectra, where several $[R\text{-}OSO_3Y]X^+$ ions were observed (X, Y = H, NH_4 or Na) it was reasoned that only a single $[M\text{-}H]^-$ ion, corresponding to an $R\text{-}OSO_3^-$ ion would be observed for each of the three sulfonated compounds detected in sub-samples of the bulk Irish extract. This proved to be the case.

An attempt was made by Irish collaborators to obtain high resolution MS data in negative ion mode for the *m/z* 925 ion, however on-going stability issues rendered the data unreliable. It was anticipated that this data, had it been interpretable, would have confirmed the presence of a sulfur atom in the sulfonated PTX-i's and differentiate between the presence of a $C_5H_{11}O_3$ or $C_4H_7O_4$ side chain (refer to Section 3.3.3). However, it would not have defined the exact structure of the C_5 or C_4 side chain that

is believed to be attached to C-35. This would require the isolation of one of the PTX-i compounds in a quantity sufficient for NMR analysis using a combination of one- and two-dimensional NMR techniques in a manner analogous to those utilised (for example) in the structure elucidation of PTX-13 and PTX-14[19].

3.5.1 MS^2 analyses of the *m/z* 925 $[M-H]^-$ ion of the sulfonated PTX-i analogues

Assuming that the molecular weight of the protonated sulfonated PTX-i compounds was 926 Da, it was reasoned that they would exhibit distinctive *m/z* 925 $[M-H]^-$ ions (see above). Full scan negative ion LCMS analyses verified this hypothesis (Figure 3-32).

In MS^2 mode, performed with a slower MeCN-H_2O gradient than that used in earlier analyses in a effort to increase the resolution of early eluting peaks, each of the three sulfonated PTX-i peaks which eluted at 8.72, 10.05 and 11.11 min respectively afforded negative ion MS^2 mass spectra which were characterised by strong *m/z* 907 (H_2O loss), *m/z* 881 (CO_2 loss) and *m/z* 845 (SO_3 loss) ions, together with less intense *m/z* 583, 597 and 615 ions (Figure 3-33).

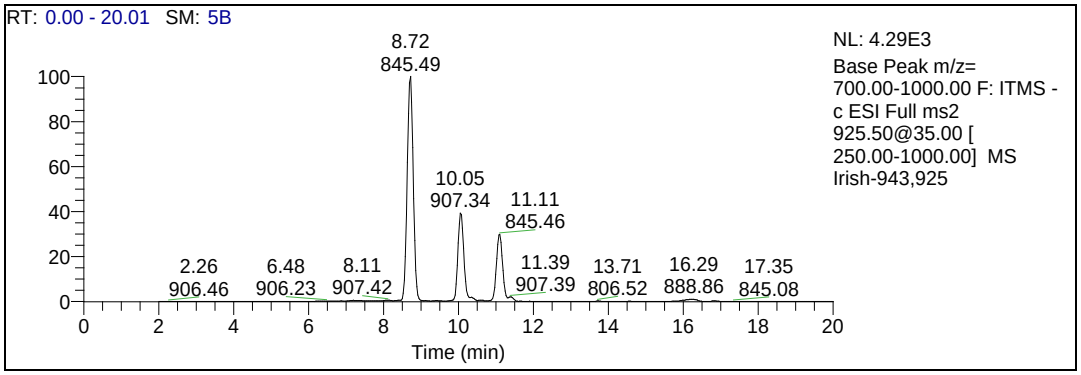

Figure 3-32: Extracted ion chromatogram of the *m/z* 925 ion showing several peaks believed to be sulfonated PTX-i analogues.

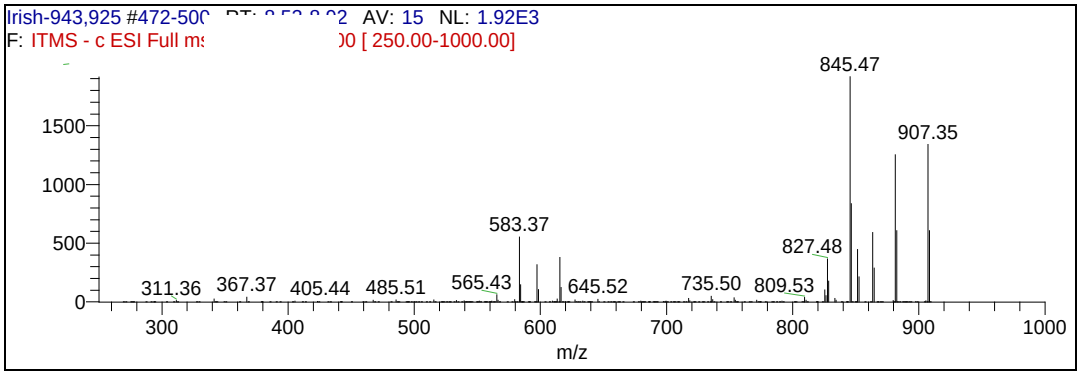

Figure 3-33: MS^2 mass spectrum of the *m/z* 925 $[M-H]^-$ ion from the dominant sulfonated PTX-i compound.

Possible structures for the *m/z* 583 ion which is believed to arise via cleavage through the C-15–C-16 bond and the C-33–O-1 bond are shown in Figure 3-34. These structures are consistent with the hypothesis that the sulfate group is believed to be associated with the $C_4H_7O_4$ or $C_5H_{11}O_3$ side chain considered to be present in PTX-i isomers.

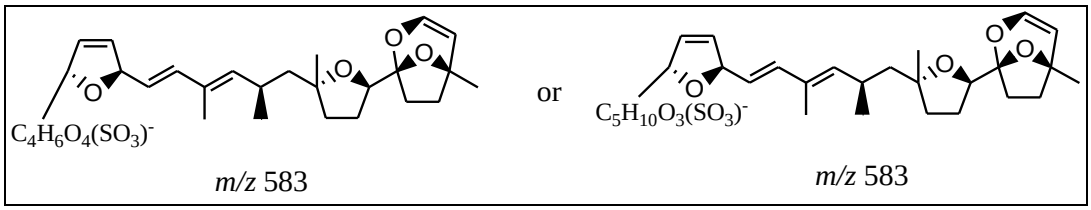

Figure 3-34: Possible structures for the *m/z* 583 ion.

3.5.2 MS^2 analyses of the *m/z* 943 $[M-H]^-$ ion of the sulfonated PTX-i analogues

The ease and clarity (sensitivity, peak resolution and in general absence of interfering responses from another sub-sample components) with which the *m/z* 925 $[M-H]^-$ negative ion of PTX-i compounds gave structurally informative MS^n results (refer to Section 3.5.1) prompted a search for the seco-analogue of sulfonated PTX-i compounds. If present, these compounds would be expected to afford $[M-H]^-$ ions at *m/z* 943.

Figure 3-35 is a full scan plot of the *m/z* 943 MS^2 ion responses determined for a sub-sample of the bulk Irish extract. Several peaks exhibited significant full scan *m/z* 943 ion responses. Examination of the MS^2 mass spectra determined for each of the peaks revealed that several of them exhibited MS^2 mass spectra which were consistent with their identification as seco analogues of the sulfonated PTX-i compounds (see above).

For example, the peak at 9.54 min (Figure 3-36) showed daughter ions at *m/z* 925 (H_2O loss), *m/z* 897 (46 Da loss, probably loss of HCOOH from the additional acid present in the seco variant) and *m/z* 863 (SO_3 loss) together with a low mass ion at *m/z* 601. This ion is believed to be 'seco' equivalent (+18) of the *m/z* 583 ion observed in the MS^2 mass spectrum of the closed ring sulfonated PTX-i isomers identified in Section 3.4.

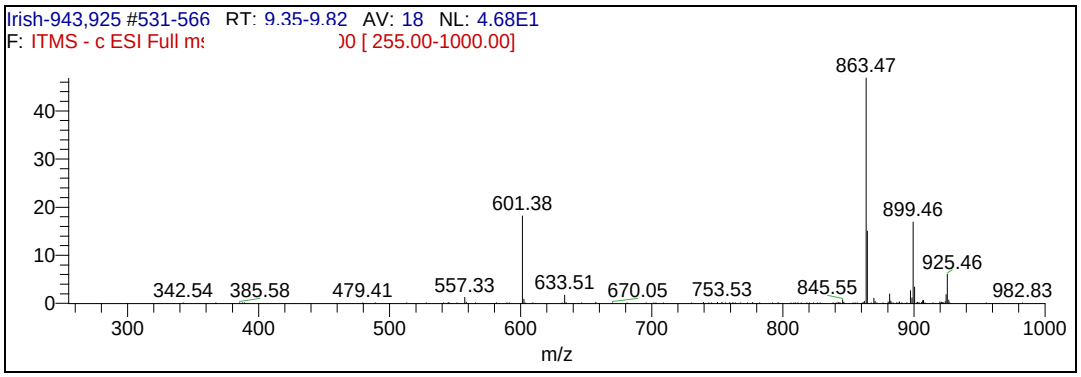

Figure 3-35: MS^2 mass spectrum of *m/z* 943 negative ion from the sulfonated PTX-i compound.

The clarity of the *m/z* 943 negative MS^2 LCMS profiles was improved by plotting only the *m/z* 863 (SO_3 loss) ion responses observed for compounds showing MS^2 *m/z* 943 ion responses. Figure 3-36 compares the parent *m/z* 943 and *m/z* 843 extracted ion (mass filtered) *m/z* 943 MS^2 chromatograms. Ghost peaks observed in the unfiltered chromatogram were suppressed in the mass filtered chromatogram.

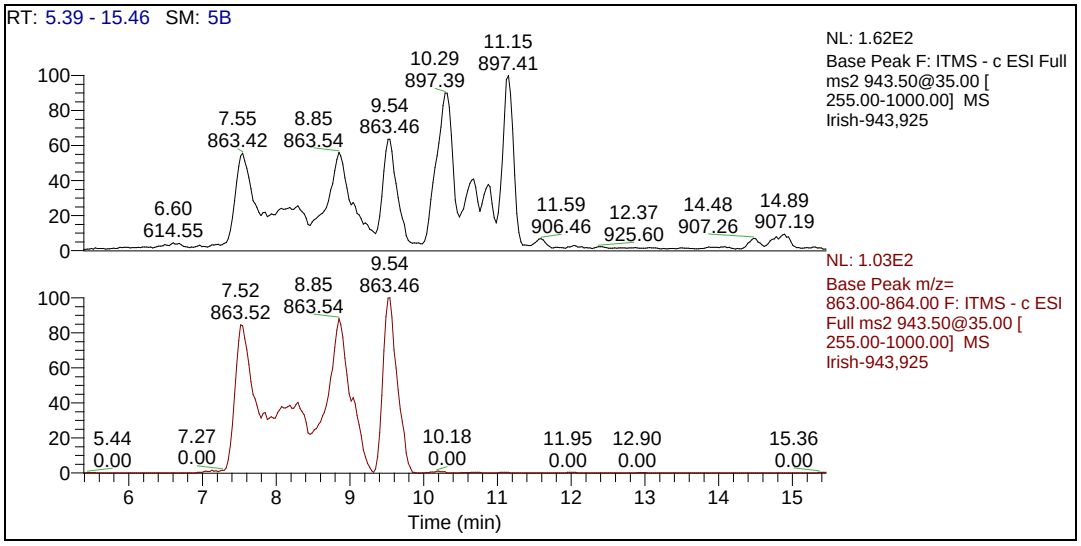

Figure 3-36: Comparison of full scan and *m/z* 863 extracted ion *m/z* 943 MS^2 chromatograms.

This mode of peak identification (namely extracted ion filtering of a full scan MS^2 mass spectrum) using ion trap MS^2 data is equivalent to selected ion reaction monitoring (SRM) detection of a specific ion transition (fragmentation) as is routinely performed using a triple quad mass spectrometer. The sensitivity of a triple quad MS when operated in SRM mode is substantially greater than that of an ion trap MS operated in SRM mode since a triple quad MS can monitor a specific ion transition for 100% of the available time, whereas a ion trap system needs to generate MS^2 daughter ions within the trap and progressively scan them out of the trap, cycle by cycle, thus only a small amount of the time per cycle can be utilised per cycle to record a specific daughter ion transition.

3.5.3 Isomeric forms of the sulfonated PTX-i compounds

As is observed for non-sulfonated PTX-i compounds (refer to Section 3.3), a series of isomers of the more dominant compound were observed in negative ion analyses directed towards the identification of sulfonated analogue. In each case, two or three such peaks were detected in MS^2 analyses which utilised *m/z* 925 and 943 ion

responses targeted towards sulfonated PTX-i and seco-PTX-i analogues respectively. Generally two of the peaks showed much stronger responses than the third such peak.

The level of sulfonated seco-PTX-i isomers in the representative sub-sample of the bulk Irish extract was typically less than was the case for the level of sulfonated PTX-i isomers. This is apparent in Figure 3-37 where the noise levels of the respective traces are $1.99E^1$ (seco isomers) and $5.14E^2$ (closed ring isomers).

The MS^2 mass spectra recorded for the two more dominant sulfonated seco-PTX-i and sulfonated-PTX-i isomers were similar but not identical (Figure 3-37).

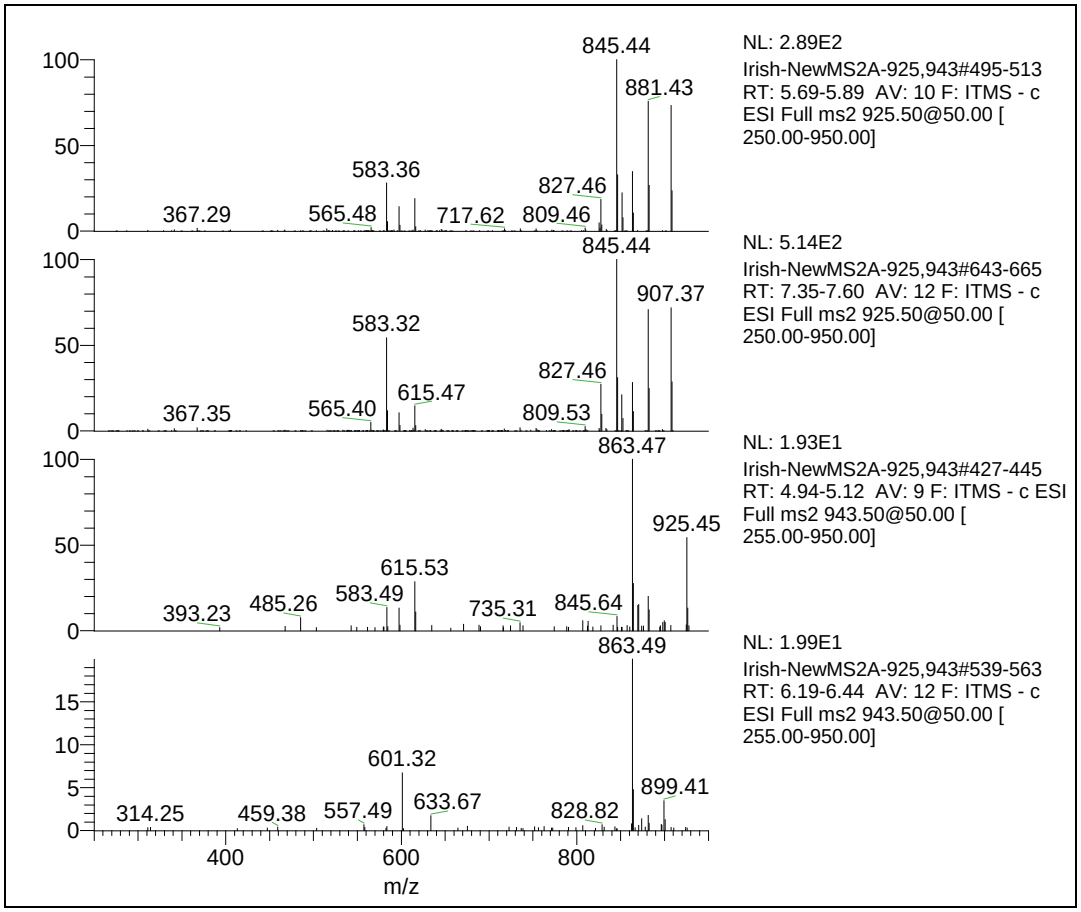

Figure 3-37: Negative ion MS^2 mass spectra of two sulfonated PTX-i compounds (upper pair of mass spectra: $[M-H]^-$ at *m/z* 925) and two sulfonated seco-PTX-i compounds (lower pair of mass spectra: $[M-H]^-$ at *m/z* 943).

In accord with the conclusion that compounds showing MS^2 *m/z* 943 ion responses were more polar (i.e. more heavily hydroxylated), open ring seco-compounds than the closed ring compounds that showed MS^2 *m/z* 925 responses, the closed ring compounds eluted before the open ring compounds on the reverse phase C-18 LC column used in this investigation.

Because the extracts used in this investigations had been stored for several years prior to the detailed LCMS analyses reported in Section 3.5 were undertaken, it cannot be ascertained with certainty whether or not only a single isomer was initially present in the bulk processed Irish extracts. Based on the documented behaviour of several shellfish compounds and observations made in the laboratory, most notably the progressive conversion of PTX-2SA to its 7-*epi* analogue and to a lesser extent other isomers, we consider it likely that some of the non sulfonated and sulfonated PTX-i peaks detected in the present study will transpire to be storage artefacts. Clarification of this situation will require the analysis of a series of freshly collected and carefully processed and stored extracts.

3.5.4 High resolution mass spectral analyses

During the write-up of this thesis, a newly obtained fraction of the Irish sample supplied by Dr C. O. Miles was analysed using the University of Waikato's high resolution MicrOTOF mass spectrometer. The sample contained a high level of OA and a moderate level of the sulfonated PTX-i compound. The negative ion direct infusion mass spectrum determined for the sample is shown by Figure 3-38. The dominant ion at *m/z* 803.4557 arises from the $[M-H]^-$ ion of OA (found 803.4557: $C_{44}H_{67}O_{13}$ requires 803.4587).

The intensity of the *m/z* 925.4275 ion was *ca.* $1/8^{th}$ that of the *m/z* 803.4557 $[M-H]^-$ ion from OA. A molecular analysis was performed on the *m/z* 925.4275 ion. This analyses, which was restricted to molecular formulation which contained between 40 and 48 carbon atoms and one or no sulfur atoms, gave the best result for the

molecular formula $C_{46}H_{69}O_{17}S$ (found 925.4275: $C_{46}H_{69}O_{17}S$ requires 925.4261). The 'fit error' for this molecular formula was -1.52 ppm or -1.47 mDa which is a very small error. The *m/z* 803 ion of OA showed a 3.78 ppm or 3.03 mDa error when compared with the known molecular formula, $C_{44}H_{67}O_{13}$ of the $[M-H]^-$ ion of OA.

The $C_{46}H_{69}O_{17}S$ molecular formula established for the *m/z* 925 ion is indicative of the PTX-i analogues possessing a PTX-2 like structure with a $C_5H_{11}O_3$ side chain attached to the C-35, rather than a C-36–C-40 hemiacetal ring as found in known pectenotoxins. While the HRMS data differentiates between the attachment of a $C_5H_{11}O_3$ or a $C_4H_7O_4$ side chain to C-35, it does not determine the isomeric form of the C-35 side chain (e.g. straight chain or branched chain forms) or the point of attachment of the sulfate and ester groups in the PTX-i analogues. There remains a need to isolate a sufficient quantity of a PTX-i compound for its structure to be determined using one and two-dimensional NMR methods.

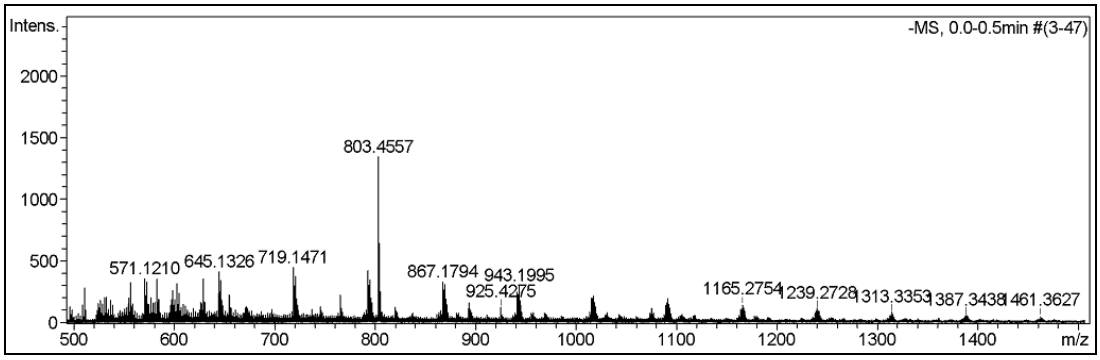

Figure 3-38: High resolution direct infusion negative ion mass spectrum of an Irish sample containing OA (*m/z* 803) and a sulfonated PTX-i compound (*m/z* 925).

3.6 Independent detection of a sulfonated PTX-i compound by Irish workers

During the write up of the investigations reported in Sections 3.4-3.5, a member of the Irish group reported that they had detected a sulfonated PTX-i compound which displayed what was believed to be a MNH_4^+ ion at *m/z* 944. The QTOF-MS/MS mass spectra which the Irish group determined for PTX-2 and the compound which they

designated as PTX-i is shown by Figure 3-39. This mass spectrum is believed to correspond to that determined for the dominant sulfonated PTX-i compound reported in Section 3.4 of this thesis.

The Irish group designated the sulfonated compound as PTX-i (Figure 3-39) whereas in this investigation the PTX-i designation was applied to the non-sulfonated compound (and structural isomers of this compound) and sulfonated analogues were collectively referred to as sulfonated PTX-i analogues. It is proposed that the convention adopted in this thesis should be applied in all future studies (i.e. the PTX-i designation should be applied to non-sulfonated analogues). When the structure of the dominant PTX-i compound is known (after isolation and NMR analysis), it would be appropriate to replace the 'i' designation by a number (e.g. PTX-15 if it transpires to be the 15th reported PTX analogue) and it may emerge that some or all of the lesser (minor, later eluting) peaks will prove to be epimerised analogues of the parent PTX-i compound such as the 7-*epi*-PTX-i analogues.

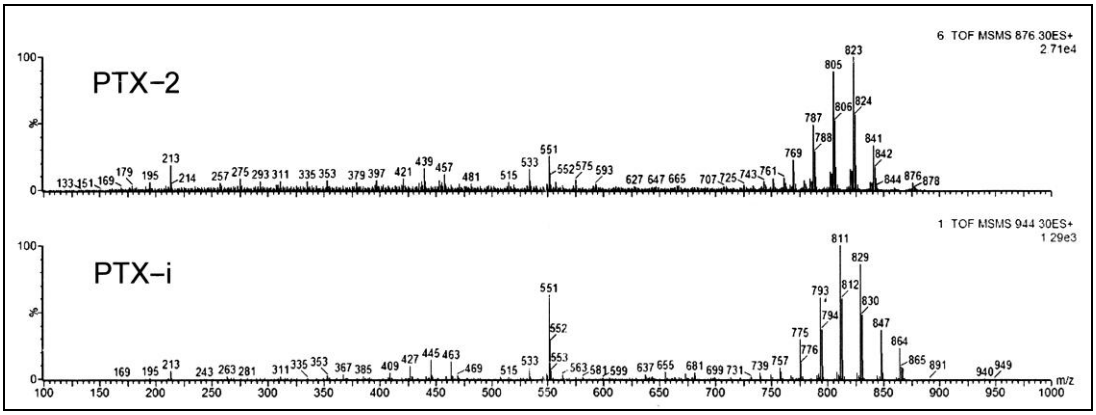

Figure 3-39: QTOF-MS/MS mass spectra determined by Irish workers for PTX-2 and the *m/z* 944 PTX-i sulfonated ion.

Following an agreement to proceed towards the formal characterisation of the new group of PTX-i compounds (non-sulfonated, sulfonated and sulfonated esters: refer to Sections 3.3, 3.4/3.5 and 3.8 respectively) on a collaborative rather than competitive basis, the Irish group was advised that it considered likely their 'PTX-i' compound would also afford a strong *m/z* 925 $[M-H]^-$ ion. This proved to be case and

the QTOF-MS/MS mass spectrum of this ion was found to be essentially identical to that determined for the dominant sulfonated PTX-i compound in this investigation, using a LTQ ion trap MS system.

3.7 Reaction of PTX-2 and related compounds with $NaBH_4$ and $NaBD_4$

The following sections provide information of the reaction of PTX-2, PTX-2SA and a mixture of sulfonated PTX-i and seco-PTX-i compounds with $NaBH_4$ and $NaBD_4$.

3.7.1 Background information on borohydride reactions

Sodium borohydride ($NaBH_4$) is used in organic synthesis to reduce aldehydes and ketones to alcohols in the presence of MeOH and H_2O at basic pHs since it reacts with both MeOH and H_2O in acidic solutions.

$NaBH_4$ rarely reacts with esters or carboxylic acids under normal conditions. Reduction of these groups is usually achieved using lithium aluminium hydride (LAH) and moderate to forcing conditions. LAH is well known to be a more reactive reagent than sodium borohydride.

In mass spectral terms, reaction of a carbonyl group with $NaBH_4$ adds two Da (two hydrogen atoms) per reacted group. If $NaBD_4$ is used in place of $NaBH_4$, three Da are introduced per reacted carbonyl group since the initially formed –CDOD- reduction is converted to the corresponding -CDOH- analogue via the rapid exchange of the deuterium atom of -OD groups with hydrogen present in protonated reaction solvents such as MeOH and H_2O.

It was anticipated that $NaBH_4$ and $NaBD_4$ reduction reactions would afford mass spectral information that would serve to define the presence of a 14-keto group in PTX-i analogues. It was also of interest to determine if the terminal hemiacetal ring system of PTX-2 and its analogues was reactive to towards $NaBH_4$, since hemiacetal

ring systems exist in equilibration with a corresponding open chain keto or aldo form (c.f. glucose). Even if only a low level of the open form of a compound is present (as is the case for glucose), reduction reactions proceed to completion via continual replacement of the minor level of the aldo form as it reduced by reagents such as $NaBH_4$ as shown in Figure 3-40.

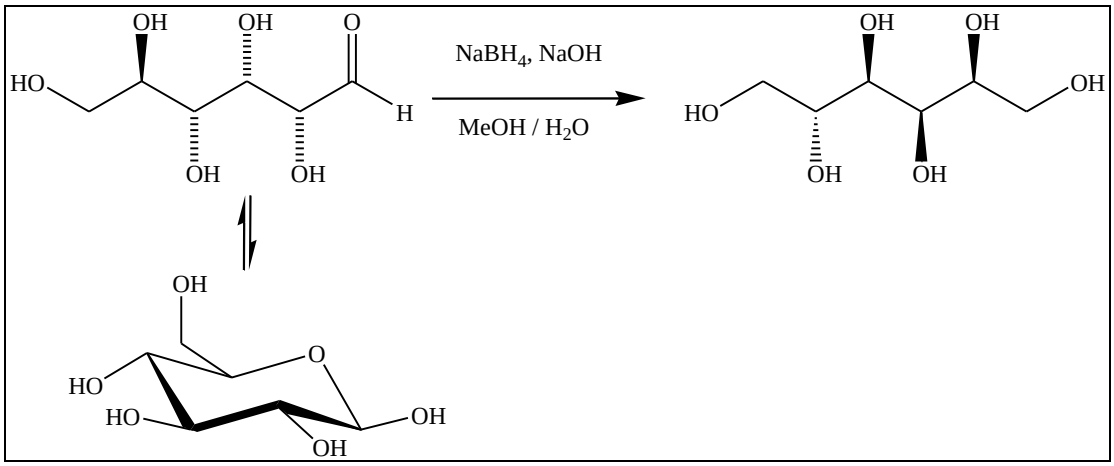

Figure 3-40: Scheme showing the reaction of glucose with $NaBH_4$ to produce glucitol.

Sodium borohydride reduction reactions can be carried out on a micro scale by the direct addition of a small quantity of $NaBH_4$ to an LCMS vial which contains a MeOH-H_2O solution, or an MeCN-MeOH-H_2O solution of target molecules. Experience in our laboratories is that the presence of some unreacted $NaBH_4$ and/or reaction by-products derived from the $NaBH_4$ does not interfere with subsequent LCMS analysis.

Three samples, containing PTX-2 and PTX-2SA and a mixture of sulfonated PTX-i and seco-PTX-i compounds were subjected to reaction with $NaBH_4$ and $NaBD_4$.

3.7.2 MS^n analyses of PTX-2/$NaBH_4$ reaction products

The reaction of PTX-2 with $NaBH_4$ was initially undertaken to determine the stability or otherwise of the PTX-2 skeleton towards $NaBH_4$ and the extent to which $NaBH_4$ would reduce the keto or hemiacetal groups present in PTX-2.

In LCMS analyses, PTX-2 exhibits MNH_4^+ and MNa^+ ions at *m/z* 876 and 881 respectively. Successful reaction should be expected to add either two or four Da to these ions, depending on whether only the 14-keto group or both of the 14-keto and 36-hemiacetal groups were reduced (Figure 3-41). Reduction of the 14-keto and 36-hemiacetal groups in each case introduces an additional asymmetric carbon, thus isomeric forms of product molecules are to be expected.

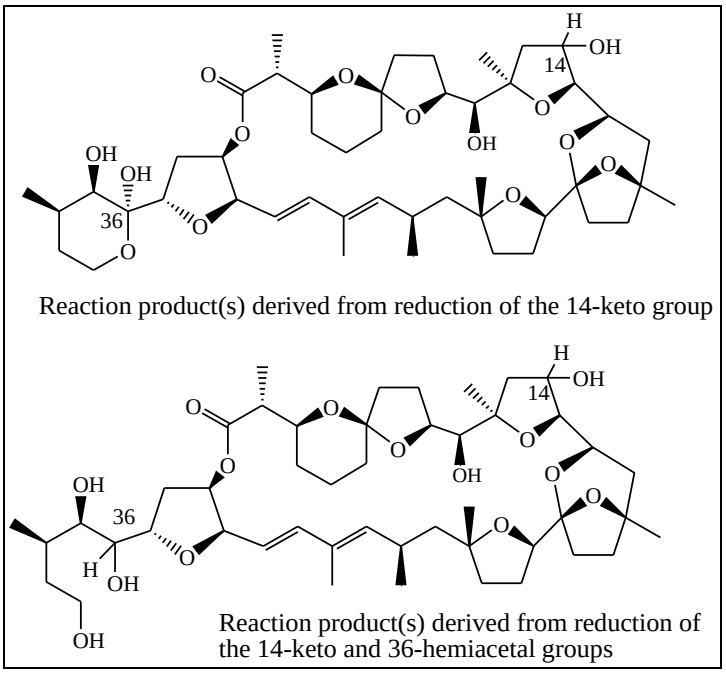

Figure 3-41: Scheme showing the possible outcomes of the $NaBH_4$ reaction with PTX-2.

Reaction of an authentic specimen of PTX-2 with a modest excess of $NaBH_4$ afforded one major and one minor product peak (Figure 3-42), which exhibited essentially identical full scan MNH_4^+ and MNa^+ MS^2 mass spectra. Both of the reduction

products exhibited MNH_4^+ and MNa^+ ions at *m/z* 880 and 885 respectively, corresponding to the addition of four hydrogen atoms thereby revealing that reduction of both the 14-keto and 36-hemiacetal groups had occurred (Figure 3-41).

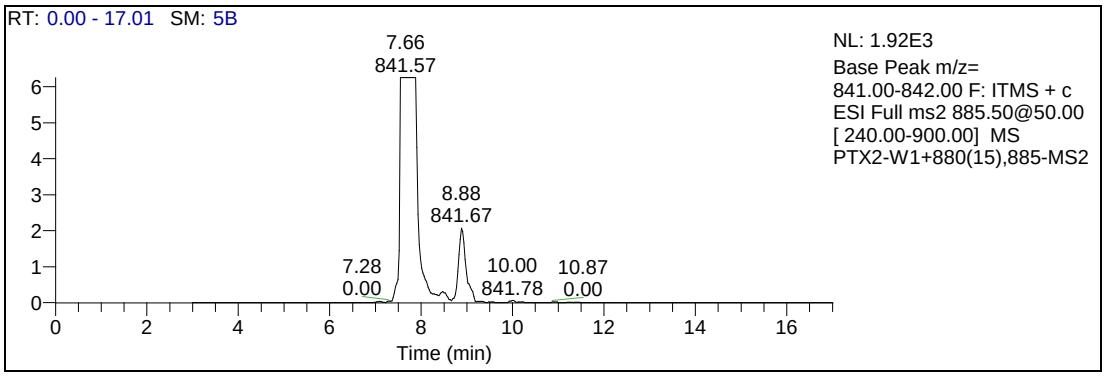

Figure 3-42: *m/z* 885 MS^2 ion chromatogram showing major and minor reduction products from the PTX-2/$NaBH_4$ reaction.

Only a low signal to noise ratio MS^2 mass spectrum could be obtained for the more dominant reduction product of the *m/z* 880 MNH_4^+ ion. This mass spectrum (Figure 3-43) was dominated by a daughter ion at *m/z* 861, attributable to the loss of NH_3 from the parent MNH_4^+ ion. The MNH_4^+ MS^2 mass spectrum of the reduction product differed greatly from that recorded for PTX-2 (refer to Section 3.1).

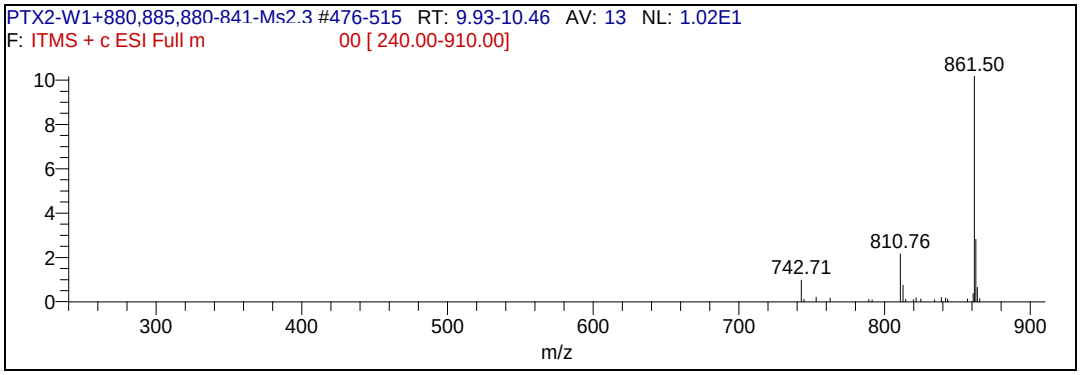

Figure 3-43: MS^2 mass spectrum of the *m/z* 880 ion of the dominant PTX-2/$NaBH_4$ reaction product.

On the other hand, the *m/z* 885 MNa^+ MS^n mass spectra of the reduction products were reminiscent of those recorded for PTX-2, other than for a two or four Da increase in the *m/z* values of appropriate ions.

The *m/z* 885 MNa^+ MS^2 mass spectrum (Figure 3-44) of each of the reduction products was, as expected, dominated by the loss of CO_2 (44 Da) to afford an *m/z* 841 daughter ion analogous to the *m/z* 837 ion observed in the corresponding PTX-2 MS^2 mass spectrum (refer to Section 3.1.2).

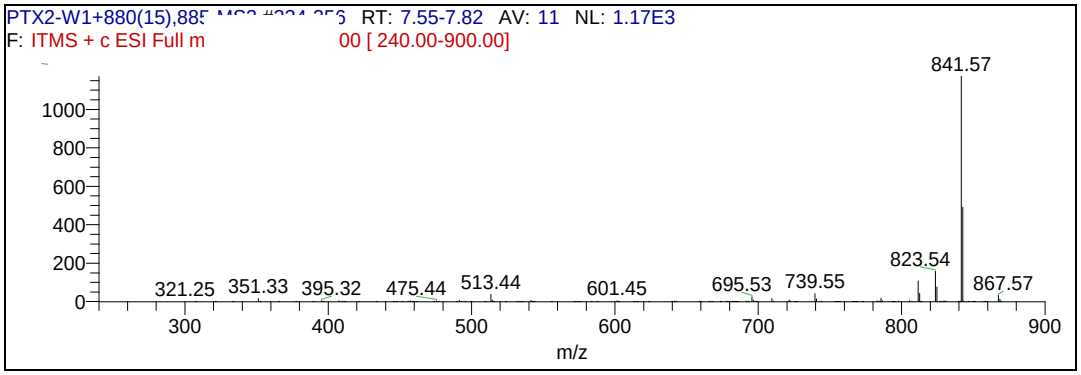

Figure 3-44: MS^2 mass spectrum of the *m/z* 885 MNa^+ of the dominant PTX-2/$NaBH_4$ reaction product.

Under MS^3 conditions, the *m/z* 841 ion (Figure 3-45) predominantly afforded an *m/z* 823 (H_2O loss) daughter ion together with minor daughter ions (of presently unknown structure) at *m/z* 739, 695, 513 and 351.

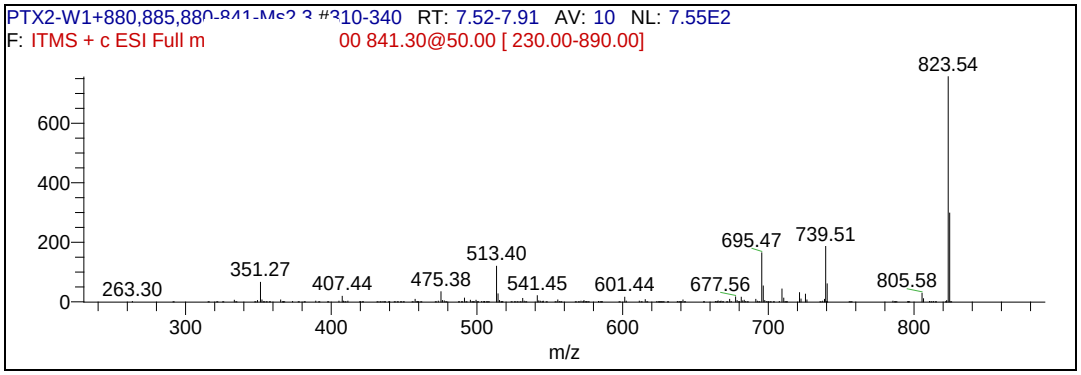

Figure 3-45: MS^3 mass spectrum of the *m/z* 885 → *m/z* 841 ion sequence from the dominant PTX-2/$NaBH_4$ reaction product.

Under MS^4 conditions, the *m/z* 823 ion (Figure 3-46) predominantly afforded an *m/z* 805 (H_2O loss daughter ion) together with minor daughter ions (of presently unknown structure) at *m/z* 721, 677 and 513. The *m/z* 721 and 677 ions are H_2O loss analogues of the *m/z* 739 and 695 analogues observed in the MS^3 mass spectrum.

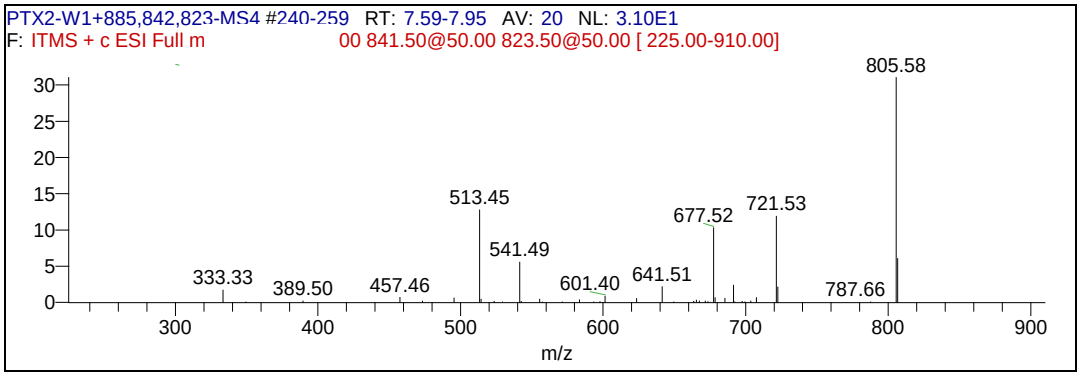

Figure 3-46: MS^4 mass spectrum of the *m/z* 885 → *m/z* 841→ *m/z* 823 ion sequence from the dominant PTX-2/$NaBH_4$ reaction product.

It is apparent from the foregoing analyses, that the reaction of PTX-2 with $NaBH_4$ proceeds smoothly to afford predictable products and that with the exception that the C-36 hemiacetal group in the PTX-2 skeleton is also reduced by sodium borohydride.

3.7.3 Reaction of PTX-2 with $NaBD_4$

When a specimen of PTX-2 was reacted with $NaBD_4$, the MNa^+ ion of the pair of reduction products formed in this reaction occurred at *m/z* 887, compared to *m/z* 885 for the products obtained when PTX-2 was reacted with $NaBH_4$. This is consistent with the introduction of two -CDOH- groups in the former compounds compared to two -CHOH- groups in the latter compounds via reduction of the 14-C=O and 36-hemiacetal groups present in the respective molecules.

The MNa^+ MS^2 mass spectrum of the more dominant of the two $NaBD_4$ reduction products formed in this reaction is shown in Figure 3-47. The dominant *m/z* 843 daughter ion seen in this mass spectrum can be attributed to the loss of CO_2 from the parent MNa^+ ion. Under MS^3 conditions, the *m/z* 843 ion (Figure 3-48) afforded an *m/z* 825 (H_2O loss) ion together with lower intensity *m/z* 741, 696, 514 and 351 ions. These ions appeared at *m/z* 739, 695, 513 and 351 in the analogous MS^3 mass spectrum of the $NaBH_4$ reduction product.

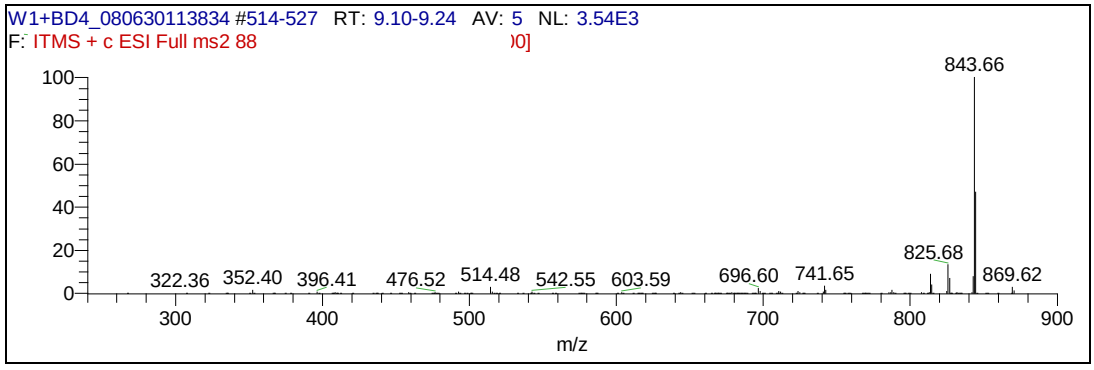

Figure 3-47: MS^2 mass spectrum of the *m/z* 887 MNa^+ ion of the major PTX-2/$NaBD_4$ reaction product.

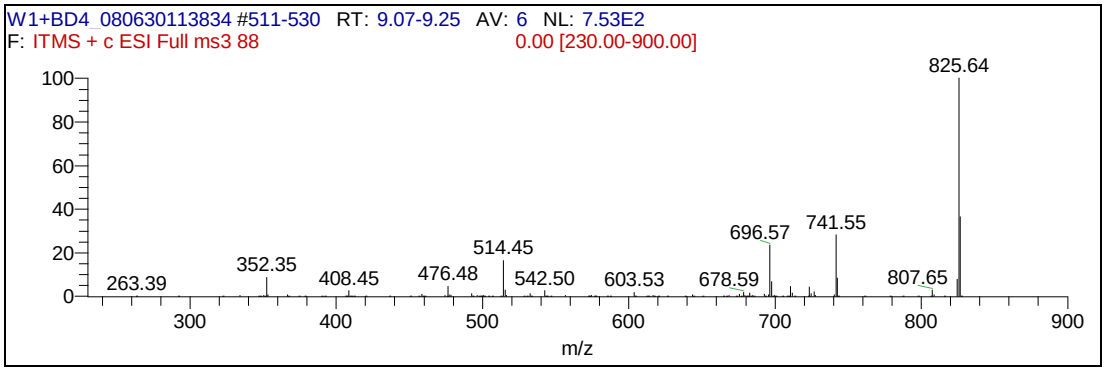

Figure 3-48: MS^3 mass spectrum of the *m/z* 887 → *m/z* 843 ion sequence from the major PTX-2/$NaBD_4$ reaction product.

3.7.4 MS^n analyses of PTX-2SA/$NaBH_4$ reaction products

The reaction of PTX-2SA with $NaBH_4$ only gave useable MNa^+ MS^2 and MS^3 mass spectra while the MNH_4^+ mass spectra were unacceptable to use for analyses. The reaction, as for the PTX-2 reaction, afforded reductions which possessed four addition hydrogen atoms. This is indicative of reduction of the 14-keto group and the 36-hemiacetal group.

The major daughter ion in the MS^2 mass spectrum (Figure 3-49) of the more dominant of the PTX-2SA reduction products occurred at *m/z* 859. This ion can be attributed to the loss of a CO_2 molecule. As was also the case for PTX-2, the *m/z* 859 ion showed a further loss of H_2O under MS^3 conditions (Figure 3-50) to afford an *m/z* 841 ion.

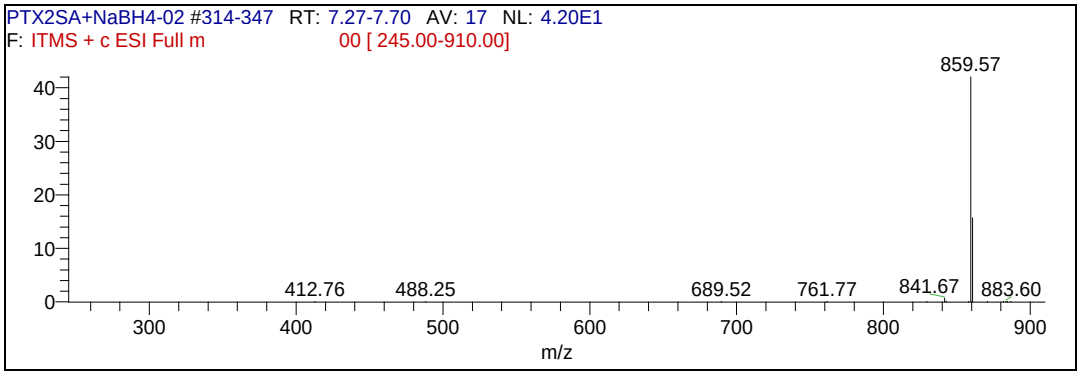

Figure 3-49: MS^2 mass spectrum of the *m/z* 903 ion from the major PTX-2SA/$NaBH_4$ reaction product.

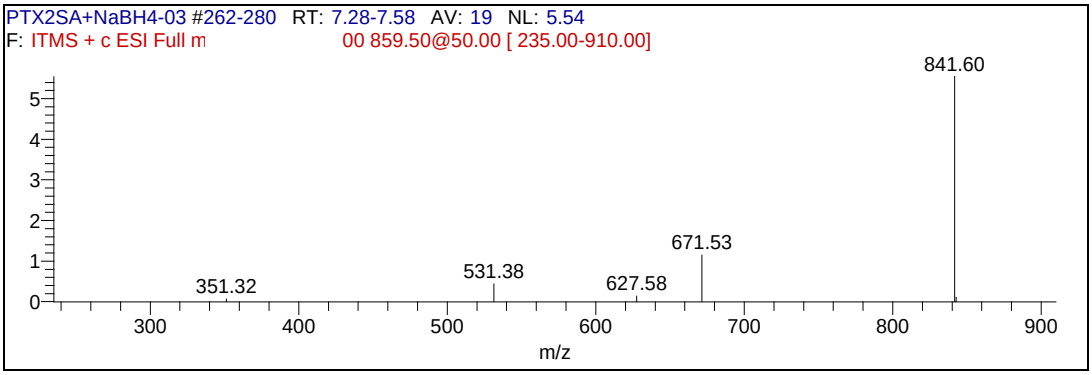

Figure 3-50: MS^3 mass spectrum of the *m/z* 903→ *m/z* 859 ion sequence from the major PTX-2SA/$NaBH_4$ reaction product.

Unlike PTX-2 (a neutral compound), PTX-2SA possesses a carboxyl group which can be ionized and consequentially afford useful negative ion mass spectral data. Only a structurally uninformative *m/z* 861 H_2O molecule loss daughter was observed in the negative ion *m/z* 879, $[M-H]^-$ MS^2 mass spectrum (Figure 3-51).

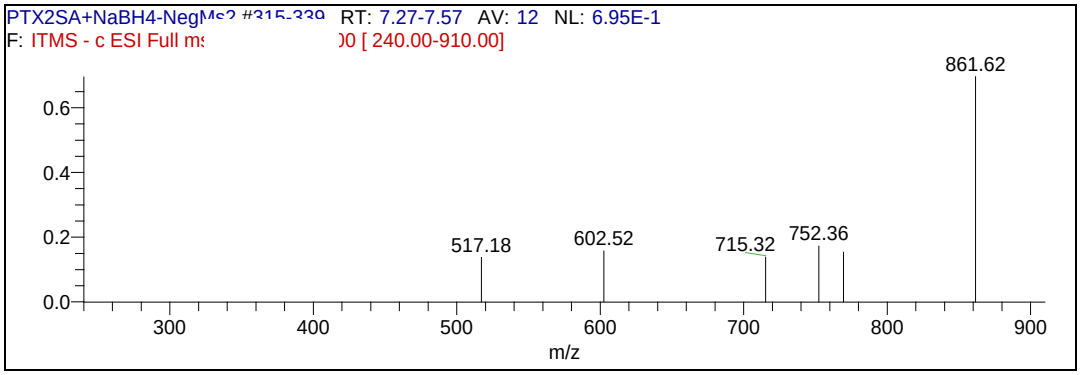

Figure 3-51: MS^2 mass spectrum of the *m/z* 879 MNa^+ ion from the major $NaBH_4$/PTX-2SA reaction product.

3.7.5 Reaction of PTX-2SA with $NaBD_4$

When a specimen of PTX-2 was reacted with $NaBD_4$ the MNa^+ ion of the pair of reduction products formed in this reaction occurred at *m/z* 905, compared to *m/z* 899 for the products obtained when PTX-2 was reacted with $NaBH_4$. This is consistent with the introduction of two -CDOH- groups in the former compounds compared to two -CHOH- groups in the latter compounds via reduction of the 14-C=O and 36-hemiacetal groups present in the respective molecules.

3.7.6 MS^n analyses of PTX-2SA/$NaBD_4$ reaction products

The MNa^+ MS^2 mass spectrum of the major $NaBD_4$ reduction product formed in this reaction is shown in Figure 3-52. The dominant *m/z* 861 daughter ion can be attributed to the loss of CO_2 from the parent MNa^+ ion. Under MS^3 conditions, the *m/z* 861 ion (Figure 3-53) afforded an *m/z* 843 (H_2O loss), together with low intensity *m/z* 672 and 532 ions. These ions occur at *m/z* 671 and 531 in the MS^3 mass spectrum of the analogous $NaBH_4$ reduction product (refer to Section 3.7.4).

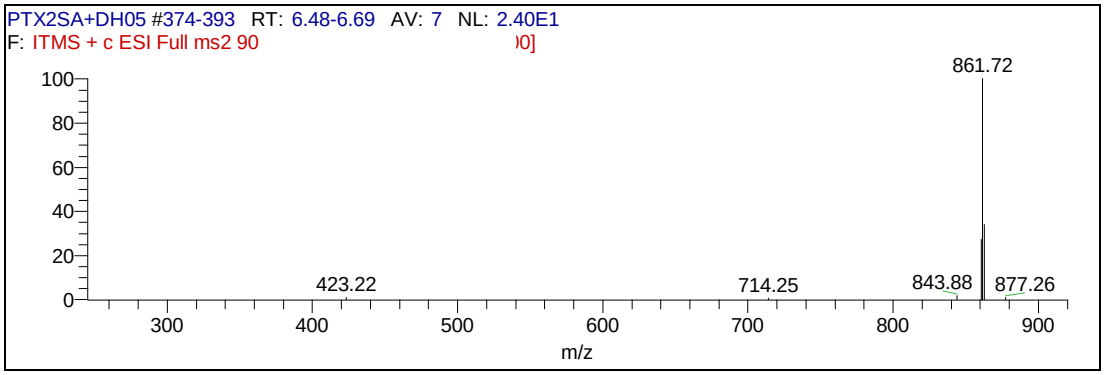

Figure 3-52: MS^2 mass spectrum of the *m/z* 905 ion from the major $NaBD_4$/PTX-2SA reaction product.

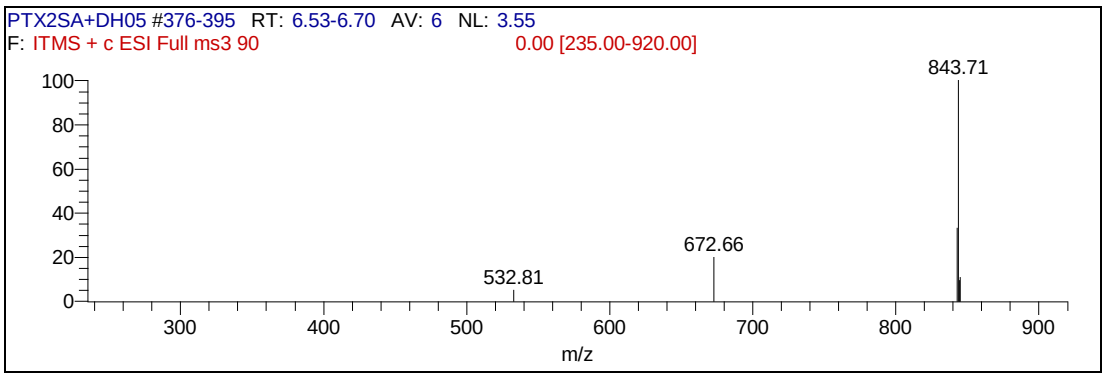

Figure 3-53: MS^3 mass spectrum of the *m/z* 905 → *m/z* 861 ion sequence from the major $NaBD_4$/PTX-2SA reaction product.

3.7.7 Reaction of the sulfonated seco-PTX-i isomers with $NaBH_4$ and $NaBD_4$

A small amount of a fraction recovered from the separation of an Irish extract during the isolation of PTX-2SA esters by other workers[20] was found to contain a moderate level of the sulfonated seco-PTX-i isomers.

Reaction of a sub-sample of this fraction with $NaBH_4$ afforded products which showed $[M-H]^-$ ions at *m/z* 945, compared to *m/z* 943 for sulfonated seco-PTX-i isomers (refer to Section 3.5.2). The addition of only two hydrogen atoms, compared to four hydrogen atoms when PTX-2SA was reacted with $NaBH_4$, is consistent with

the proposal that PTX-i and seco-PTX-i and sulfonated analogues of these compound posses a reducible 14-keto, but lack a 36-hemiacetal group.

3.7.8 MS^n analyses of sulfonated seco-PTX-i isomers/$NaBH_4$ reaction products

The dominant daughter ion observed for reaction products in *m/z* 945 negative ion $[M-H]^-$ MS^2 mass spectrum (Figure 3-54) occurred at *m/z* 865. This ion can be attributed to the loss of an SO_3 (an 80 Da loss).

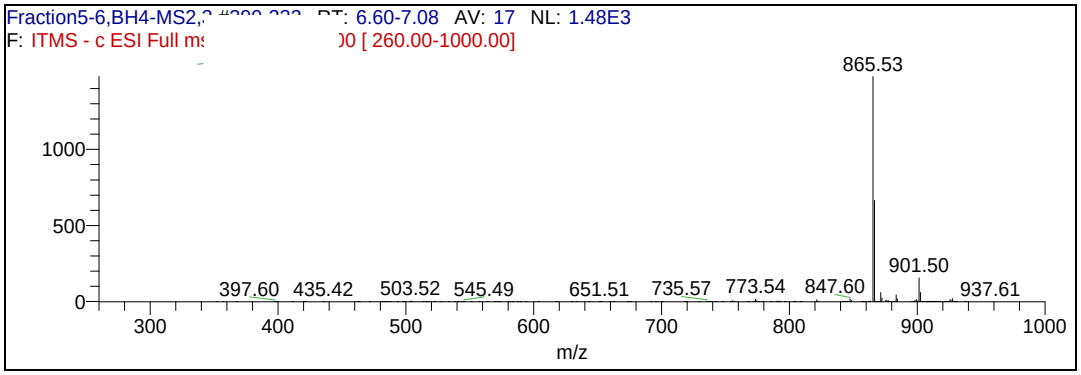

Figure 3-54: MS^2 mass spectrum of the *m/z* 945 ion from the major sulfonated seco-PTX-i isomers/$NaBH_4$ reaction product.

Under MS^3 conditions, the *m/z* 865 ion (Figure 3-55) afforded *m/z* 847 (H_2O loss), 821 (CO_2 loss), 773 and 545 ions.

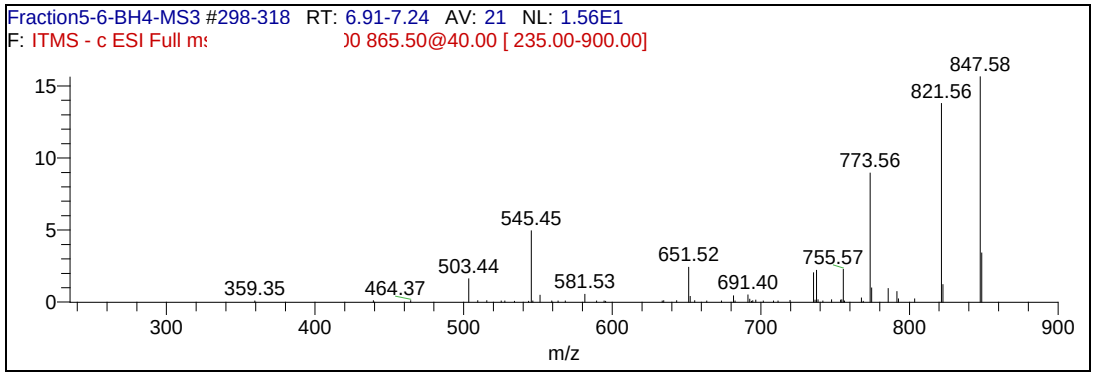

Figure 3-55: MS^3 mass spectrum of the *m/z* 945 → *m/z* 865 ion sequence from the major sulfonated seco-PTX-i isomers/$NaBH_4$ reaction product.

3.7.9 MS^n analyses of sulfonated seco-PTX-i isomers/$NaBD_4$ reaction products

Reaction of a sub-sample of this fraction with $NaBD_4$ afforded products which $[M-H]^-$ ions at *m/z* 946, compared to *m/z* 943 for parent sulfonated seco-PTX-i isomers (refer to Section 3.5.2). The three Da increase observed for the $[M-H]^-$ ion of the former compounds is consistent with the reduction of a 14-keto group to 14-CDOH group (refer to Section 3.7.3).

Under MS^2 conditions, the parent *m/z* 946 $[M-H]^-$ ion (Figure 3-56) afforded a daughter ion at *m/z* 866, attributable to the loss of a SO_3 group. Under MS^3 conditions, the *m/z* 866 ion (Figure 3-57) afforded *m/z* 848 (H_2O loss), 822 (CO_2 loss), 774, 652 and 546 ions. In the each case the mass of these ions is one greater than those seen in the MS^3 mass spectrum of the corresponding $NaBH_4$ reduction products (refer to Section 3.7.8).

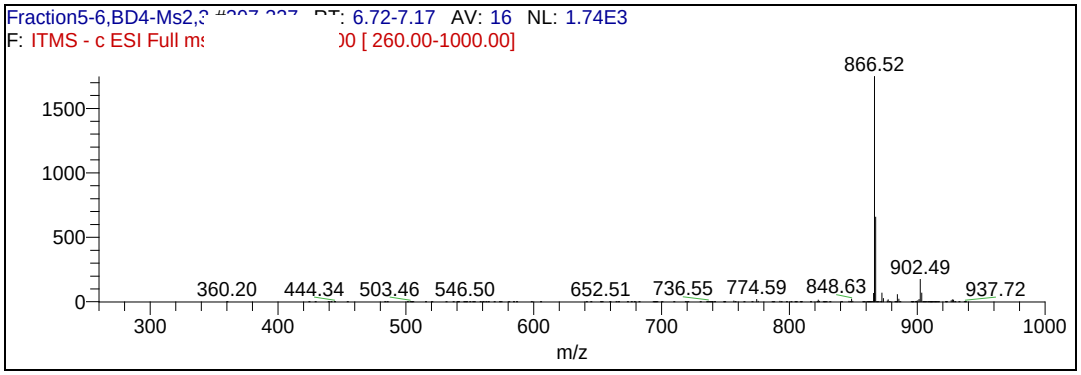

Figure 3-56: MS^2 mass spectrum of the $[M-H]^-$ *m/z* 946 ion from the major sulfonated seco-PTX-i isomers/$NaBD_4$ reaction product.

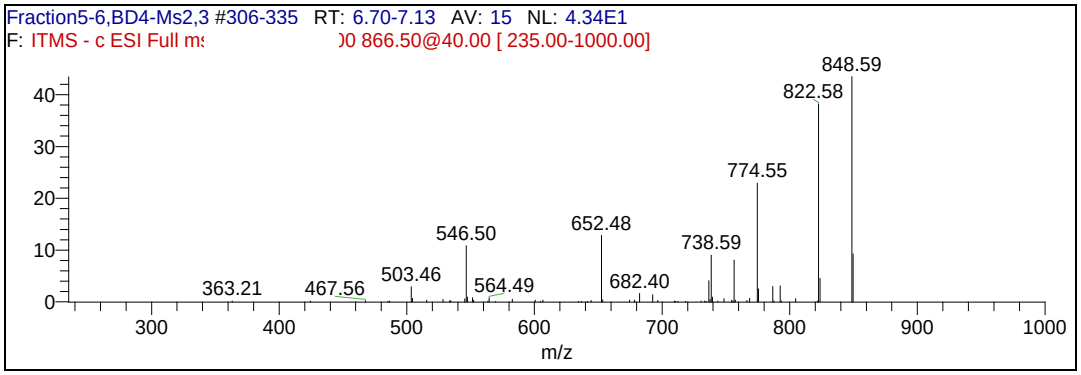

Figure 3-57: MS^3 mass spectrum $[M-H]^-$ of the *m/z* 946 → *m/z* 866 ion sequence from the major sulfonated seco-PTX-i isomers/$NaBD_4$ reaction product.

3.8 Sulfonated PTX-i esters

The following sections describe the detection and mass spectral analyses of the sulfonated PTX-i esters.

3.8.1 Introduction

Fatty acid esters of several groups of shellfish toxins have been reported. For example, fatty acids of okadaic acid are collectively known as DTX-3[14]. The dominant DTX-3 ester is the 16:0 ester – i.e. the palmitic acid ester. Fatty acids of spirolides and PTX-2SA are also known[20].

A series of PTX-2SA esters with 14 to 22 carbon ester groups were first detected in the LCMS analyses of sub-samples of the Irish extracts[20]. Subsequently, a separation of a bulk quantity of the Irish material afforded sufficient quantities of the dominant 16:0 and 22:6 esters for their structures to be defined using one and two-dimensional 600 MHz NMR data[20]. This data showed that the ester moieties were attached to C-37. Detailed MS^n LCMS analyses showed that in addition to C-37 esters, lower levels of C-35 and C-11 esters were also present in the extracts. Appreciable quantities of the 14:0, 16:0, 16:1, 18:4, 20:5 and 22:6 esters of PTX-2SA

and 7-*epi*-PTX-2SA were identified in $LCMS^n$ analyses, together with low to trace levels of some other esters including 15:0, 16:2, 17:0, 18:2 and 18:1 analogues[20].

The known presence of PTX-2SA ester in the bulk Irish extracts which were found to contain non-sulfonated and sulfonated PTX-i compounds (refer to Sections 3.3-3.5), prompted a search for esters of PTX-i and sulfonated analogue of PTX-i. These searches, which were performed in both positive and negative ion modes, revealed the presence of esters (predominantly the 16:0 ester) of sulfonated PTX-i compounds. Non-sulfonated PTX-i esters were not detected.

3.8.2 MS^n analyses of the $[M-H]^-$ ions of the 16:0 esters of sulfonated PTX-i

An account of the MS^n characterisation of the dominant sulfonated-PTX-i 16:0 ester is presented in the following sections.

3.8.2.1 MS^2 analyses of *m/z* 1163 $[M-H]^-$ ion of the 16:0 ester of sulfonated PTX-i

Since sulfonated PTX-i compounds were more readily detected in negative ion LCMS analyses than in positive ion analyses, the presence of the 16:0 ester (and also related analogues: refer to Table 3-1, Section 3.8.4) was initially probed in negative ion *m/z* 1163 MS^2 analyses.

Given the general esterification formula (acid + ROH → ester + H_2O), it was reasoned that the $[M-H]^-$ ion of 16:0 ester of PTX-i sulfates would occur at *m/z* 1163 (since 925+256-18 = 1163). Accordingly, a negative ion *m/z* 1163 MS^2 LCMS analyses was undertaken. The resulting full scan MS^2 profile is shown in Figure 3-58. Several of the peaks exhibited MS^2 mass spectra which were consistent with their identification as the 16:0 esters of sulfonated PTX-i compounds, including the dominant peak which occurred at 8.96 min.

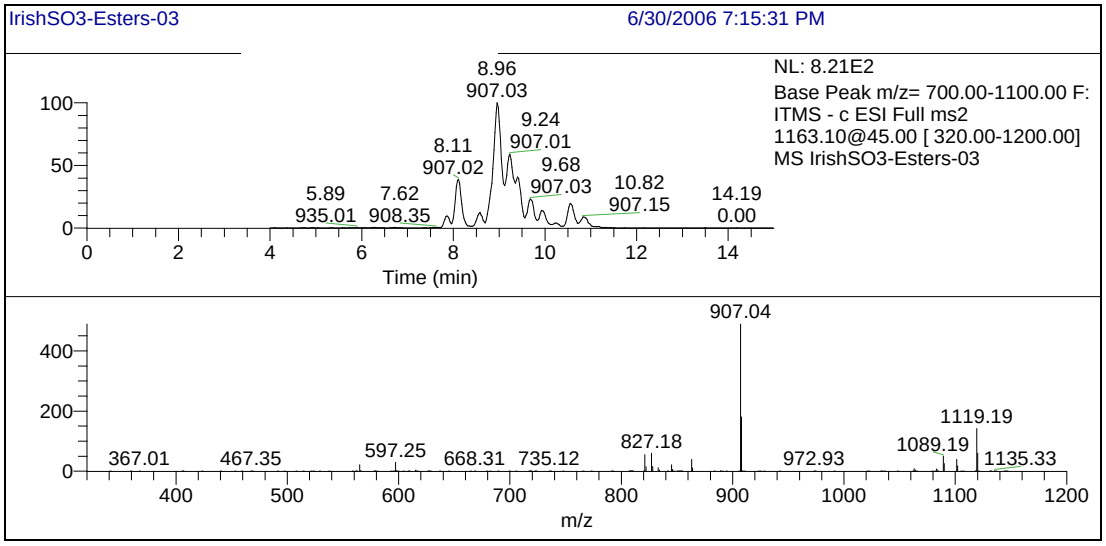

Figure 3-58: Extracted ion trace (top) and MS^2 mass spectrum of the dominant *m/z* 1163 16:0 fatty acid ester ion (bottom).

The daughter ion which appeared at *m/z* 907 can be attributed to the loss of the 16:0 ester moiety as palmitic acid (256 Da) while the *m/z* 1119 daughter ion can be attributed to the loss of a CO_2 molecule (44 Da) as is commonly seen in the MS^2 mass spectra of PTX-2 analogues.

3.8.2.2 MS^3 analyses of the *m/z* 1163 → *m/z* 907 ion sequence of the of the 16:0 ester of sulfonated PTX-i

The MS^3 mass spectrum determined for the *m/z* 907 daughter ion (Figure 3-59) was consistent with it arising for a sulfonated PTX-i analogue. The *m/z* 889 ion seen in the MS^3 mass spectrum can be attributed to the loss of H_2O from the *m/z* 907 ion while the *m/z* 863 and 827 ions can be attributed to the loss of CO_2 (44 Da) and SO_3 (80 Da) molecules respectively.

Since the ion at *m/z* 565 has a difference of 342 Da from the *m/z* 907 ion (or 298 Da from the *m/z* 863 ion) it can be attributed to the loss of the upper portion of the PTX-2 like skeleton believed to be present in PTX-i analogues (refer to Sections 3.1, 3.2 and 3.3).

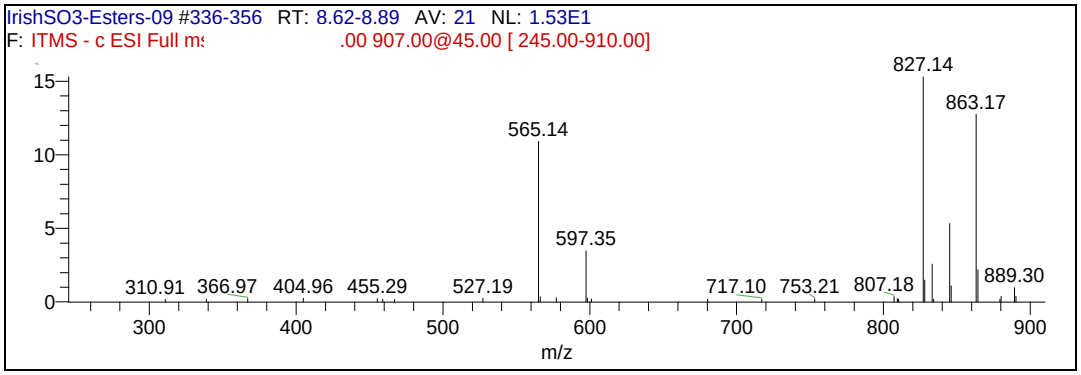

Figure 3-59: MS^3 mass spectrum of the *m/z* 1163 → *m/z* 907 ion sequence for the dominant sulfonated PTX-i 16:0 ester.

The *m/z* 500-700 region of the negative ion *m/z* 925 MS^2 and *m/z* 925 → *m/z* 907 MS^3 mass spectra of the dominant sulfonated PTX-i compound (upper two mass spectra) and the negative ion 1163 MS^2 and *m/z* 1163 → *m/z* 907 of the dominant sulfonated PTX-i 16:0 ester are compared in Figure 3-60. It is readily apparent that there are marked similarities in the pairs of MS^2 and MS^3 mass spectra. In particular, *m/z* 565 and 597 ions appear in each of the MS^2 and MS^3 mass spectra.

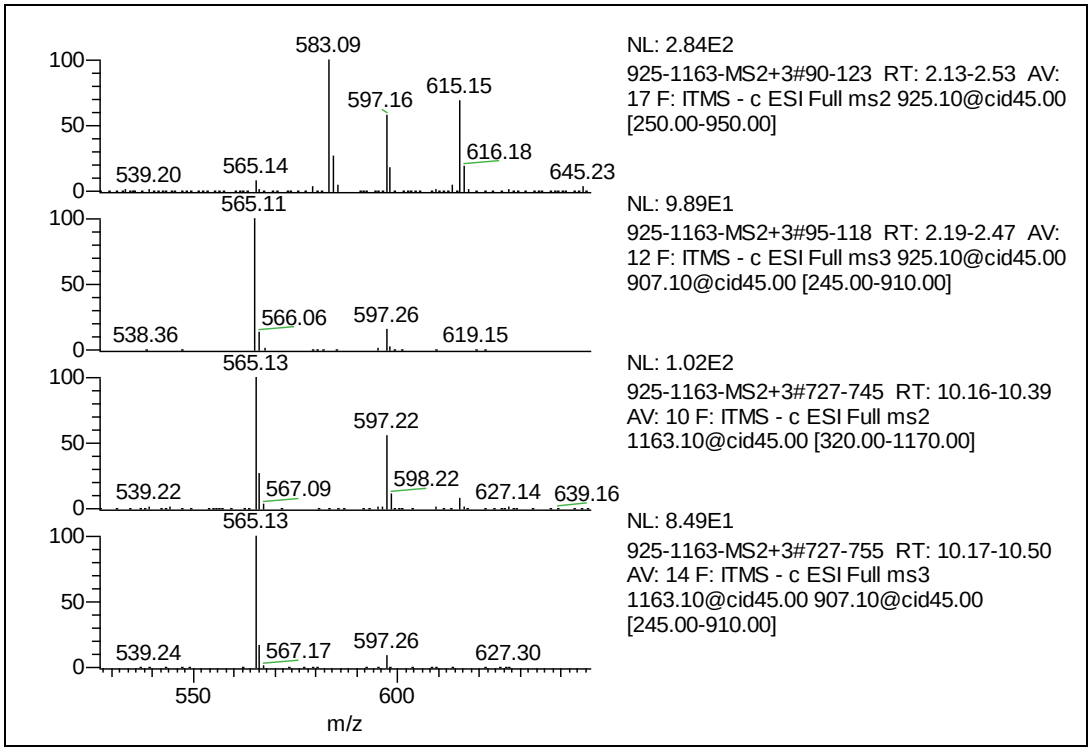

Figure 3-60: Comparison of the negative ion *m/z* 925 MS^2 and *m/z* 925 → *m/z* 907 MS^3 mass spectra (upper pair) and *m/z* 1163 MS^2 and *m/z* 1163 → *m/z* 907 MS^3 mass spectra (lower pair) determined for the dominant sulfonated PTX-i and sulfonated PTX-i 16:0 ester.

3.8.2.3 MS^4 analyses of the *m/z* 1163 → *m/z* 907 → *m/z* 863 ion sequence for the dominant sulfonated PTX-i 16:0 ester

Two useable MS^4 mass spectra were obtained for daughter ions derived from the *m/z* 1163 ion. The first of these spectra was derived from the *m/z* 1163 → *m/z* 907 (-256 Da) → *m/z* 863 (-44 Da) ion sequence (Figure 3-61). The resulting MS^4 mass spectrum showed the loss of 298 Da to afford an *m/z* 565 ion analogous to that seen in some MS^3 mass spectra (see above).

The loss of 44 Da followed by the 298 Da (total 342 Da) is a well known feature of the positive ion MNa^+ MS^2 and MS^3 mass spectra of PTX-2 and PTX-2SA analogues (refer to Sections 3.1, 3.2 and 3.3). It is apparent that in sulfonated PTX-i analogues

the loss of 298 or 342 Da residues can also occur in negative ion MS^n mass spectra where a readily ionisable group such as a sulfate group is present.

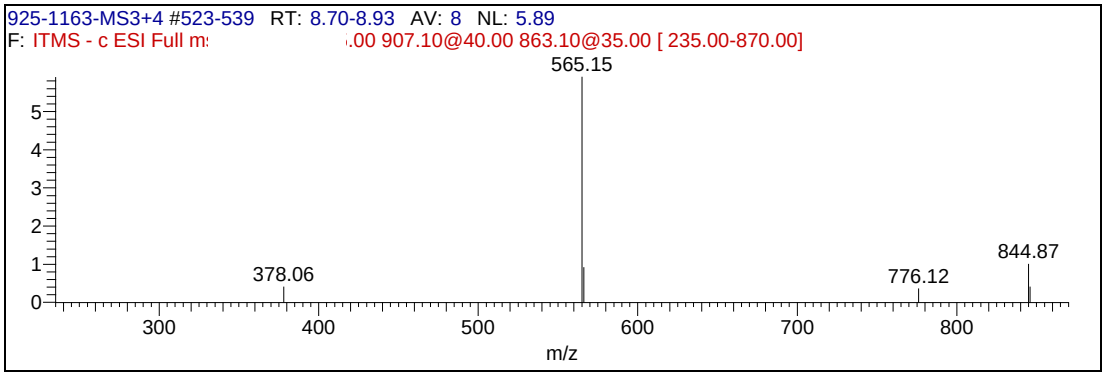

Figure 3-61: MS^4 mass spectrum of the ions *m/z* 1163 → *m/z* 907 → *m/z* 863 ion sequence for the dominant sulfonated PTX-i 16:0 ester.

3.8.2.4 MS^4 analyses of the *m/z* 1163 → *m/z* 907 → *m/z* 827 ion sequence for the dominant sulfonated PTX-i 16:0 ester

The second MS^4 mass spectrum was obtained from the *m/z* 1163 → *m/z* 907 (-256 Da) → *m/z* 827 (-SO_3) ion sequence. The resulting MS^4 mass spectrum has little structural significance since only a H_2O loss *m/z* 809 could be recognised in the low signal to noise spectrum (Figure 3-62).

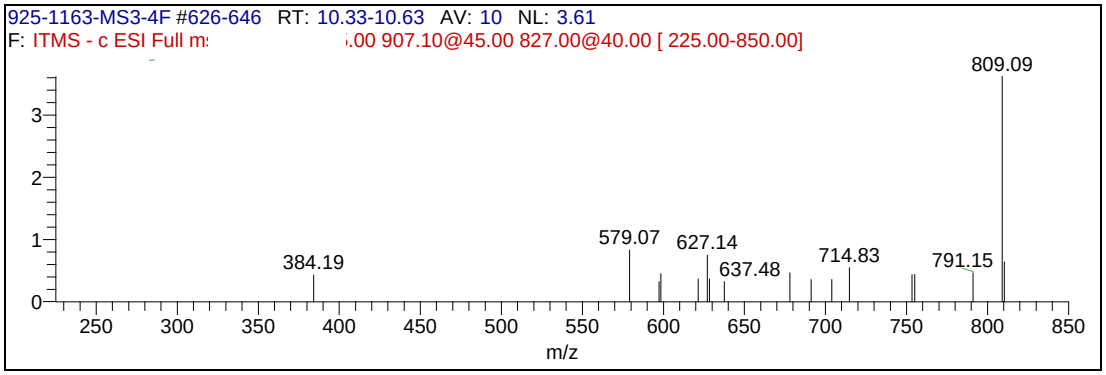

Figure 3-62: MS^4 mass spectrum of the *m/z* 1163→ *m/z* 907→ *m/z* 827 ion sequence for the dominant sulfonated PTX-i 16:0 ester.

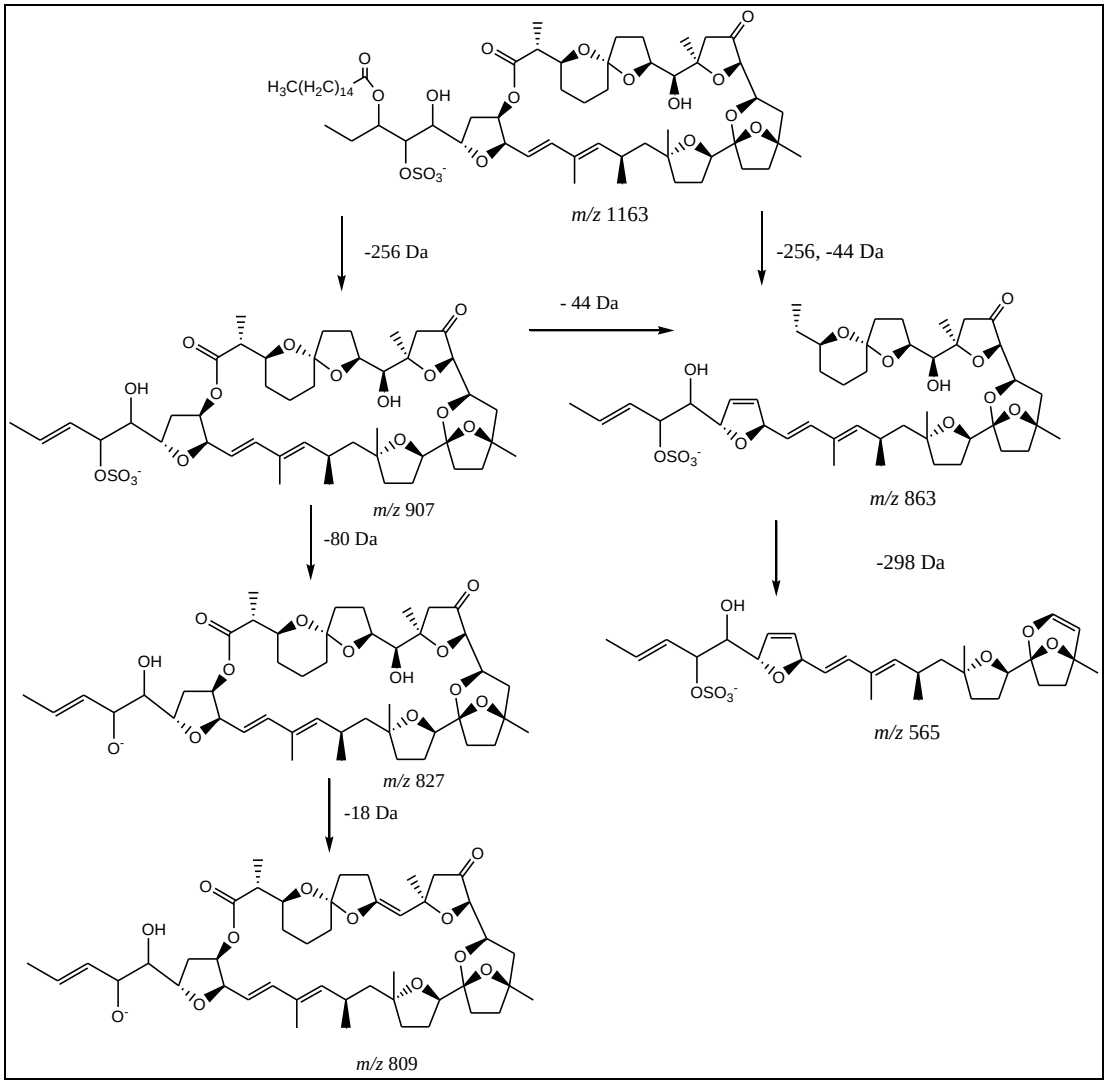

Figure 3-63: Scheme showing possible structures of some ions seen in MS^2, MS^3 and MS^4 mass spectra of the sulfonated PTX-i 16:0 ester.

A scheme of the possible structures of ions seen in the various MS^2, MS^3 and MS^4 mass spectra of the *m/z* 1163 $[M-H]^-$ 16:0 sulfonated ester ion is given in Figure 3-63. Two possible routes are shown depending on which ion is formed first.

3.8.3 MS^n analyses of the MNa^+ and MNH_4^+ ions of the sulfonated PTX-i 16:0 ester

The following sections describe the mass spectral analyses of the sulfonated PTX-i 16:0 ester.

3.8.3.1 MS^2 analyses of the *m/z* 1209 MNa^+ ion

It can be reasoned that in positive ion mode, the 16:0 ester analogue of the *m/z* 971 $[R\text{-}OSO_3Na]Na^+$ type ion which characterised sulfonated PTX-i compounds (refer to Section 3.4.1), would occur at *m/z* 1209 (971+256-18 = 1209). Coincidentally, this is the same *m/z* value as that of the 20:5 ester of PTX-2SA and its 7-*epi* isomer[20].

Examination of historic *m/z* 1209 MNa^+ MS^2 data files (Figure 3-64) available from the investigation that lead to the identification of the 20:5 ester of PTX-2SA and the 7-*epi* isomer of this compound[20] revealed the presence of an earlier eluting peak (18.1 min), *ca.*10% the size of the PTX-2SA ester peak (21.0 min), that exhibited a MS^2 mass spectrum for an $[R\text{-}OSO_3Na]Na^+$ type ion that showed it to be a sulfonated PTX-i 16:0 ester. The MS^2 mass spectrum shown included in Figure 3-64 is identical to that shown in Figure 3-65.

It is of note that there were fewer sulfonated PTX-i ester peaks seen in this plot which was recorded in 2005 than was the case for data recorded in later years. These observations support the belief that some of the PTX-i and PTX-i analogue peaks detected in the more recent investigations are storage artefacts (isomers) of compound(s) originally present in the bulk Irish extracts.

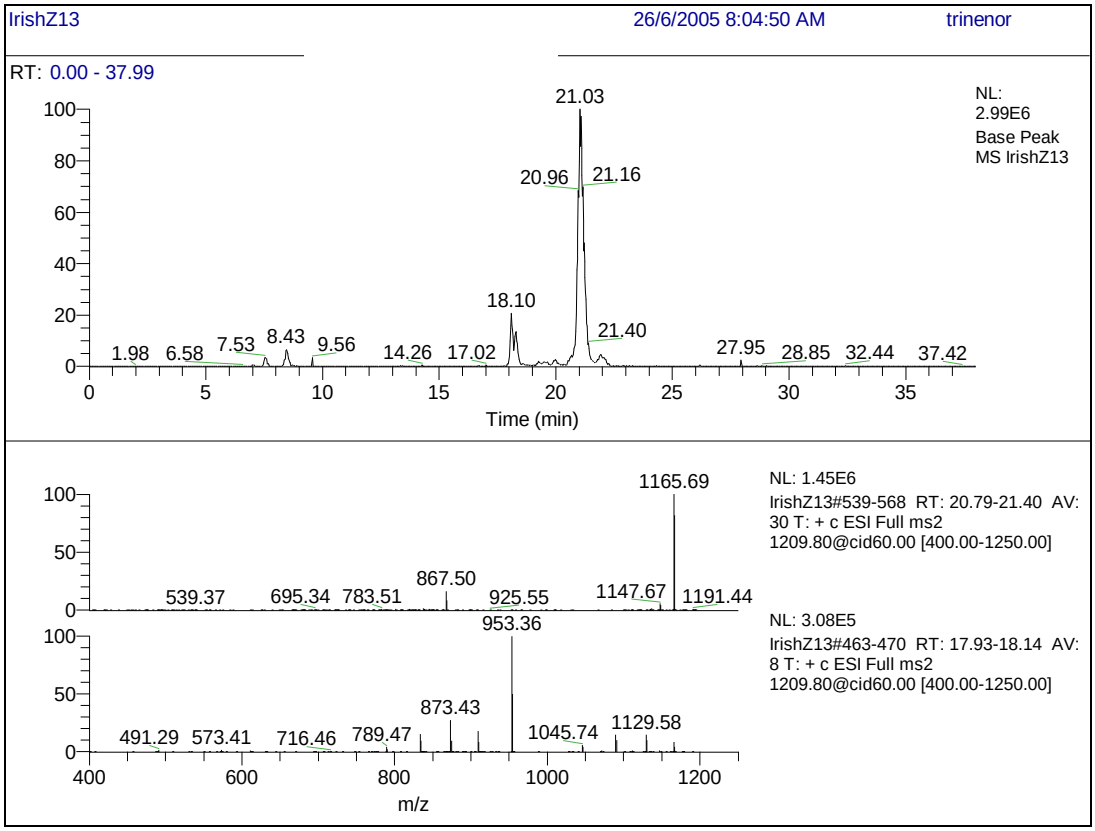

Figure 3-64: Extracted ion trace of *m/z* 1209 (upper) determined in 2005 for a bulk Irish extract sub-sample and MS^2 mass spectra of peaks eluting at 21.03 min (PTX-2SA 22:6 ester: base peak at *m/z* 1165) and 18.10 min (sulfonated PTX-i 16:0 ester: base peak at *m/z* 953) (lower).

Positive ion analyses were performed on sub-samples of the bulk Irish extract and a fraction recovered from a small scale C-18 column separation of portion of the bulk Irish sample by a co-worker (Mr K. Larsen) 12 months earlier as part of another investigation under way in our laboratories. LCMS analyses of retained sub-samples of the C-18 column fractions in both positive and negative ion modes identified a fraction that possessed a level of the sulfonated PTX-i 16:0 ester that was sufficient for the determination of the positive ion MS^2, MS^3 and MS^4 mass spectra of several sulfonated PTX-i 16:0 esters (see below).

When the C-18 column fraction was examined in *m/z* 1209 MS^2 mode, several peaks were found to exhibit MS^2 mass spectra which were consistent with their

identification as sulfonated PTX-i 16:0 esters. For example, the peak which eluted at 25.47 min (Figure 3-65) showed a dominant daughter at *m/z* 953 attributable to the loss of the ester moiety.

Other structurally significant daughter ions appeared at *m/z* 1165 (CO_2 loss), *m/z* 1129 (SO_3 loss), *m/z* 1089 ($NaHSO_4$ loss), *m/z* 1045 ($NaHSO_4$ and CO_2 loss), *m/z* 909 (loss of palmitic acid and CO_2), *m/z* 873 (loss of palmitic acid and SO_3), *m/z* 833 (loss of palmitic acid and $NaHSO_4$) and *m/z* 789 (loss of palmitic acid, $NaHSO_4$ and CO_2).

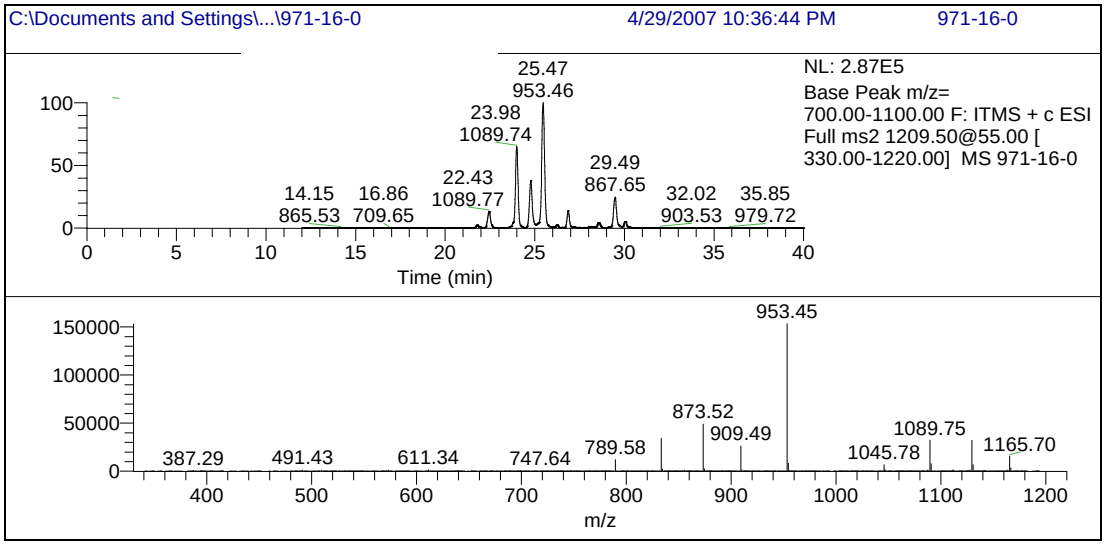

Figure 3-65: Extracted ion trace of the *m/z* 1209 ion (top) with the MS^2 mass spectrum of the *m/z* 1209 ion (bottom).

3.8.3.2 MS^3 and MS^4 analyses of the *m/z* 1209 daughter ions of the sulfonated PTX-i 16:0 ester

Under MS^3 conditions, the *m/z* 1191 (H_2O loss) ion (Figure 3-66) afforded *m/z* 1147, 1071 and 867 ions, attributable to losses of CO_2 (44 Da), SO_3 (80 Da) and 324 Da. The 324 Da loss can be attributed to the loss of the upper portion of the PTX-2 skeleton (342 Da) believed to present in PTX-i analogues, after the loss of H_2O for

this portion of the structure in the initial MS^2 step, thus a loss of 324 Da (342-18 Da) is seen in the MS^3 mass spectrum.

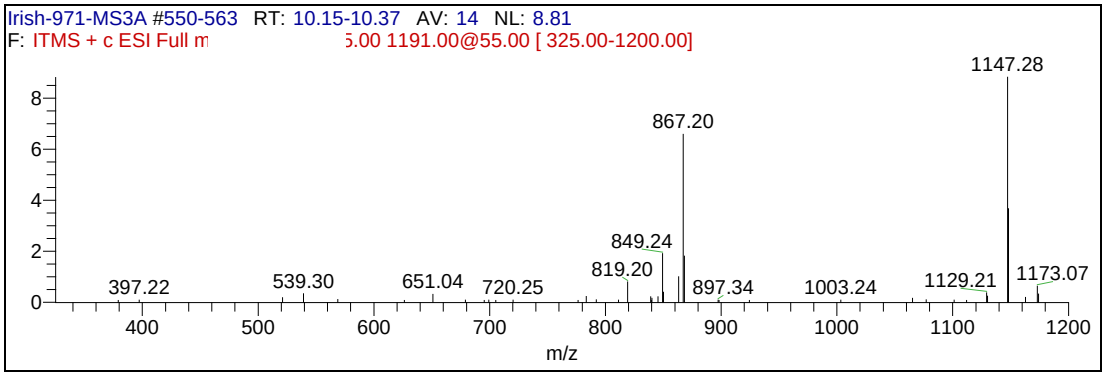

Figure 3-66: MS^3 mass spectrum of the *m/z* 1209 → *m/z* 1191 ion sequence from the dominant *m/z* 1209 compound.

Under MS^3 conditions, the *m/z* 1165 (CO_2 loss) ion (Figure 3-67) predominantly afforded an *m/z* 867 ion, attributable to the loss of the upper portion the PTX-2 skeleton (342 Da) believed to be present in PTX-i analogues after prior loss of CO_2 in the MS^2 step.

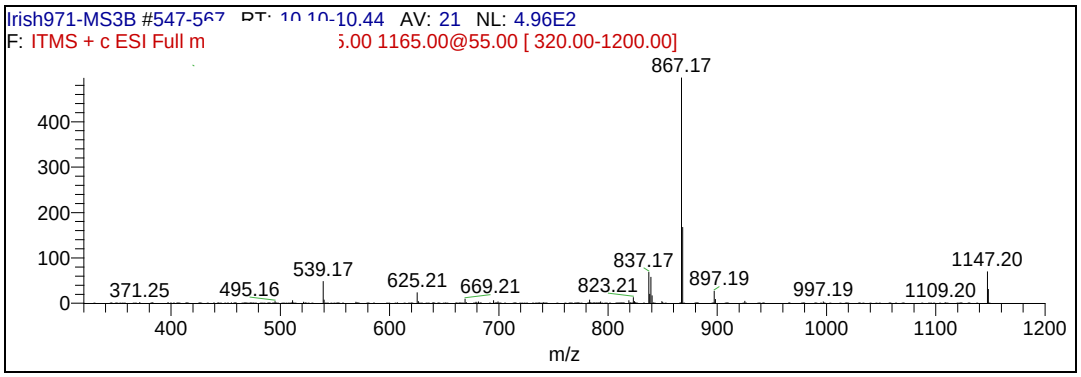

Figure 3-67: MS^3 mass spectrum of the *m/z* 1209 → *m/z* 1165 ion sequence from the dominant *m/z* 1209 compound.

Under MS^3 conditions, the *m/z* 1129 (SO_3 loss) ion (Figure 3-68) included *m/z* 1033 and *m/z* 873 ions attributable to loss of a 96 Da residue and loss of palmitic acid (256 Da) respectively.

In the absence of high resolution mass data, the 96 Da loss cannot be formulated with certainty however it appears to be associated with the prior loss of an SO_3 molecule from the sulfonated and presumably also an esterfied $C_5H_{11}O_3$ side chain (refer to Section 3.3.3) attached to C-36. The 96 Da loss appears to be analogous to that observed in the *m/z* 971 → *m/z* 891 MS^3 mass spectrum of sulfonated PTX-i compounds (refer to Section 3.4.3.3).

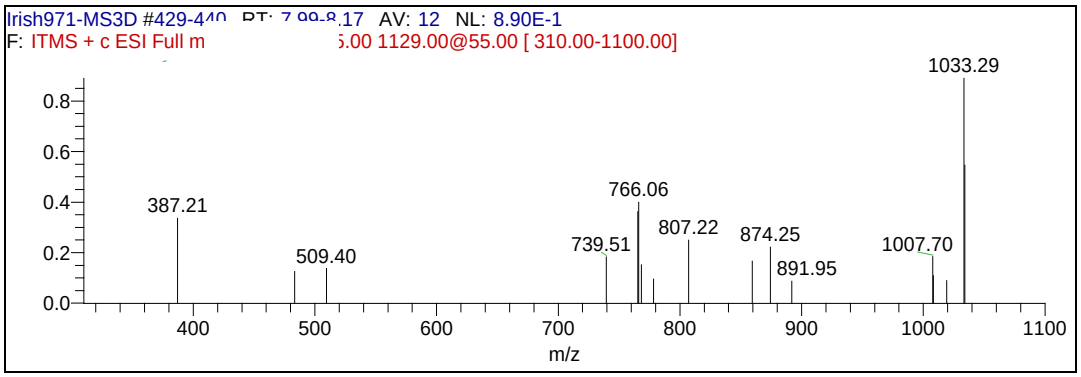

Figure 3-68: MS^3 mass spectrum of the *m/z* 1209 → *m/z* 1129 ion sequence from the dominant *m/z* 1209 compound.

Under MS^3 conditions, the *m/z* 1089 ($NaHSO_4$ loss) ion (Figure 3-69) afforded *m/z* 104, 833 and 747 ions, attributable to the loss of CO_2 (44 Da), palmitic acid (256 Da) and the upper portion of the PTX-2 skeleton (342 Da) believed to be present in PTX-i analogues respectively.

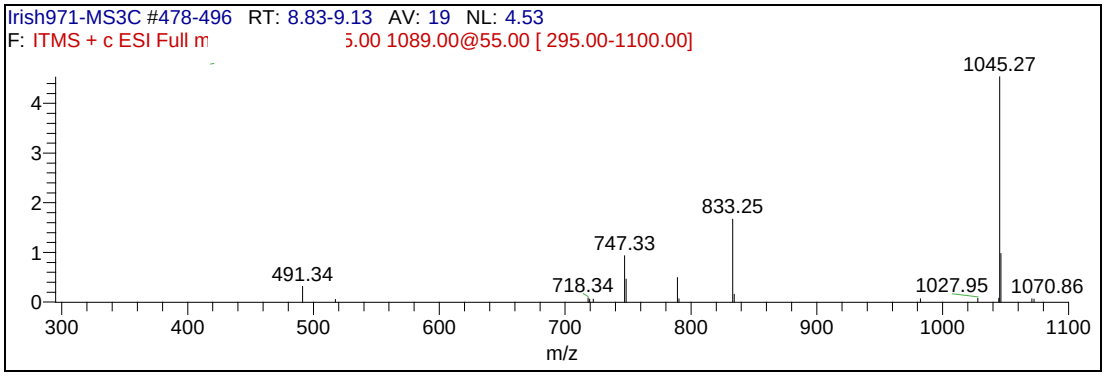

Figure 3-69: MS^3 mass spectrum of the *m/z* 1209 → *m/z* 1089 ion sequence from the dominant *m/z* 1209 compound.

Attempts were made to acquire MS^3 mass spectra from some of the lower mass daughter ions seen in the MS^2 mass spectrum of the parent sulfonated 16:0 ester however this only produced unsatisfactory spectra.

MS^4 fragmentation of the ions detected in the foregoing MS^3 mass spectra was also attempted. Only one, the *m/z* 1209 → *m/z* 1165 → *m/z* 1045 ion sequence afforded a satisfactory MS^4 mass spectrum (Figure 3-70).

MS^4 fragmentation of the *m/z* 1045 ion generated via *m/z* 1165 (CO_2 loss) and *m/z* 1045 ($NaHSO_4$ loss) in prior MS^2 and MS^3 steps respectively afforded *m/z* 789 and *m/z* 747 ions attributable to the loss of palmitic acid (256 Da) and the upper portion of the PTX-2 skeleton (298 Da) after prior loss of C-1 carboxyl group as CO_2 in the MS^2 step.

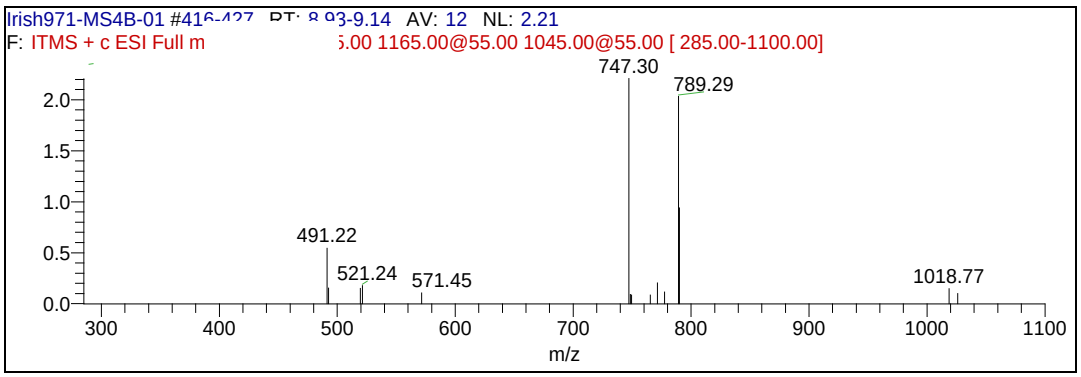

Figure 3-70: MS^4 mass spectrum of the *m/z* 1209 → *m/z* 1165 → *m/z* 1045 ion sequence from the dominant *m/z* 1209 compound.

Positive ion MS^2 analyses targeting the $[R–OSO_3NH_4]NH_4^+$ variant (*m/z* 1199) of the *m/z* 1209 $[R\text{-}OSO_3Na]Na^+$ ion utilised in the MS^2 studies described in preceding sections, afforded the MS^2 mass spectrum shown in Figure 3-71. This spectrum included daughter ions at *m/z* 1181, 1155 and 857, attributable to the loss of H_2O (18 Da), CO_2 (44 Da) and the upper portion of the PTX-2 skeleton (342 Da) believed to be present in PTX-i analogues.

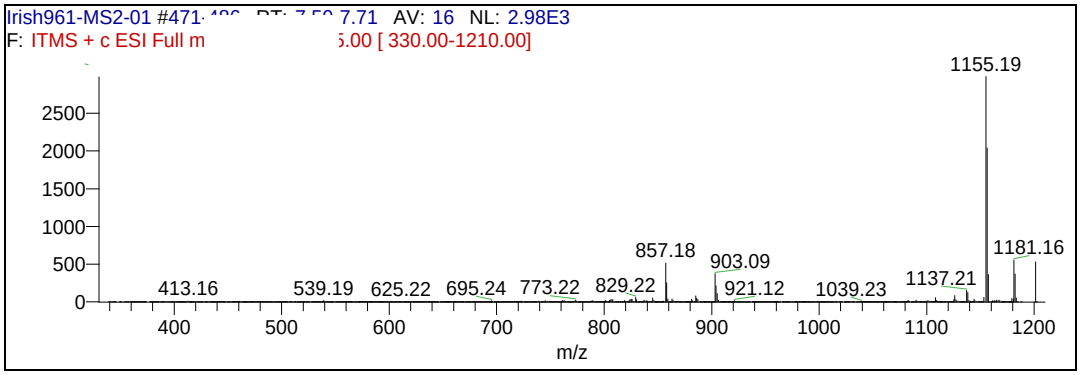

Figure 3-71: MS^2 mass spectrum of the *m/z* 1199 ion from the dominant *m/z* 1199 compound.

3.8.4 Characterisation of other esters

Examination of unseparated sub-samples of the bulk Irish extracts in targeted MS^2 mass spectral analyses performed in both positive and negative ion modes showed that while sulfonated 16:0 PTX-i esters were the dominant esters present in the Irish extracts that were available for LCMS, lesser amounts of other esters were also present.

Irrespective of the ester chain length, negative ion MS^2 mass spectra were characterised by a dominant *m/z* 907 ion (refer to Section 3.5.1) arising to the loss of the ester group as the corresponding fatty acid.

Integration of the *m/z* 907 peak areas observed for the dominant peak observed in each of the MS^2 analyses, which were performed under identical condition (gradient elution conditions, amount injected etc) afforded an estimate of the relative contributions of detected esters (refer to Table 3-1).

The most abundant of the esters was the 16:0 ester (64.1% of total detected esters) followed by the 16:1 ester (11.7%) and low levels of the 14:0, 15:0, 17:0, 18:4, 22:5 and 22:6 esters. 16:3, 16:2, 18:3, 18:2, 18:1 and 18:0 esters were not detected.

Table 3-1: Negative ion $[M-H]^-$ ions, *m/z* 907 ion peak areas, relative levels of *m/z* 907 ion areas and % total detected fatty acid esters detected in a bulk Irish extract.

Ester	MS^2 ion (*m/z*)	*m/z* 907 ion peak area	Relative level of *m/z* 907 ion areas	% total detected fatty acid esters
14:0	1135	525	0.06	4.2
15:0	1149	130	0.02	1.0
16:3	1157	-	-	-
16:2	1159	-	-	-
16:1	1161	1469	0.18	11.7
16:0	1163	8084	1.00	64.1
17:0	1177	605	0.07	4.8
18:4	1183	744	0.09	5.9
18:3	1185	-	-	-
18:2	1187	-	-	-
18:1	1189	-	-	-
18:0	1191	-	-	-
20:5	1209	526	007	4.2
22:6	1235	328	0.06	4.4

The data presented in Table 3-1 needs to be interpreted with caution since, based on LCMS results recorded over a 2 year period, it is believed that a number of the PTX-i isomer peaks detected in stored (aged) Irish samples has increased with time. It is also of note that the sulfonated PTX-i 16:0 ester fraction recovered from a small scale C-18 column by Mr K. Larsen appeared to contain more of the sulfonated PTX-i 16:0 ester isomer peaks than was the case before the extract was applied to the C-18 column.

The progressive conversion of PTX-2SA to 7-*epi*-PTX-2SA over time is well documented[13]. Given this tendency, it is considered likely that some of the PTX-i peaks detected in the LCMS studies described in preceding Sections of this chapter

will transpire to be artefacts of compound(s) originally present in the aged (stored) extracts that were available for analysis in the present study.

Extraction and processing of newly collected mussel and algal water extracts under carefully controlled conditions needs to be undertaken in order to identify naturally occurring PTX-i type compounds and processing/handling induced conversion of naturally occurring compounds to artefact variants.

3.9 Examination of three NZ extracts for PTX-i analogues

The three newly prepared extracts from stored New Zealand algal water extracts were systematically examined in positive and negative ion full scan and MS^2 modes for the presence of the PTX-i analogue reported in this thesis, namely free, sulfonated and sulfonated esters, using the Waikato LCQ system and the NVI LTQ system. PTX-i and its analogues were not detected in any of the New Zealand extracts.

3.10 Summary

The investigations reported in this chapter have identified the MS characteristics of a hitherto unknown group of PTX-2 like analogues and defined the MS^n ions (ion trap based LCMS systems) or SRM ion data (triple quad MS systems) that can be used to detect the new compounds in mussel or algal water extracts.

Whilst the gross structures of the new group of PTX-i compounds have not been established, it is apparent that they possess a PTX-2 like structure that is devoid of a 36-hemiacetal group. The terminal hemiacetal ring system is believed to have been replaced by a $C_5H_{11}O_3$ side chain attached to C-35. Sulfate and fatty acid residues are believed to be attached to two of the hydroxyl groups present in the C-35 side chain. Possible structures for the C-35 side chain include those presented in Figure 3-18. It is possible there may be major and minor isomeric forms of the oxygenated five carbon side chain believed to be attached to C-35.

Further work should be directed towards the isolation of a quantity of one or more of the new PTX-i compounds sufficient for one and two-dimensional NMR analysis. Based on the results reported in the Sections 3.3-3.7, the best isolation candidates appear to be the PTX-i sulfate and its 16:0 ester.

Chapter 4

MS^n Characterisation of Reduced PTX-2SA Analogues

4.0 Introduction

During searches for other previously unidentified algal toxins in several historic Irish and three newly prepared New Zealand algal water extracts, two peaks were detected in positive ion full scan analyses that showed *m/z* 896 and 901 ion responses. A five mass difference is characteristic of a MNH_4^+/MNa^+ ion pair. This pair of ions, if they arise for a PTX-like compound, differ by 20 Da from the MNH_4^+/MNa^+ ion pair observed for PTX-2 (*m/z* 876 and *m/z* 881 respectively) or two Da from the MNH_4^+/MNa^+ ion pair observed for PTX-2SA (*m/z* 894 and 899 respectively).

4.1 MS^n analyses of the *m/z* 896 and *m/z* 901 ions

The following sections describe the mass spectral analyses of the *m/z* 896 and 901 ions.

4.1.1 MS^2 analyses of the *m/z* 896 MNH_4^+ ion

The MNH_4^+ MS^2 mass spectrum of the *m/z* 896 ion is shown in Figure 4-1. The higher mass region included a weak 18 Da (H_2O) loss ion at *m/z* 878 together with a 35 Da (NH_4OH) loss ion at *m/z* 861 and a subsequent series of H_2O loss ions at *m/z* 843 ($-H_2O$), *m/z* 825 ($-2H_2O$), *m/z* 807 ($-3H_2O$) and *m/z* 789 ($-4H_2O$).

Comparison of the *m/z* 894 MS^2 mass spectrum of PTX-2SA NH_4^+ (*m/z* 894) and the MS^2 mass spectrum of one of the peaks which showed a *m/z* 896 MNH_4^+ ion response is presented in Figure 4-2. This figure highlights the two Da difference between the daughter ions in the *m/z* 880-900 regions of the two mass spectra.

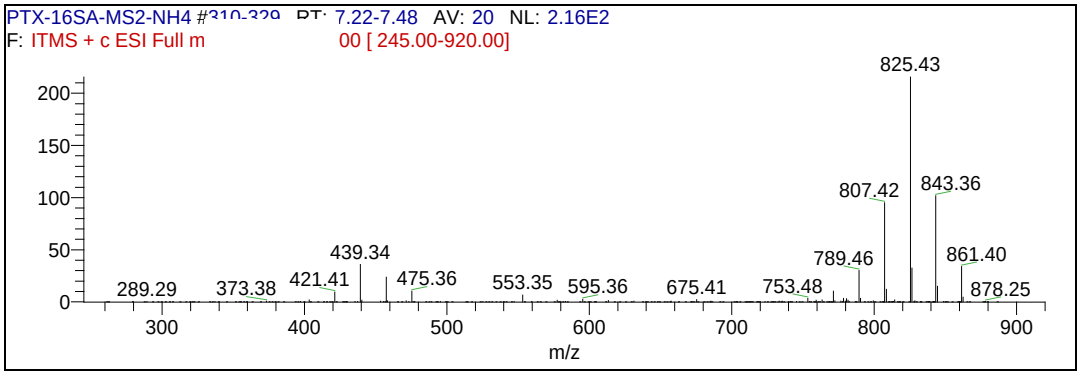

Figure 4-1: MS^2 mass spectrum of the *m/z* 896 MNa^+ ion from the '896/901' compound.

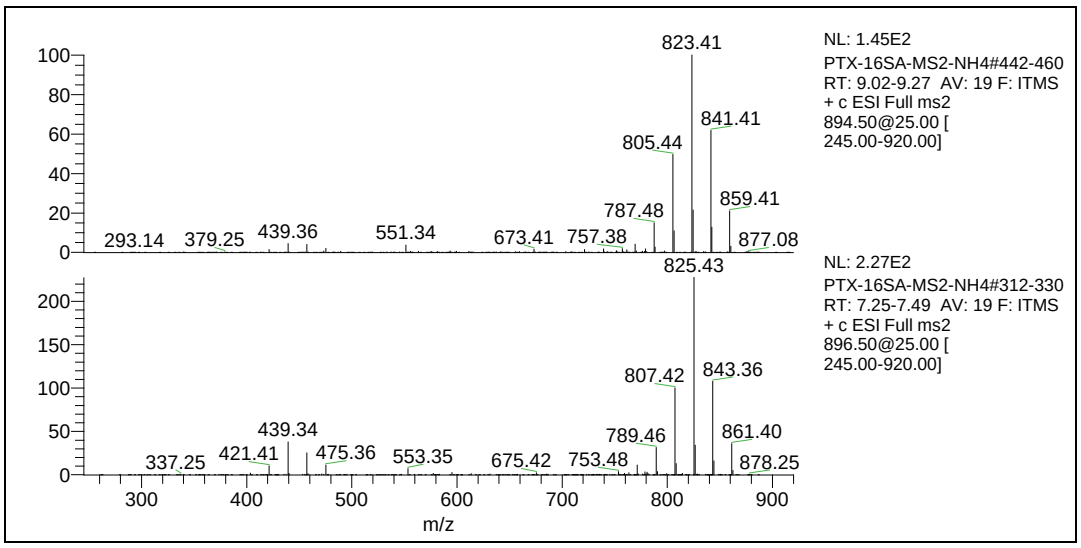

Figure 4-2: Comparison of the MS^2 mass spectra of PTX-2SA *m/z* 894 ion (top) and the *m/z* 896 ion (bottom) from the '896/901' compound.

Less obvious but more structurally significant is the mass difference between the *m/z* 551 ion seen in the MS^2 mass spectrum of PTX-2SA and the *m/z* 553 ion seen in the MS^2 mass spectrum of the *m/z* 896 ion. The structure of the low intensity *m/z* 551 ion that appears in MNH_4^+ MS^2 mass spectrum of PTX-2 is known to include a 14-keto group. Reduction of this group to afford a 14-CHOH group would increase the mass of the *m/z* 551 ion to *m/z* 553. Other lower mass fragment ions occur at the same mass in the MS^2 mass spectra of both compounds (for example ions that occur at *m/z* 475, 457, 439 and 421), which is consistent with the proposal that the point of

structural variation between the two compounds is associated with the upper portion of the two compounds structures (Figure 4-4).

Expanded views of the low intensity daughter ions observed in the respective MNH_4^+ MS^2 mass spectra are presented in Figure 4-3. This figure highlights the similarities and differences in ion masses discussed in the previous paragraph.

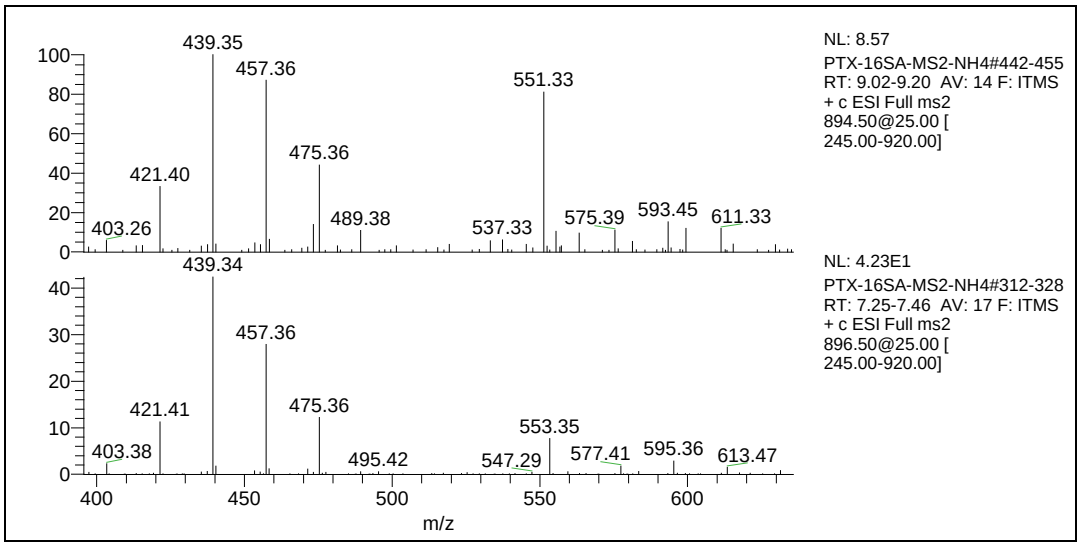

Figure 4-3: Expanded lower mass region comparison of the MS^2 mass spectra of PTX-2SA *m/z* 894 ion (top) and the unknown *m/z* 896 ion (bottom) from the '896/901' compound.

A scheme showing the proposed origin of some of the lower mass ions seen in the MS^2 mass spectrum of PTX-2SA is shown in Figure 4-4, some of which are analogous to those seen in PTX-2[6]. This scheme can be adapted to account for ions seen in the *m/z* 896 MNH_4^+ MS^2 mass spectrum of the '896/901' compound, assuming the presence of a 14-CHOH group (Figure 4-5).

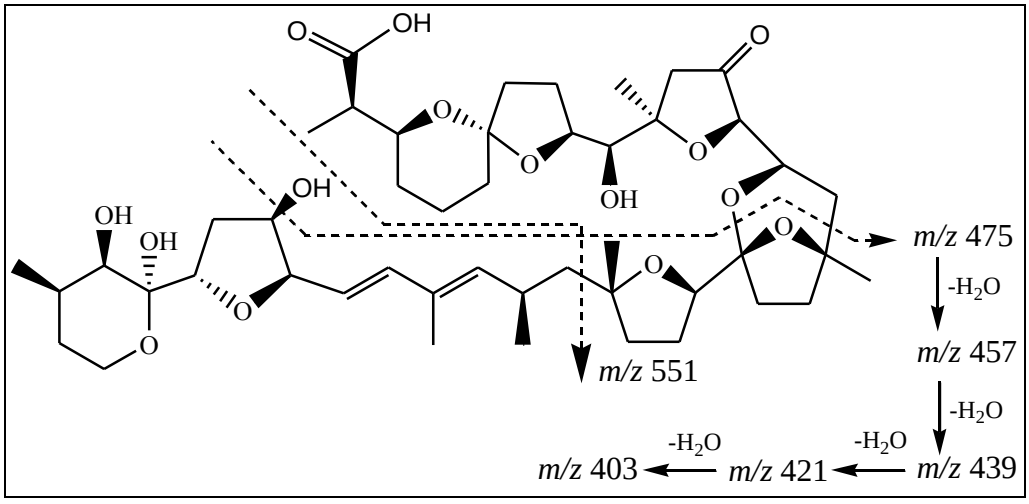

Figure 4-4: Scheme showing the proposed origins of some daughter ions in the MNH_4^+ MS^2 mass spectrum of PTX-2SA.

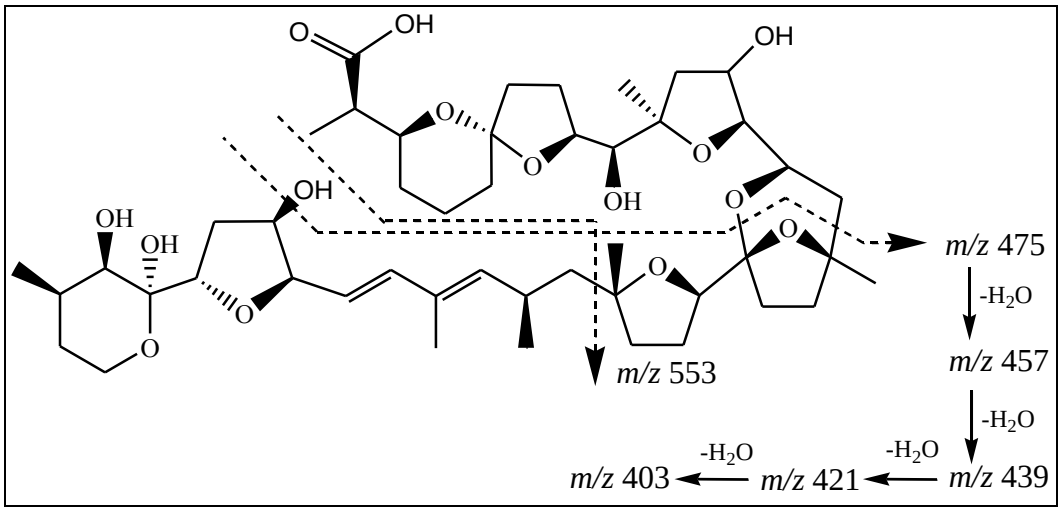

Figure 4-5: Scheme showing the possible origin of ions from the *m/z* 896 MS^2 mass spectrum of the '896/901'compound.

4.1.2 MS^2 and MS^3 analyses of the *m/z* 901 MNa^+ ion

The MS^2 mass spectrum of the *m/z* 901 ion observed for the '896/901' compound is shown in Figure 4-6. The dominant daughter ion which appeared at *m/z* 857 can be considered to originate by loss of a CO_2 molecule (44 Da) from the parent MNa^+ ion, as also seen in the MNa^+ MS^2 mass spectrum of PTX-2SA, however in this case the ion appears at *m/z* 855.

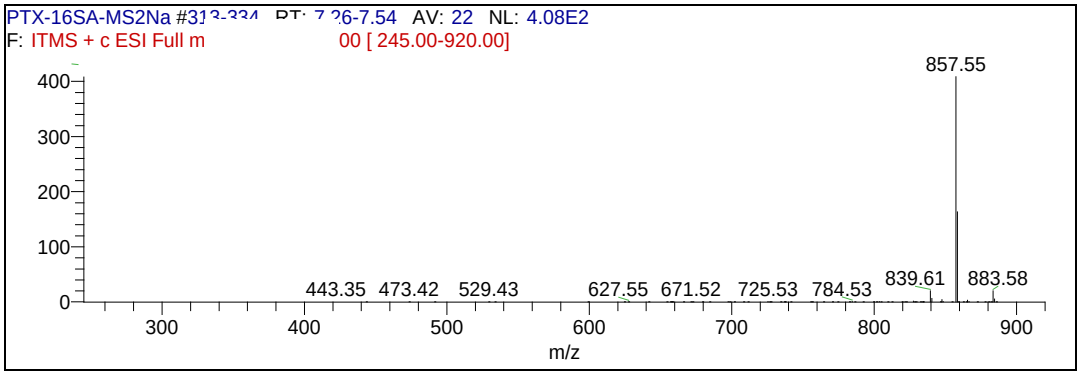

Figure 4-6: MS^2 mass spectrum of the *m/z* 901 MNa^+ ion from the '896/901'compound.

The MNa^+ MS^2 mass spectrum of PTX-2SA also included a modest intensity *m/z* 557 ion, corresponding to the loss of either a 298 Da residue from the *m/z* 855 ion, or the loss of a 342 Da residue from the MNa^+ ion (refer to Section 3.4.3). The absence of equivalent low intensity 298 or 342 Da losses in the MNa^+ *m/z* 901 MS^2 mass spectrum (Figure 4-7) is consistent with the proposal that the point of structural variation between PTX-2SA and the '896/901' compound is associated with the upper portion of the PTX-2SA structure, namely the part of the structure that is responsible for the 298 and 342 losses. The presence of a 14-CHOH group rather than a 14-C=O group in the '896/901' compound is consistent with this proposal.

Under MS^3 conditions, the *m/z* 857 ion (CO_2 loss) ion (Figure 4-8) of the '896/901' compound afforded an *m/z* 839 ion (H_2O loss) together with lower intensity *m/z* 529, 627 and 671 ions. In the absence of high resolution mass spectral data, the molecular composition and possible origin of these ions has not, as yet, been determined. There was no evidence of a 298 Da loss as seen in the MNa^+ MS^3 mass spectrum of PTX-2SA (refer above and to Section 3.2.2). The respective MS^3 mass spectra are compared in Figure 4-9.

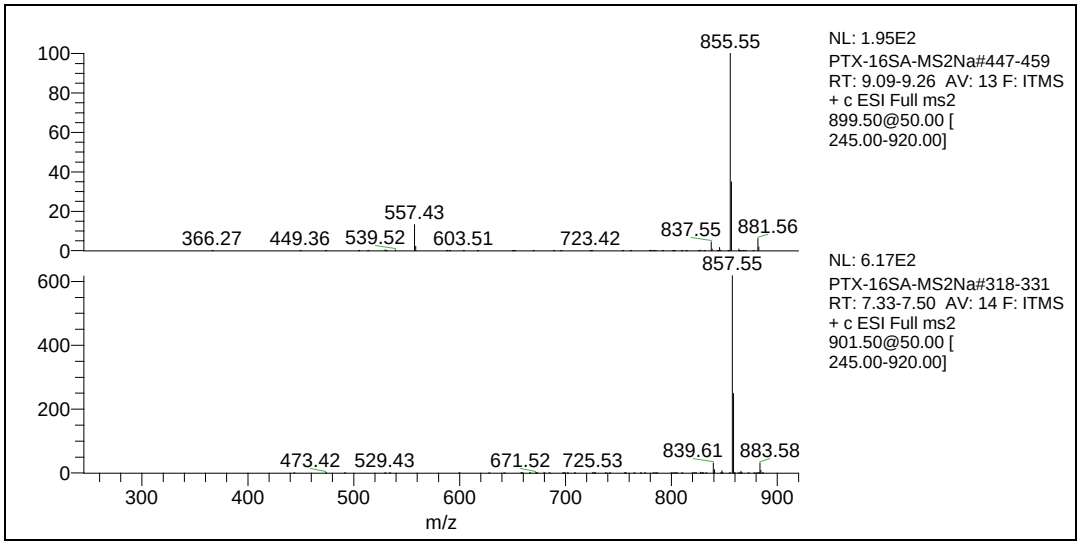

Figure 4-7: Comparison of the MS^2 mass spectrum of the PTX-2SA *m/z* 899 MNa^+ ion (top) and the MS^2 mass spectrum of the *m/z* 901 ion (bottom) from the '896/901' compound.

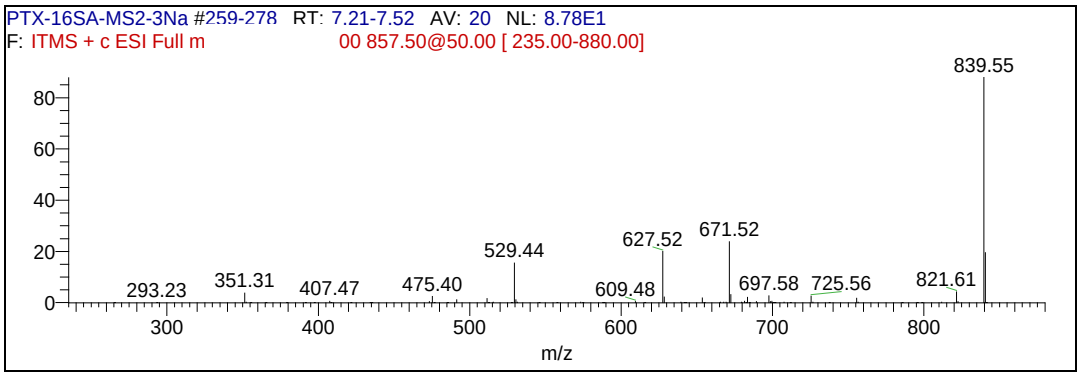

Figure 4-8: MS^3 mass spectrum of the *m/z* 901 → *m/z* 857 ion sequence from the '896/901' compound.

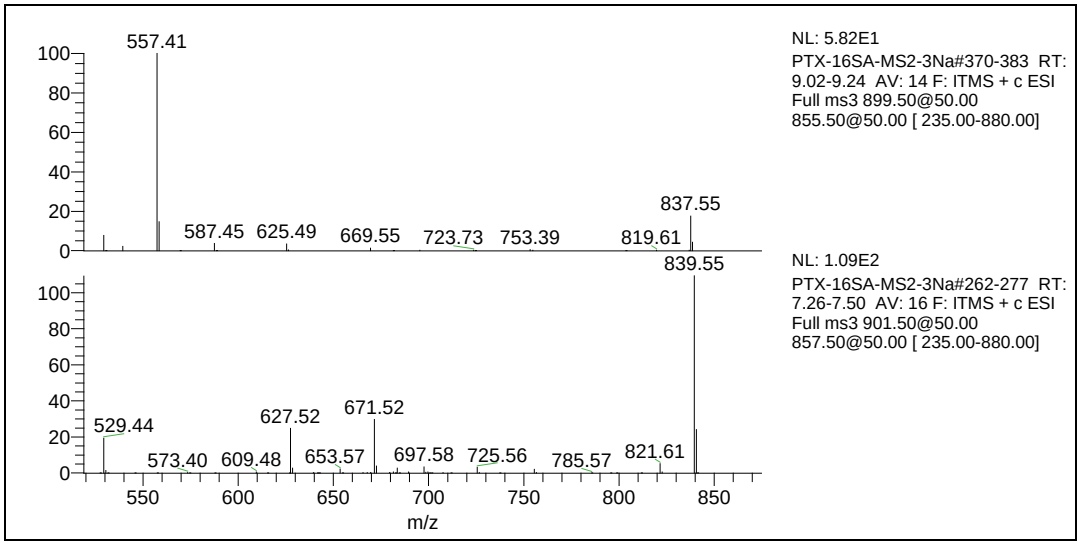

Figure 4-9: Comparison of the MS^3 mass spectra of the *m/z* 899 → *m/z* 855 ion sequence from PTX-2SA (upper) and the *m/z* 901 → *m/z* 857 ion sequence from the '896/901' compound (lower).

4.2 MS^2 analyses of the *m/z* 877 $[M-H]^-$ ion

Since the MNH_4^+ and MNa^+ ions are observed at *m/z* 896 and 901 respectively, it can be reasoned that the molar mass of the '896/901' compound is 878 Da, and that if it was observable, an $[M-H]^-$ ion should occur at *m/z* 877. The MS^2 mass spectrum determined when this ion was targeted in an MS^2 experiment is shown in Figure 4-10.

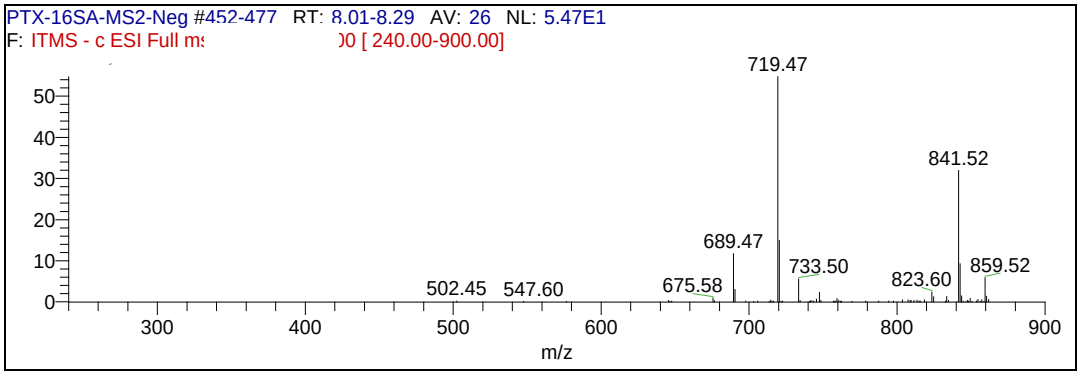

Figure 4-10: MS^2 mass spectrum of the *m/z* 877 $[M-H]^-$ ion of the '896/901' compound.

In the absence of high resolution MS^2 mass spectral data, the molecular composition and possible origin of the *m/z* 719 ion (158 Da loss) has not, as yet, been determined. The *m/z* 859 and 841 ions can be ascribed to the successive loss of H_2O molecules.

4.3 $NaBH_4$ reduction of the '896/901' compound

The proposal that the '896/901' compound might be a 14-CHOH analogue of PTX-2SA was explored in a LCMS vial scale $NaBH_4$ reaction. This afforded major and minor product peaks, both of which in full scan mode exhibited *m/z* 898 and 903 ions attributed to MNH_4^+ and MNa^+ ions respectively. The retention time of one of the products peaks corresponded to that of one of products obtained when PTX-2SA was reacted with $NaBH_4$. The MNH_4^+ MS^2 and MNa^+ MS^2 and MS^3 mass spectra of the foregoing series of PTX-2SA/$NaBH_4$ reaction products and series of '898/903' reaction products were essentially identical.

These observations, in combination with the MS^n features described in Sections 4.1-4.2 above, were consistent with the proposal that '896/901' compound possesses a 36-hemiacetal group and a reduced 14-CHOH group and that the reaction of the '896/901' compound with $NaBH_4$ resulted in the reduction (opening) of the 36-hemiacetal group.

The mass spectral data presented above does not however define the stereochemistry of the 14-CHOH group (α- or β-oriented) present in the '896/901' compound. This will require the isolation of a quantity of the reduced compound sufficient for NMR analyses. ^{1}H NMR coupling constant data together with NOE-difference, or 2D-NOESY or ROESY data should suffice to define the C-14 stereochemistry.

4.4 Examination of three NZ extracts the '896/901' compounds

The three newly prepared samples from stored New Zealand algal water extracts were systematically examined in both positive and negative ion full scan and MS^2 modes

for the presence of the '896/901' compounds reported in this thesis. The MNH_4^+ and MNa^+ ions were searched for using the Waikato LCQ system and the NVI LTQ system. The results of these analyses showed that two samples (the 1A/1B and 2A/2B samples) possessed detectable levels of the '896/901' compounds while the 3A/3B sample showed no detectable trace of the '896/901' compounds.

4.5 Detection of the '878/883' closed ring analogue of the '896/901' compound by co-workers

During the course of the write-up of the investigations reported in this thesis, Dr C. O. Miles and colleagues in Oslo and Ireland detected the presence of a compound that in full scan exhibited *m/z* 878 MNH_4^+ and *m/z* 883 MNa^+ ions. On a reverse phase C-18 column developed with a 2 mM NH_4COOH/HCOOH buffered MeCN-H_2O gradient, this peak eluted slightly before the peak that arose from the much greater level of PTX-2 in the sample. Preliminary MNH_4^+ and MNa^+ MS^2 mass spectral analyses, performed in Oslo and New Zealand (Dr C. O. Miles, personal communication) were consistent with the view that the Irish '878/883' compound is the 14-CHOH PTX-2 analogue of the 14-CHOH PTX-2SA compound reported in Sections 4.1-4.3 of this thesis.

It is intended that a detailed series of MS^2 and MS^3 mass spectral analyses and $NaBH_4$ and $NaBD_4$ reactions analogous to those described in Section 3.6 will be performed in Oslo by Dr C. O. Miles and co-workers during April-May 2009. It can be anticipated that these analyses will verify that the '878/883' compound is the closed ring PTX-2 like variant of the open ring PTX-2SA like '896/901' compound detected in the present investigation.

Chapter 5

MS^n Characterisation of OA and DTX-2 Glycosides

5.0 Introduction

As part of an on-going collaborative research effort in our laboratories for new toxins in mussel and algal water extracts that have been retained by the National Veterinary Institute, Oslo, after known algal toxins had been identified, or recovered from them, a set of 11 water samples that had previously had the bulk of the extractable organic part recovered from them by extraction with CH_2Cl_2 and/or other solvents, were subjected to LCMS analyses to determine if it new, more polar, analogues of known toxins were present in the residual water samples.

One of the water samples (the W8 sample collected during a *Dinophysis acuta* bloom, 2005) was found to possess residual levels of OA and DTX-2 along with what appeared to be a glycoside analogue of these compounds.

Okadaic acid and DTX-2 exhibit $[M-H]^-$, MH^+, MNH_4^+, and MNa^+ ions at *m/z* 803, 805, 822 and 827 respectively. Of these ions, the $[M-H]^-$ and MNa^+ ions are the most useful in MS^n analysis, since their MS^2 and MS^3 characteristics are now well established[39]. It was anticipated that MS^n analyses, of primarily the MNa^+ and $[M-H]^-$ ions of the proposed glycosylated compounds, would verify that they were definitely OA and DTX-2 analogues. The point of attachment of the glycosyl residue may also possibly be defined by this analyses.

A comparison of MS^n characteristics of OA and DTX-2, and what were believed to be hitherto unreported glycosylated analogues of these compounds is presented below. Since the MS^n characteristics of OA and DTX-2 are essentially identical, the account presented here is illustrated primarily for the first eluting peak, believed to be an OA-glycoside.

5.1 MS^n analyses of the MNa^+ mass spectra of OA and OA-glycoside

This section describes the mass spectral analyses of the MNa^+ ions of OA and OA-glycoside.

5.1.1 MS^2 and MS^3 analyses of the MNa^+ mass spectra of OA and OA-glycoside

The MNa^+ *m/z* 827 MS^2 mass spectra of OA and DTX-2 are characterised by high intensity daughter ions at *m/z* 809 (H_2O loss) and *m/z* 723 (104 Da loss). This 104 Da loss has been ascribed to the loss of $HOOC\text{-}COH(CH_3)_2$ from the C-1–C-3 portion of OA as illustrated in Figure 5-1.

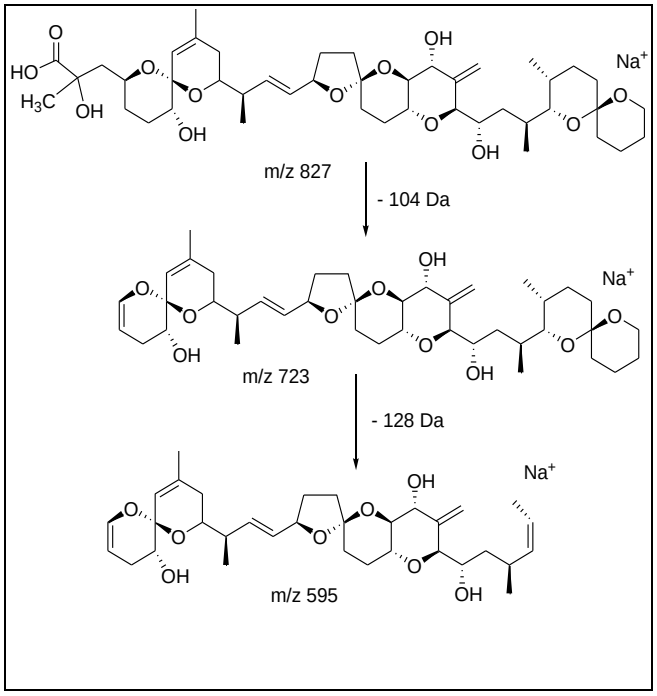

Figure 5-1: Proposed structures for some ions seen in the MS^2 mass spectrum of the MNa^+ *m/z* 827 ion of OA.

A pair of peaks which eluted at 5.14 and 5.50 min on a C-18 column when it was developed with a 2 mM NH_4COOH/HCOOH buffer on a H_2O-MeCN gradient from 30% MeCN to 100% MeCN over 20 min, afforded MS^2 mass spectra (Figure

5-2) that were also characterised by the loss of 18 Da (H_2O) and 104 Da (HOOC-$COH(CH_3)_2$) from a parent MNa^+ ion which occurred at *m/z* 989. A 104 Da loss is seen in the MS^2 mass spectrum of the OA-glycoside, showing that the glycosyl residue is not attached to the tertiary 2-OH group.

The difference between the masses of the MNa^+ ions of the early and later peaks was 162 Da (989-827 = 162). This difference is suggestive of the presence of a six carbon glycosyl residue, such as a glucopyranosyl residue.

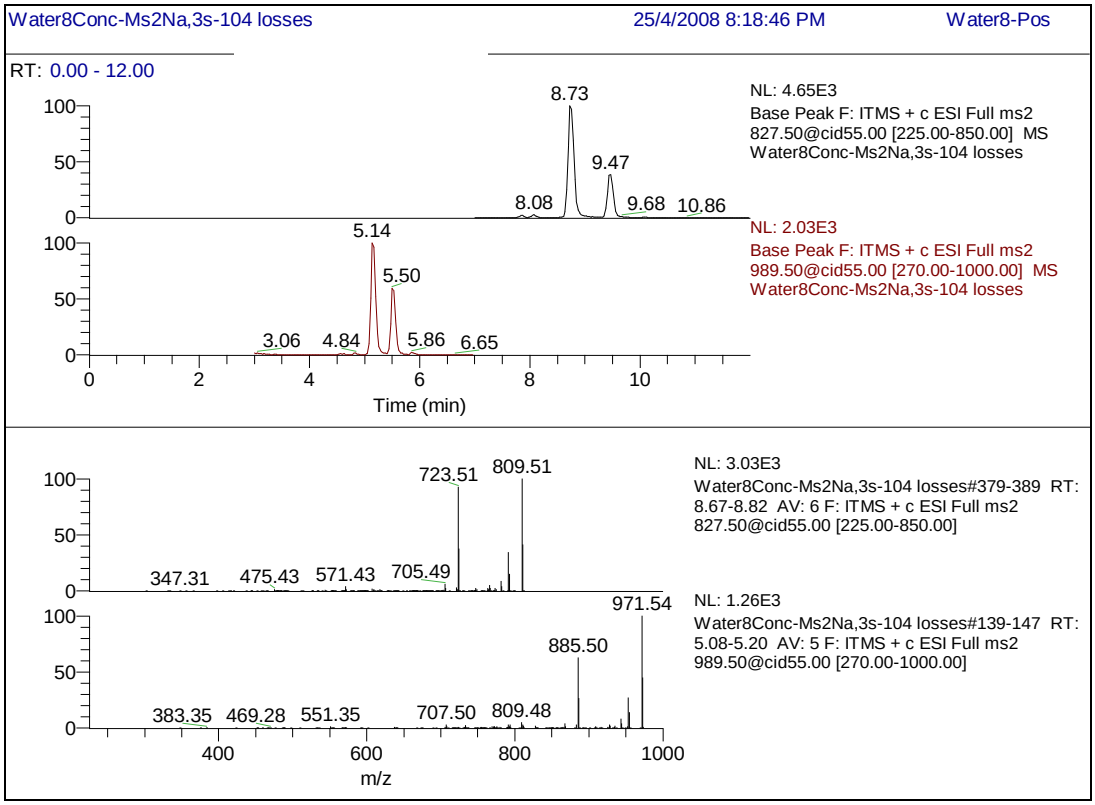

Figure 5-2: *m/z* 827 and 989 MS^2 extracted ion chromatograms (upper pair) and *m/z* 827 and 989 MS^2 mass spectra (lower pair) for the peaks eluting at 8.73 min and 5.14 min respectively.

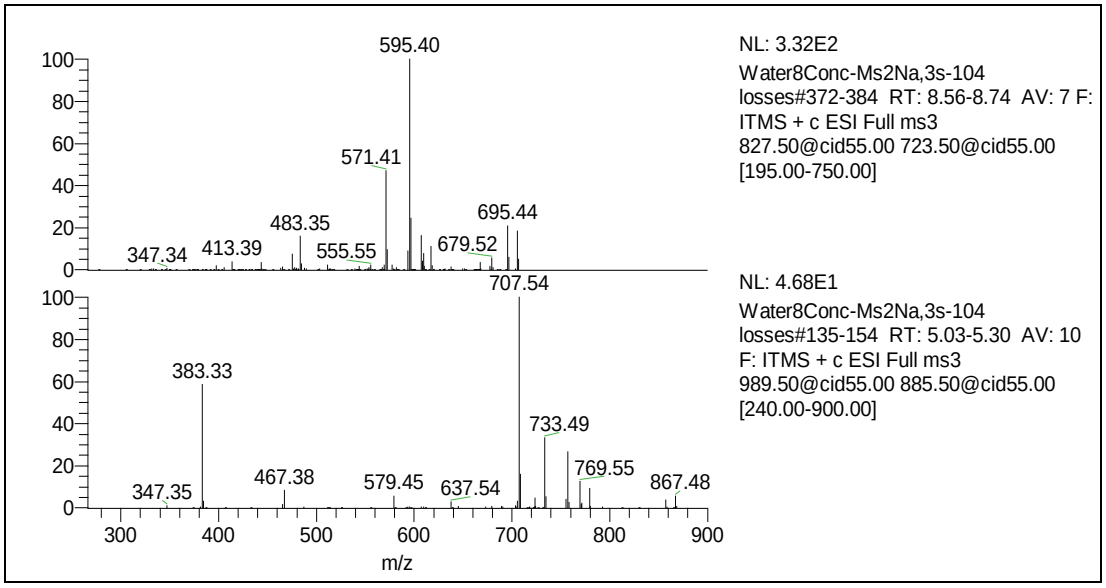

Figure 5-3: MS^3 mass spectra of the *m/z* 827 → *m/z* 723 ions (top) and the *m/z* 989 → *m/z* 885 ions (bottom) for the peaks eluting at 8.73 min and 5.14 min respectively.

The MS^3 mass spectra of the *m/z* 723 and 885 ions (104 Da loss daughter ions) of OA and its proposed glycosyl analogue respectively are compared in Figure 5-3. The moderate intensity *m/z* 733 and 757 ions which are seen in the later compounds MS^3 mass spectrum appear to be glycosylated analogues of the *m/z* 571 and 595 ions seen in the MS^2 mass spectrum of OA. The detection of these ions indicates that the glycosyl group is attached to either the C-7 or the C-24 hydroxyl groups of the OA structure (Figure 5-7).

The origin of the dominant *m/z* 707 daughter ion (178 Da loss) seen in the MS^3 mass spectrum of the *m/z* 885 is intriguing since a glycosyl residue is generally characterised by the loss of 162 or 180 Da, as illustrated in Figure 5-4 for a glucose residue. Possibly, the 178 Da loss may arise from the loss of the glycosyl residue in an oxidised form (Figure 5-4, illustrated for a glucose residue).

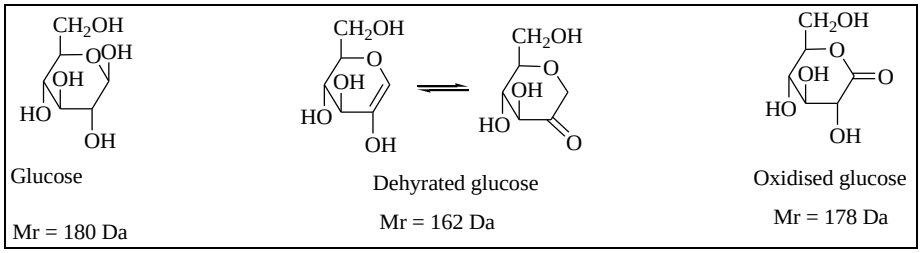

Figure 5-4: Structures and molecular masses of possible glucose related losses seen in MS^n mass spectra.

Possibly, the *m/z* 383 ion seen in the MS^3 mass spectrum of the proposed glycoside is a rearrangement ion in the fourth ring (Figure 5-5) analogous to that proposed for the *m/z* 483 ion seen in some negative ion MS^n mass spectra (refer to Section 5.2).

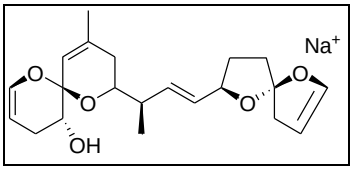

Figure 5-5: Possible structure for the *m/z* 383 ion.

5.1.2 MS^2 and MS^3 analyses of the MNH_4^+ mass spectra of OA and OA-glycoside

The MNH_4^+ MS^2 mass spectra determined for OA and the proposed glycosylated analogue of OA are compared in Figure 5-6.

Each of the MS^2 mass spectra were characterised by NH_4OH (35 Da loss) and subsequent series of H_2O loss ions. The glycosylated analogue shows two such sets of peaks: one which retains the glycosyl residue and the other which has lost the glycosyl residue.

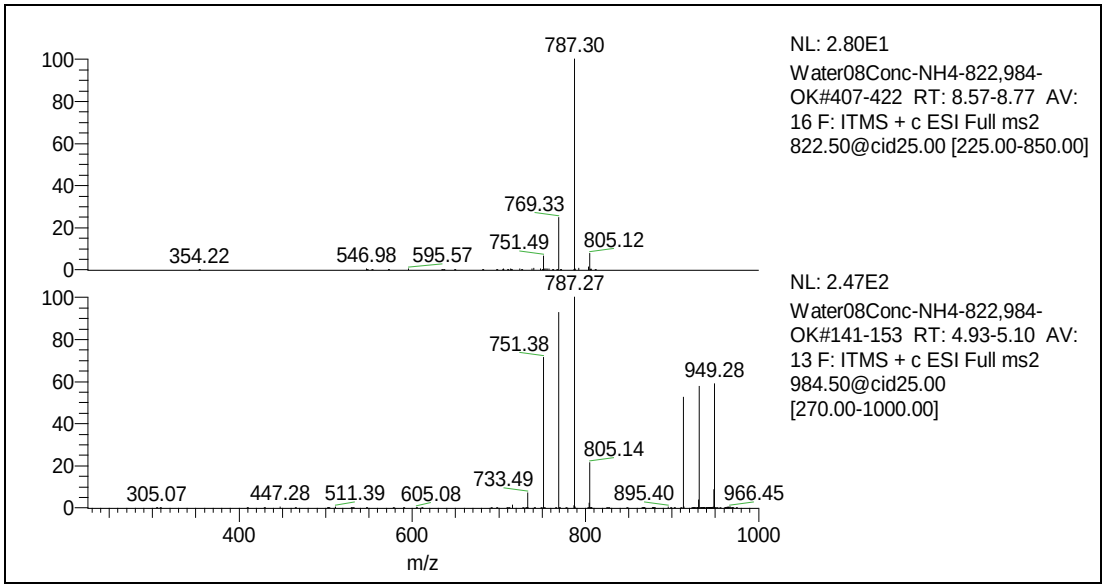

Figure 5-6: Comparison of the *m/z* 822 and *m/z* 984 MNH_4^+ MS^2 mass spectra of OA (upper) and its glycosylated analogue (lower).

5.2 MS^2 and MS^3 analyses of the $[M-H]^-$ mass spectra of OA and OA-glycoside

The negative ion MS^2 mass spectrum of OA and the proposed OA-glycoside are compared in Figure 5-8. The origin of the OA daughter ions at *m/z* 563 and *m/z* 255 is well established[40] as shown in Figure 5-7. The *m/z* 255 ion can arise via a Retro

Diels-Alder (RDA) rearrangement pathway either directly from either the $[M-H]^-$ ion or from the *m/z* 563 daughter ion.

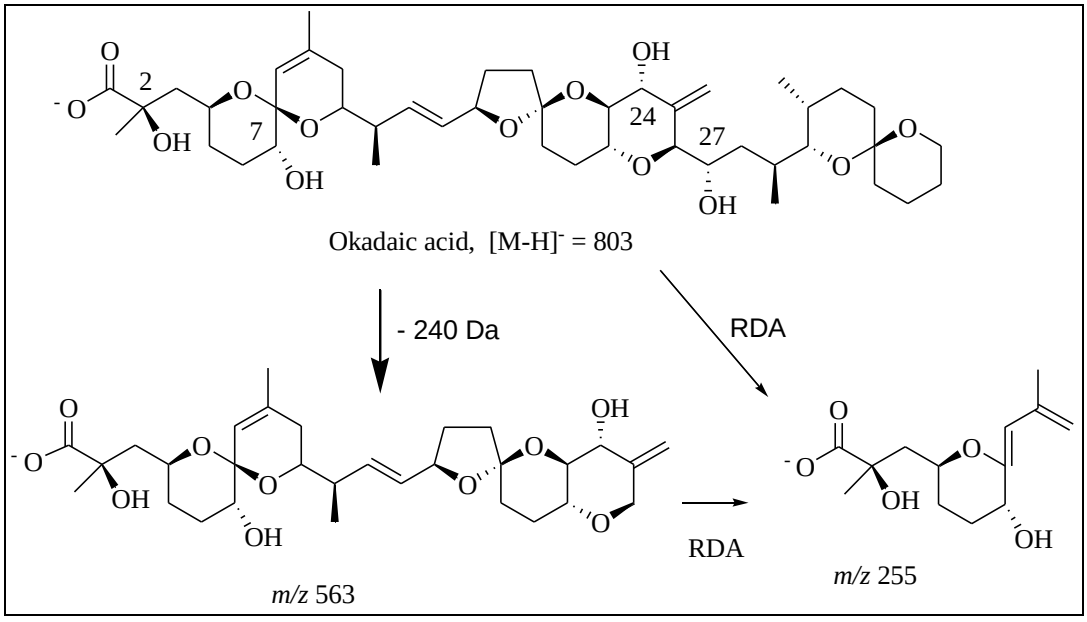

Figure 5-7: Scheme showing the structures of the ions seen in the negative MS^2 mass spectrum of *m/z* 803.

The *m/z* 725 daughter ion seen in the MS^2 mass spectrum of the glycoside can be ascribed to the glycosylated version of the *m/z* 563 seen in MS^2 mass spectrum of OA, thus it can be reasoned that glycosyl group is attached to either C-7 or C-24, but not C-27.

Loss of 18 Da (H_2O) and 162 Da (dehydrated glucose) or 180 Da (glucose) would afford the *m/z* 947, 803 and 785 ions respectively seen in the MS^2 mass spectrum of the glycosyl compound (Figure 5-8). Possible structures for ions seen in this mass spectrum are given in Figure 5-9. Since the origin of the *m/z* 463 ion was not obvious, its MS^3 fragmentation was probed (see below).

.

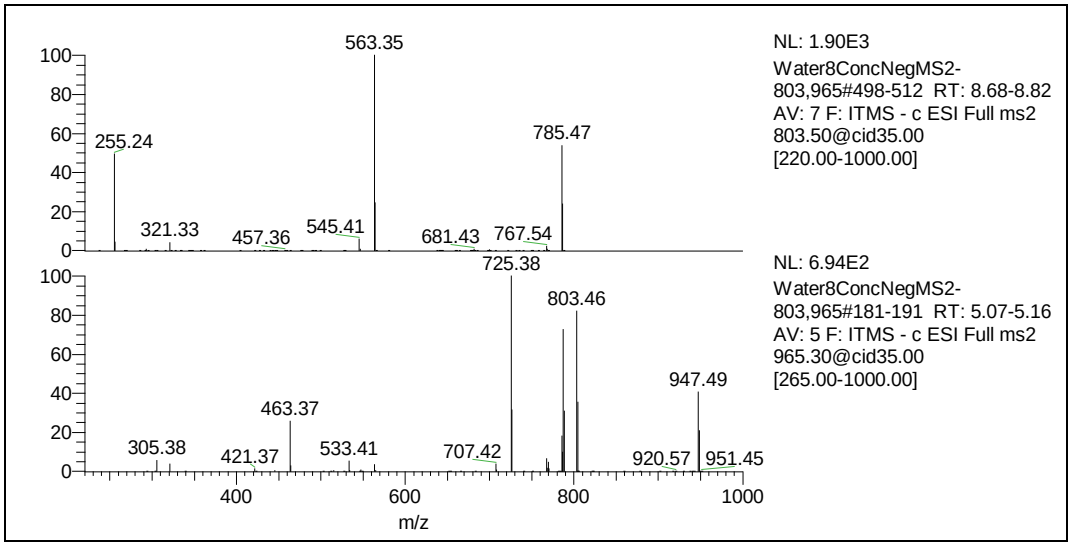

Figure 5-8: Comparison of the $[M-H]^-$ MS^2 mass spectra of OA (*m/z* 803) and the OA-glycoside (*m/z* 965).

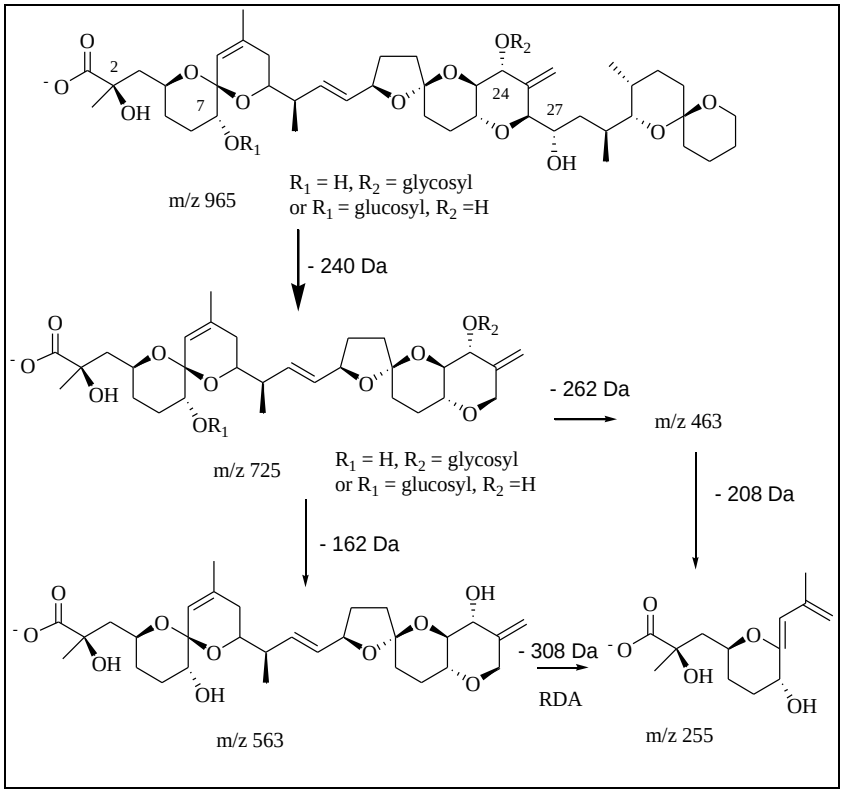

Figure 5-9: Proposed structures for the ions seen in the $[M-H]^-$ MS^2 mass spectrum of the OA-glycoside.

MS^3 fragmentation of the *m/z* 463 ion predominantly afforded an *m/z* 255 ion, as shown in Figure 5-10 suggesting, but not equivocally establishing, that the glycosyl residue was not attached to C-7. Consideration of possible formulations for the *m/z* 463 ion (which must include the atoms associated with the *m/z* 255 fragment ion) leads to the conclusion it cannot be formulated as a simple one or two bond cleavage process. Rather it appears to arise via a rearrangement pathway involving the cleavage and rearrangement of three (or more) bonds which is induced in some way by the presence of a glycosyl group, which if it is not attached to C-7, must be attached to C-24. A possible structure for *m/z* 463 ion is shown in Figure 5-11.

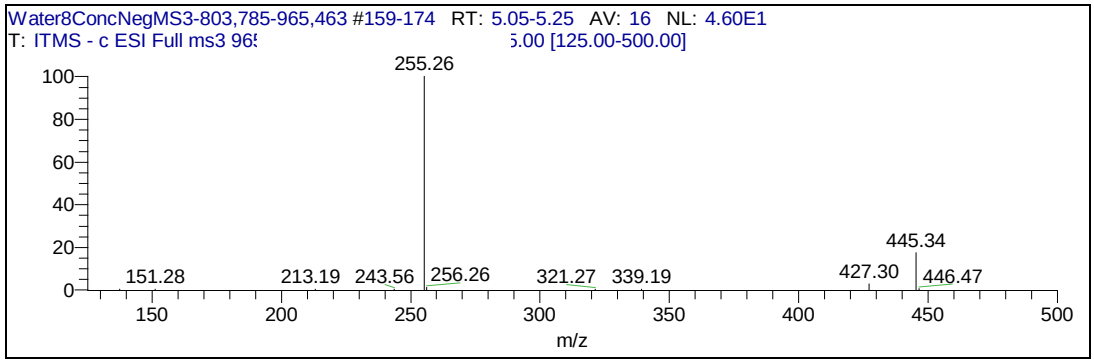

Figure 5-10: MS^3 mass spectrum of the *m/z* 965 → *m/z* 463 ion sequence from the *m/z* 965 $[M-H]^-$ ion.

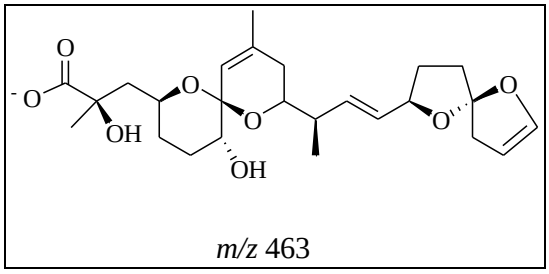

Figure 5-11: Possible structure of the *m/z* 463 ion.

The MS^3 mass spectrum of the *m/z* 725 ion predictably afforded *m/z* 563 and *m/z* 255 ions, as did the fragmentation of the *m/z* 803 ion. Strong H_2O loss ions were also seen in the respective MS^3 mass spectra at *m/z* 707 and *m/z* 785. These spectra are shown in Figure 5-12 and Figure 5-13.

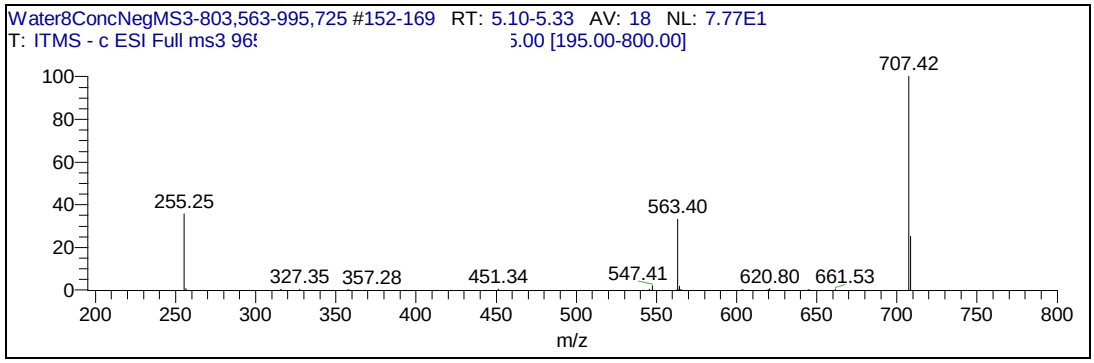

Figure 5-12: MS^3 mass spectrum of the *m/z* 965 → *m/z* 725 ion sequence from the *m/z* 965 $[M-H]^-$ ion.

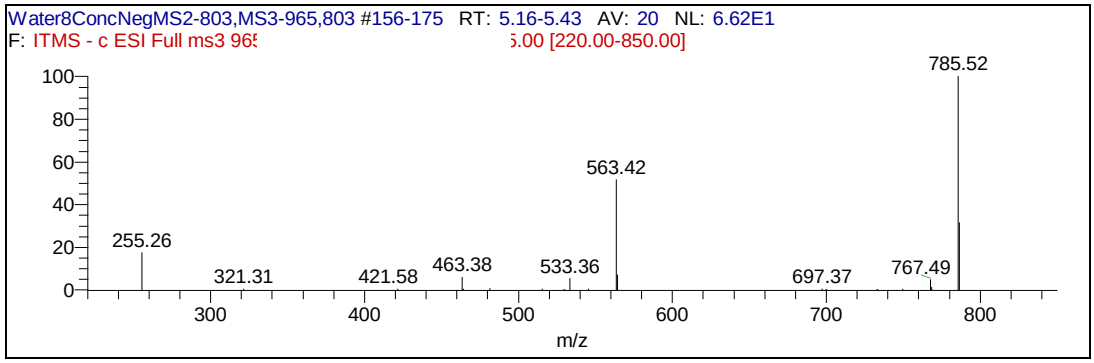

Figure 5-13: MS^3 mass spectrum of the *m/z* 965 → *m/z* 803 ion sequence from the *m/z* 965 $[M-H]^-$ ion.

The foregoing mass spectral data shows that the glycosyl residue is not attached to C-2 or C-27, and is most likely attached to C-24 rather than C-7. Since the mass spectral features of the first and second eluting MNa^+ OA peaks were essentially identical, it can be concluded this is also the case for both of the glycosylated peaks (Figure 5-2). The second of these peaks is believed to be the DTX-2 analogue of the first eluting OA-glycoside, based on the reasonable assumption that the order in which their glycoside will elute on a C-18 column will be the same as for the parent compounds.

5.3 600 MHz ^{1}H NMR data determined for the OA-glycoside

Whilst the foregoing mass spectral data is consistent with the identification of the pair of early eluting peaks as C-7 or C-24 substituted OA and DTX-2 glycosides, it did not unequivocally establish the point of glycosylation, or identify the glycosyl residue, be it a glucose, galactose or other residue.

During May-June 2007 an opportunity arose, in collaboration with co-workers at the National Veterinary Institution laboratory, Oslo, including Dr C. O. Miles, and Oslo University (Professor Riste), for Professor Wilkins to attempt the isolation of a sufficient quantity of the more dominant (1st eluting) of the glycosides from a retained portion of the W8 water sample whilst he was seconded to the NVI as a visiting scientist.

A quantity of the glycoside (estimated to be of the order 50 µg) was isolated in a sufficient purity for its ^{1}H NMR, two-dimensional COSY and TOCSY spectra and several 1D-selected TOCSY spectra to be determined using a 600 MHz NMR spectrometer at Oslo University. The quality of the ^{1}H NMR data thus obtained was such that it proved possible to define the point of attachment of the glycosyl residue and to demonstrate via coupling constant information elucidated in 1D-selective TOCSY spectra that the glycosyl residue was a β-glucopyranosyl residue.

A comparison of the H-7, H-11 and 25=CH_2 chemical shift (Figure 5-14; data reproduced with permission from Professor Wilkins and Dr C. O. Miles) showed that the glucose residue was attached to C-24 (rather than C-7 as is the case for OA/DTX-3 esters) and that one of the protons of the 25=CH_2 group experienced a moderate downfield shift that could be attributed to the introduction of 24-O-β-glucopyranosyl residue.

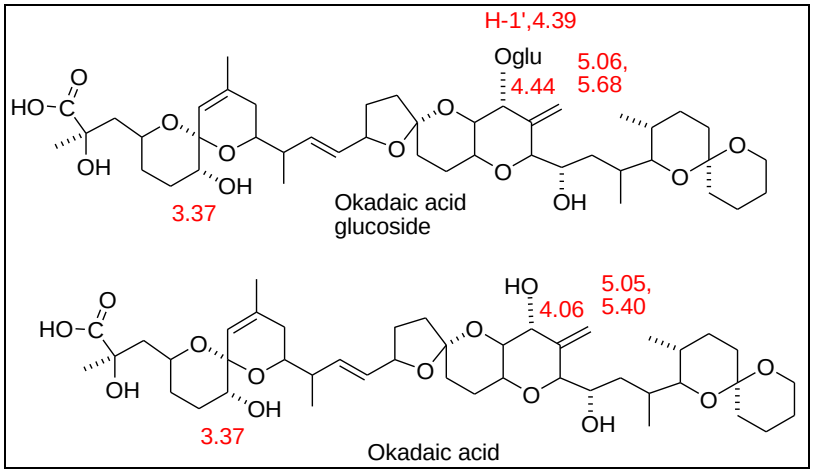

Figure 5-14: Chemical shifts determined for selected protons of OA and OA 24-glucoside (ppm in CD_3OD).

An account of the isolation of a specimen of OA 24-glucoside and the NMR analyses, carried out in Oslo by Professor Wilkins, Dr C. O. Miles and others, is beyond the scope of the mass spectral investigation reported in this thesis. In due course, the NMR anayses will be reported elsewhere by Professor Wilkins and Dr C. O. Miles.

5.4 Examination of three New Zealand extracts for OA and DTX glucosides

The three newly prepared extracts from stored New Zealand algal water extracts were systematically examined in both positive and negative ion full scan and MS^2 modes for the presence of the OA and/or DTX-glycosides detected in the W8 and related algal water extracts. The New Zealand samples, prepared as described in Chapter 2, were examined using the Waikato LCQ system and the more sensitive NVI LTQ system. OA and/or DTX-glycosides were detected in the 2A/2B sample (Akaroa Harbour) from the three New Zealand extracts but not detected in the 1A/1B or 3A/3B (West Coast) samples.

Chapter 6

Summary and Conclusions

The approach adopted in the investigations reported in this thesis is one that has proved productive in the past when working in a collaborative environment. There is an initial requirement for a systematic and often tedious/repetitive examination of historic extracts prior to their disposal in the expectation this will result in the detection of peaks attributable to unreported compounds in the extracts.

Thereafter, there is a need to determine if unexpected or new peaks arise from innocuous, natural compounds of little interest to researchers, or if they are potentially toxic compounds derived from algal sources. Often this can be deduced from a series of both positive and negative ion LCMS analyses conducted in full scan, MS^2, MS^3 and MS^4 modes. Although this can be a time consuming process, it frequently serves to identify substances which are modified analogues of known algal toxins as exemplified in this thesis wherein a series of a PTX analogues, the reduced PTX-2SA compounds and the OA/DTX-2 glucosides were identified.

It is known that other unreported substances are present in other historic extracts available in our laboratories that have not as yet been subjected to the same level of $LCMS^n$ analyses as described in this thesis (Professor Wilkins and Dr C. O. Miles, personal communication).

Ion trap mass spectrometers are well suited to this approach since a prior knowledge of SRM daughter ion transitions is not required. Once the MS^n characteristics have been identified in ion trap based analyses, including suitable daughter ions for use in SRM methods, higher sensitivity triple quad SRM methods can be developed to detect newly discovered algal toxins.

Subsequent to the initial LCMS detection of a potential new algal toxin using full scan and MS^n methods there is a need to:

(i) define the occurrence of it across a range of recently collected and carefully processed extracts with the intention of excluding the formation of artefact compounds such as 7-*epi*-PTX-2SA isomers and

(ii) identify samples/sources that may contain a quantity of a new toxin sufficient for its isolation and structural elucidation using NMR methods.

A collaborative approach is frequently more productive in this environment than a researcher or Masters or PhD student working alone. While one group of workers and Masters or PhD students associated with them may have access to a wide range of extracts arising from the routine screening of mussel and algal water samples, a second group may have high level $LCMS^n$ and isolation skills and a third group may have the ability to secure high quality NMR data from sub-milligram samples.

The work presented in this thesis has identified three new groups of algal toxins, namely:

(i) a series of PTX-i analogues,

(ii) two reduced PTX-2SA analogues (one which may be the 7-*epi* isomer of the parent compound),

(iii) and OA and DTX-2 24-*O*-glycosides.

Co-workers are now endeavouring to isolate these compounds in sufficient quantity to determine their structures using advanced one and two-dimensional NMR spectroscopic methods.

In the case of the OA and DTX-2 glycosides, this approach has already resulted in the collaborative acquisition of preliminary ^1H NMR data by co-workers that has defined the structure of a new OA glucoside and, by implication, also a DTX-2 glucoside.

Additionally, based on an analysis of LCMS, MS^2 and MS^3 mass spectral data analogous to those reported above for the OA and DTX-2 glycosides, another historic algal water extract available in the NVI, Oslo, is believed to contain a moderate level of the corresponding DTX-1 glucoside (Professor Wilkins and Dr C. O. Miles, personal communication).

References

1. Toyofuku, H., Joint FAO/WHO/IOC activities to provide scientific advice on marine biotoxins (research report). *Mar. Poll. Bull.* **2006,** 52, 1735-1745.
2. Daiguji, M., Satake, M., James, K. J., Bishop, A., MacKenzie, L., Naoki, H., Yasumoto, T., Structures of new pectenotoxin analogs, pectenotoxin-2 seco acid and 7-*epi*-pectenotoxin-2 seco acid, isolated from a dinoflagellate and greenshell mussels. *Chem. Lett* **1998**, 653-654.
3. James, K. J., Bishop, A. G., Draisci, R., Palleschi, L., Marchiafava, C., Ferretti, E., Satake, M., Yasumoto, T, Liquid chromatographic methods for the isolation and identification of new pectenotoxin-2 analogues from marine phytoplankton and shellfish. *J. Chromatogr. A* **1999,** 844, 53-65.
4. MacKenzie, L., Holland, P., McNabb, P., Beuzenberg, V., Selwood, A., Suzuki, T., Complex toxin profiles in phytoplankton and Greenshell mussels (*Perna canaliculus*), revealed by LC-MS/MS analysis. *Toxicon* **2002,** 40, 1321-1330.
5. Miles, C. O., Wilkins, A. L., Samdal, I. A., Sandvik, M., Petersen, D., Quilliam, M. A., Naustvoll, L. J., Rundberget, T., Torgersen, T., Hovgaard, P., Jensen, D. J., Cooney, J. M., A novel pectenotoxin, PTX-12, in *Dinophysis* Spp. and shellfish from Norway. *Chem. Res. Toxicol.* **2004,** 17, 1423-1433.
6. Suzuki, T., Beuzenberg, V., Mackenzie, L., Quilliam, M. A., Liquid chromatography-mass spectrometry of spiroketal stereoisomers of pectenotoxins and the analysis of novel pectenotoxin isomers in the toxic dinoflagellate *Dinophysis acuta* from New Zealand. *J. Chromatogr. A* **2003,** 992, 141-150.
7. Fernández, M. L., Reguera, B., First report of pectenotoxin-2 in isolated *Dinophysis caudata* cells determined by liquid chromatography-mass spectrometry, Book of Abstracts. 10th International Conference on Harmful Algae, St. Petersburg Beach, FL, Oct 21-25; Florida Fish and Wildlife Conservation Commission, Florida Institute of Oceanography, and Intergovernmental Oceanographic Commission of UNESCO: St. Petersburg, FL. **2002**, 91.
8. MacKenzie, L., Beuzenberg, V., Holland, P., McNabb, P., Suzuki, T., Selwood, A., Pectenotoxin and okadaic acid-based toxin profiles in *Dinophysis acuta* and *Dinophysis acuminata* from New Zealand. *Harmful Algae* **2005,** 4, 75-85.
9. Draisci, R., Lucentini, L., Giannetti, L., Boria, P., Poletti, R., First report of pectenotoxin-2 (PTX-2) in algae (*Dinophysis fortii*) related to seafood poisoning in Europe. *Toxicon* **1996,** 34, 923-935.
10. Suzuki, T., Mitsuya, T., Matsubara, H., Yamasaki, M., Determination of pectenotoxin-2 after solid-phase extraction from seawater and from the dinoflagellate *Dinophysis fortii* by liquid chromatography with electrospray mass spectrometry and ultraviolet detection: evidence of oxidation of

pectenotoxin-2 to pectenotoxin-6 in scallops. *J. Chromatogr. A* **1998,** 815, 155-160.

11. Lee, J., Igarashi, T., Fraga, S., Dahl, E., Hovgaard, P.,Yasumoto, T., Determination of diarrhetic shellfish toxins in various dinoflagellate species. *J. Appl. Phycol.* **1989,** 1, 147-152.
12. Suzuki, T., Mackenzie, L., Stirling, D., Adamson, J., Pectenotoxin-2 seco acid: a toxin converted from pectenotoxin-2 by the New Zealand Greenshell mussel, *Perna canaliculus*. *Toxicon* **2001,** 39, 507-514.
13. Miles, C. O., Wilkins, A. L., Munday, R., Dines, M. H., Hawkes, A. D., Briggs, L. R., Sandvik, M., Jensen, D. J., Cooney, J. M., Holland, P. T., Quilliam, M. A., MacKenzie, A. L., Beuzenberg, V., Towers, N. R., Isolation of pectenotoxin-2 from *Dinophysis acuta* and its conversion to pectenotoxin-2 seco acid, and preliminary assessment of their acute toxicities. *Toxicon* **2004,** 43, 1-9.
14. Yasumoto, T., Murata, M., Oshima, Y., Sano, M., Matsumoto, G. K., Clardy, J., Diarrhetic shellfish toxins. *Tetrahedron* **1985,** 41, 1019-1025.
15. Burgess, V., Shaw, G., Pectenotoxins -- an issue for public health: a review of their comparative toxicology and metabolism. *Environ. Int.* **2001,** 27, 275-283.
16. Miles, C. O., Pectenotoxins, In Botana, L.M. (Ed.). **2007,** Phycotoxins: Chemistry and Biochemistry. Blackwell Publishing Ltd., Oxford, 159-186.
17. Yasumoto, T., Murata, M., Lee, J., Torigoe, K., Polyether toxins produced by dinoflagellates, In Natori, S., Hashimoto, K., Ueno, Y. (Eds.). Mycotoxins and phycotoxins '88. **1989,** Elsevier Science Publishers, Amsterdam, 375-382.
18. Suzuki, T., Walter, J. A., LeBlanc, P., MacKinnon, S., Miles, C. O., Wilkins, A. L., Munday, R., Beuzenberg, V., MacKenzie, A. L., Jensen, D. J., Cooney, J. M., Quilliam, M. A., Identification of pectenotoxin-11 as 34*S*-hydroxypectenotoxin-2, a new pectenotoxin analogue in the toxic dinoflagellate *Dinophysis acuta* from New Zealand. *Chem. Res. Toxicol.* **2006,** 19, 310-318.
19. Miles, C. O., Wilkins, Alistair L., Hawkes, A. D., Jensen, D. J., Selwood, A. I., Beuzenberg, V., MacKenzie, A. L., Cooney, J. M., Holland, P. T., Isolation and identification of pectenotoxins-13 and -14 from *Dinophysis acuta* in New Zealand. *Toxicon* **2006,** 48, 152-159.
20. Wilkins, A. L., Rehmann, N., Torgersen, T., Rundberget, T., Keogh, M., Petersen, D., Hess, P., Rise, F., Miles, C. O., Identification of fatty acid esters of pectenotoxin-2 seco acid in Blue mussels (*Mytilus edulis*) from Ireland. *J. Agric. Food Chem.* **2006,** 54, 5672-5678.
21. Tachibana, K., Scheuer, P. J., Tsukitani, Y., Kikuchi, H., Van Engen, D., Clardy, J., Gopichand, Y., Schmitz, F. J., Okadaic acid, a cytotoxic polyether from two marine sponges of the genus *Halichondria*. *J. Am. Chem. Soc.* **1981,** 103, 2469-2471.
22. Yasumoto, T., Oshima, Y., Sugawara, W., Fukuyo, Y., Oguri, H., Igarashi, T., Fujita, N., Identification of *Dinophysis fortii* as the causative organism of diarrhetic shellfish poisoning. *Bull. Jpn Soc. Sci. Fish.* **1980,** 46, 1405-1411.

23. Hu, T., Doyle, J., Jackson, D., Marr, J., Nixon, E., Pleasance. S., Quilliam, M.A., Walter, J.A., Wright, J.L.C., Isolation of a new diarrhetic shellfish poison from Irish mussels. *J. Chem. Soc., Chem. Commun* **1992**, 39-41.
24. Marr, J. C., Hu, T., Pleasance, S., Quilliam, M. A., Wright, J. L. C., Detection of new 7-*O*-acyl derivatives of diarrhetic shellfish poisoning toxins by liquid chromatography-mass spectrometry. *Toxicon* **1992,** 30, 1621-1630.
25. Suzuki, T., Ota, H., Yamasaki, M., Direct evidence of transformation of dinophysistoxin-1 to 7-*O*-acyl-dinophysistoxin-1 (dinophysistoxin-3) in the scallop *Patinopecten yessoensis*. *Toxicon* **1999,** 37, 187-198.
26. Takai, A., Bialojan, C., Inhibitory effect of a marine-sponge toxin, okadaic acid, on protein phosphatases. *Biochem. J.* **1988,** 256, 283-290.
27. Terao, K.; Ito, E.; Yanagi, T.; Yasumoto, T., Histopathological studies on experimental marine toxin poisoning. I. Ultrastructural changes in the small intestine and liver of suckling mice induced by dinophysistoxin-1 and pectenotoxin-1. *Toxicon* **1986,** 24, 1141-1151.
28. Suganuma, M., Fujiki, H., Suguri, H., Yoshizawa, S., Hirota, M., Nakayasu, M., Ojika, M., Wakamatsu, K., Yamada, K., Sugimura, T., Okadaic acid: an additional non-phorbol-12-tetradecanoate-13-acetate-type tumor promoter. *Proc. Natl. Acad. Sci. USA* **1988,** 85, 1768-1771.
29. Larsen, K., Petersen, D., Wilkins, A. L., Samdal, I. A., Sandvik, M., Rundberget, T., Goldstone, D., Arcus, V., Hovgaard, P., Rise, F., Rehmann, N., Hess, P., Miles, C. O., Clarification of the C-35 stereochemistries of dinophysistoxin-1 and dinophysistoxin-2 and its consequences for binding to protein phosphatase. *Chem. Res. Toxicol.* **2007,** 20, 868-875.
30. Nishiwaki, S., Fujiki, H., Suganuma, M., Furuya-Suguri, H., Matsushima, R., Iida, Y., Ojika, M., Yamada, K., Uemura, D., Yasumoto, T., Schmitz, F. J., Sugimura, T., Structure-activity relationship within a series of okadaic acid derivatives. *Carcinogenesis* **1990,** 11, 1837-1841.
31. Mountfort, D. O., Suzuki, T., Truman, P., Protein phosphatase inhibition assay adapted for determination of total DSP in contaminated mussels. *Toxicon* **2001,** 39, 383-390.
32. Fernandez, J. J., Suarez-Gomez, B., Souto, M. L., Norte, M., Identification of new okadaic acid derivatives from laboratory cultures of *Prorocentrum lima*. *J. Nat. Prod.* **2003,** 66, 1294-1296.
33. Hu, T., Marr, J., de Freitas, A. S. W., Quilliam, M. A., Walter, J. A., Wright, J. L. C., Pleasance, S., New diol estersisolated from cultures of the dinoflagellates *Prorocentrum lima* and *Prorocentrum concavum*. *J. Nat. Prod.* **1992,** 55, 1631-1637.
34. Norte, M., Padilla, A., Fernández, J. J., Souto, M. L., Structural determination and biosynthetic origin of two ester derivatives of okadaic acid isolated from *Prorocentrum lima*. *Tetrahedron* **1994,** 50, 9175-9180.
35. Suarez-Gomez, B., Souto, M. L., Cruz, P. G., Fernandez, J. J., Norte, M., New targets in diarrhetic shellfish poisoning control. *J. Nat. Prod.* **2005,** 68, 596-599.
36. Miles, C. O., Wilkins, A. L., Hawkes, A. D., Jensen, D. J., Cooney, J. M., Larsen, K., Petersen, D., Rise, F., Beuzenberg, V., MacKenzie, A. L.,

Isolation and identification of a cis-C_8-diol-ester of okadaic acid from *Dinophysis acuta* in New Zealand. *Toxicon* **2006,** 48, 195-203.

37. Torgersen, T., Miles, C. O., Rundberget, T., Wilkins, A. L., New esters of okadaic acid in seawater and Blue mussels (*Mytilus edulis*). *J. Agric. and Food Chem.* **2008,** 56, 9628-9635.
38. Gerssen, A., Mulder, P., van Rhijn, H., de Boer, J., Mass spectrometric analysis of the marine lipophilic biotoxins pectenotoxin-2 and okadaic acid by four different types of mass spectrometers. *J. Mass Spectr*. **2008,** 43, 1140-1147.
39. Suzuki, T., Beuzenberg, V., Mackenzie, L., Quilliam, M.A., Discovery of okadaic acid esters in the toxic dinoflagellate *Dinophysis acuta* from New Zealand using liquid chromatography/tandem mass spectrometry. *Rapid Commun. Mass Spectrom.* **2004,** 18, 1131-1138.
40. Bencsath, F. A., Dickey, R.W., Edmonds, C. G., Mass spectral characteristics of okadaic acid and simple derivative. *Rapid Commun. Mass Spectrom.* **1991,** 5, 283-290.